Spring 2018

Characterization of triboelectric charging in data centers/display panel manufactures, and EMI visualization based on energy parcels method in high speed interconnections

Atieh Talebzadehghahroudi

Department: Electrical and Computer Engineering

CHARACTERIZATION OF TRIBOELECTRIC CHARGING IN DATA CENTERS/DISPLAY PANEL MANUFACTURES, AND EMI VISUALIZATION BASED ON ENERGY PARCELS METHOD IN HIGH SPEED INTERCONNECTIONS

by

ATIEH TALEBZADEHGHAHROUDI

A DISSERTATION

Presented to the Faculty of the Graduate School of the

MISSOURI UNIVERSITY OF SCIENCE AND TECHNOLOGY

In Partial Fulfillment of the Requirements for the Degree

DOCTOR OF PHILOSOPHY

in

ELECTRICAL ENGINEERING

2018

Approved by:
Prof. David Pommerenke, Advisor
Prof. James L. Drewniak
Prof. Jun Fan
Prof. Victor Khilkevich
Dr. Ki-Hyuk Kim

PUBLICATION DISSERTATION OPTION

This dissertation consists of the following five papers, formatted in the style used by the Missouri University of Science and Technology, listed as follows:

Paper I (pages 3-27), A. Talebzadeh, M. Moradian, Y. Han, A Patnaik, D. Swenson, D. Pommerenke, "Dependence of ESD charge voltage on humidity in data centers (Part 1 - test methods)", has been published in ASHRAE Journal, vol. 121, pp. 58-70, 2015.

Paper II (pages 28-55), A. Talebzadeh, A. Patnaik, X. Gao, M. Moradian, Y. Han, D. Swenson, D. Pommerenke, "Dependence of ESD charge voltage on humidity in data centers (Part 2 - data analysis)", has been published in ASHRAE Journal, vol. 121, pp. 37-48, 2015.

Paper III (pages 56-81), A. Talebzadeh, M. Moradian, Y. Han, D. Swenson, D. Pommerenke, "Effect of human activities and environmental conditions on electrostatic charging", has been published in IEEE Transactions on Electromagnetic Interference, vol. 58, no. 4, pp. 1266-1273, 2016.

Paper IV (pages 82-112), A. Talebzadeh, K. Kim, D. Pommerenke, "Triboelectric charging between display glass panels and dissipative/insulative rollers", has been published in IEEE Transactions on Electromagnetic Interference, vol. 59, no. 6, pp. 1755-1764, 2017.

Paper V (pages 113-139), A. Talebzadeh, , P. Sochoux, J. Li, Q. Liu, K. Ghosh, D. Pommerenke, "Shielding effectiveness, coupling path, and EMI mitigation for QSFP cages with heatsink", accepted for publication in IEEE Transactions on Electromagnetic Interference, DOI: 10.1109/TEMC.2018.2813889, 2018.

ABSTRACT

This dissertation is composed of five papers. In the first three papers, triboelectric charging, which is the underlying cause of most electrostatic discharge (ESD), during daily human activities in data centers such as well-defined pattern walking, random walking, standing up from a chair, and taking off a sweater is investigated. Further, the effect of environmental condition (temperature and relative humidity), the footwear, and flooring material in building the static voltage and the discharge process are studied.

In the fourth paper, triboelectric charge generation on the glass is investigated during the glass transportation by roller conveyor systems in display manufacturing. The underlying parameters that affect the static charging on both glass and rollers consisting of roller material, roller radius, transfer velocity, transfer acceleration, traveling distance, and relative humidity are explored.

The fifth paper focuses on the shielding effectiveness (SE) of quad form-factor pluggable (QSFP) interconnections cages with heatsinks, which are often only optimized for thermal, mechanical, and volume manufacturing. Energy parcels and their trajectory concept are applied to electromagnetic waves (EM) to visualize the coupling paths in a QSFP cage with a rising heatsink. The rising heatsink creates a new coupling path for EM waves to leak to the cage and emit from the routers/switches chassis faceplate. An EMI mitigation technique is introduced and its performance is evaluated with SE measurement for the frequency of 1-40 GHz with and without the active operational of 40 Gbps optical module in a dual reverberation chamber.

ACKNOWLEDGMENTS

I would like to express my great gratitude to Prof. David Pommerenke, my Ph.D. advisor, for his guidance on my research work and direction for this dissertation during my pursuit of the Ph.D. degree. I learned a lot from him during the projects and also taking his invaluable classes.

My special thanks to Prof. James Drewniak for his encouragement, trust, and support during my research. I was very fortunate to take the advantage of his immense knowledge by taking his classes. Additionally, I would like to thank all other professors in EMC Laboratory, especially Prof. Jun Fan and Prof. Victor Khilkevich for participating in my Ph.D. advisory committee, providing helpful guidance in my research, and teaching useful classes. Further, I appreciate Dr. Ki-Hyuk Kim for being on my advisory committee and his helpful discussions.

I would like to thank Mr. Philippe Sochoux, my manager in Juniper Netwroks Inc., for his kind mentoring during my six months internship. Not only did my work at Juniper Netwroks Inc. result in a part of this dissertation, it also helped me to achieve industrial experience.

I would also like to express my thanks to all the former and current members of the EMC Laboratory for their teamwork and help in my coursework and research.

Last but not least, I want to thank my whole family and all my friends for their support and encouragement towards achieving this degree. For most, I am sincerely thankful to my dear parents and my dear husband, Ali, for their emotional support and love.

TABLE OF CONTENTS

LIST OF ILLUSTRATIONS

PAPER I

PAPER II

PAPER V

LIST OF TABLES

PAPER I Page

PAPER II

PAPER III

PAPER IV

PAPER V

NOMENCLATURE

Symbol	Description
τ	decay time constant
V	voltage
t	time
V_T	transfer velocity
R_R	roller's radius
ω	angular velocity
Q	charge
SE	shielding effectiveness
P	power
E	electric field
H	magnetic field
J	electric current source
M	magnetic current source
ε	permittivity
μ	permeability
S	instantaneous Poynting vector
u	total magnetic and electric energy density
v	instantaneous velocity of EM energy parcels

SECTION

1. INTRODUCTION

This dissertation is composed of five papers that focuses on triboelectric charge voltage generation during daily activities in data centers, triboelectric charge voltage generation during glass transfer system in display manufacturing, and shielding effectiveness of quad small form-factor pluggable (QSFP) interconnections cage with a heatsink and visualizing the coupling path by applying the energy parcels concept to electromagnetic (EM) waves.

In the first three papers, the generation of electrostatic charge is considered for the cases of walking, standing up from a chair, and for taking off a sweater at seven different environmental conditions. Further, the effect of utilizing ESD-mitigation shoes and floors on building the static charge and the discharge process are presented.

In the fourth paper, triboelectric charge generation on the glass is explored during the glass transportation by a roller conveyor system in display manufacturing. The paper presents an intensive study to understand the underlaying parameters including the effect of roller material (insulative vs. dissipative), roller radius (small vs. large), transfer velocity (slow vs. fast), transfer acceleration (medium vs. high), traveling distance (200 m vs. 400 m). In addition, a comprehensive study of the surface potential distribution on the glass and rollers by utilizing a 2D automated scanner is given.

In the fifth paper, the shielding effectiveness of QSFP interconnections cages with heatsinks, which are often optimized for thermal, mechanical, and volume manufacturing, is investigated. Energy parcels and their trajectory concept are applied to EM waves to visualize the coupling paths in a QSFP cage with a rising heatsink. The rising heatsink

creates a new coupling path for EM waves to leak to the cage and emit from the routers/switches chassis faceplate. An EMI mitigation technique is introduced and evaluated by SE measurement for the frequency of 1-40 GHz, and by an active operational of 40 Gbps optical module in dual reverberation chamber.

The primary contributions of this dissertation include:

- Analyzing triboelectric charging during daily human activities in data centers and understanding the dependency of the risk of ESD-related failure on the environmental conditions and materials of foot wearing and flooring (Paper I-III).
- Studying triboelectric charging on the display glass during the glass transportation in LCD display manufacturing and the underlaying parameters (Paper IV).
- Exploring the electromagnetic shielding effectiveness in QSFP cages with heatsink and applying energy parcels concept to EM waves to visualize the coupling path created by a rising heatsink (Paper V).

PAPER

I. DEPENDENCE OF ESD CHARGE VOLTAGE ON HUMIDITY IN DATA CENTERS (PART 1 - TEST METHODS)

ABSTRACT

The effect of absolute and relative humidity on the charge generated on the human body during different human activities was investigated. Environmental conditions were altered between a relative humidity of 8% to 45% in a temperature range of 5˚C to 38˚C; additionally, a wide range of footwear and flooring types were considered. The human activities studied included well-defined walking, random walking and scraping feet, taking off a sweater and dropping it, and sitting up from a chair. The first part of this three-part article mainly describes the test and data analysis methodology. One conclusion based on the voltages generated across different footwear and flooring combinations is that charge generation depends on the particular activity and associated materials. However, low relative humidity and a low, but not very low, dew point in general produce conditions favorable for high voltage generation. Among all the experiments performed, sitting up from a chair yielded the highest body voltage. Two other parts of the three-part article present a detailed analysis.

1. INTRODUCTION

Increasing demands for energy efficient data centers leads to a strong drive towards identifying the optimal environmental operating conditions. Studies have shown that humidity affects the static charge that can be generated on a body [1]-[3]. The sudden discharge of these static voltages can damage or destroy data center equipment. In order to

have reliable operation and considerable amount of energy savings ASHRAE has guidelines for operating different types of data centers in different environmental condition envelops as indicated in Figure 1. Envelopes A1 – A4 show the different permissible envelopes for different types of data centers [4]. Operating a data center for prolonged times in the lower humidity range of A3 and A4 increases the risk of ESD induced upset or damage.

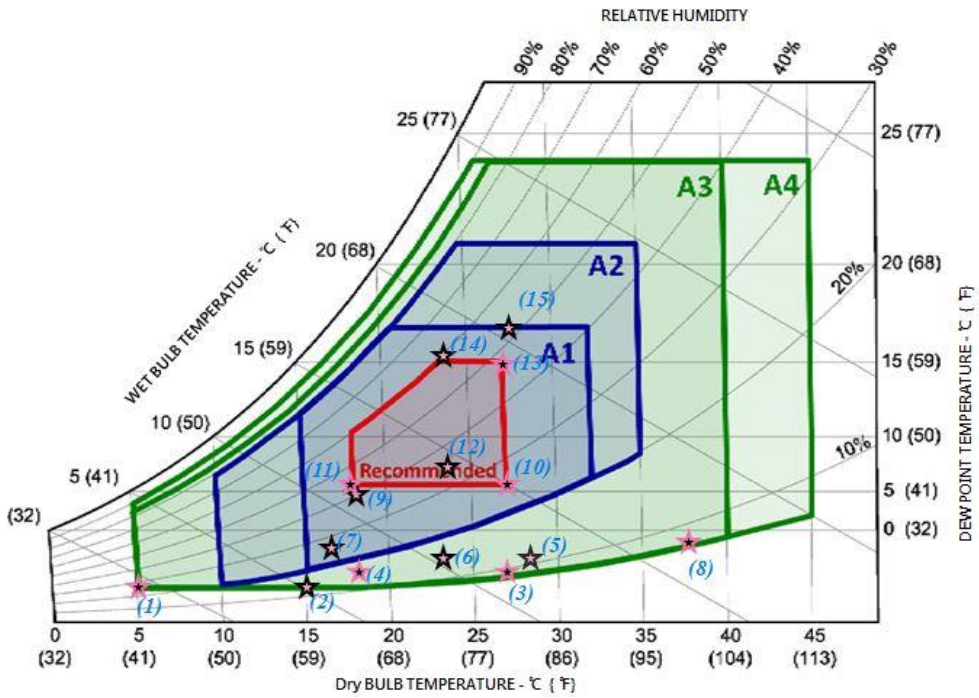

Figure 1 - ASHRAE psychometric chart. Pink stars indicate the seven environmental conditions in this study, while black stars indicate the environmental conditions used in previous studies [5] and [6].

Figure 1 and Table 1 show the ASHRAE Psychometric Chart [4] and indicate the environmental test points at which experiments have been performed. One previous study concentrated more on regions A1 and A2 [5] and [6]. However, due to the large energy-

saving potential in the even wider ranges of A3 and A4, a second study was initiated to determine how much the risk of upset or failure in a data center would increase if the environmental conditions in data centers extended to the lower humidity range of A3 and A4. To answer this question, a large set of voltage measurements were taken under well-controlled conditions. These measurements recorded the voltage as a function of time while the operator was performing an action, such as walking, sitting up from a chair, or removing a sweater and dropping it. The parameter set included a wide range of flooring systems, from conductive floors to insulated floors, as well as a range of footwear, from standard to electrostatic discharge (ESD)-preventing. During the second study, 4000 additional experiments were performed, providing more than 6500 minutes of recorded voltage waveforms. This database allows multiple types of analysis:

- Voltage levels created by user actions,
- Voltage levels as a function of environmental conditions,
- Voltage levels as a function of footwear and flooring,
- Discharge times for different flooring and footwear combinations,
- Comparison of voltage levels for different types of operator actions, such as walking vs. sitting up from a chair,
- Extrapolation of voltage levels using the probability density function to estimate the occurrence rate of voltages over time frames much longer than the 1-minute recorded waveforms,
- Estimation of the failure risk in data centers caused by the surpassing of robustness thresholds when a person charged above the threshold touches the data center serve.

The first part of the article, presented here, focuses on the description of the test method, measurement definitions, and initial data analysis. The environmental points selected for the second study primarily included those from regions A3 and A4 that allowed the effect of humidity changes to be predicted. It needs to be noted that a recent publication [7] that shows measured environmental conditions inside of data centers shows a large variation which often exceeds the targeted range.

Table 1 - List of selected environmental conditions.

Data Points	Temperature (°C)	RH (%)	Dew Point(°C)
1	5	25	-13.1
2	15	15	-11.67
3	27	8	-10
4	18	15	-8.9
5	28	10	-6.11
6	23	15	-5
7	17	25	-3.4
8	38	8	-1.7
9	18	40	3.89
10	27	25	5
11	18	45	5.6
12	23	35	6.7
13	27	45	13.9
14	23	60	15
15	27	53	16.7

2. WELL-DEFINED WALKING PATTERN EXPERIMENT

A well-defined walking pattern (WDP) has been created to allow repeatable results in comparing floor and shoe combinations. This pattern is described in the ANSI/ESD STM97.2 standard. Additionally, we introduced a "random" walking test that provides less reproducible results but better simulates real, uncontrolled walking.

The ANSI/ESD STM97.2 test method [8] involves a person walking on a floor sample in a well-defined walking pattern while wearing a specific shoe type under controlled environmental conditions. The person repeats the walking pattern a minimum of 10 times while holding an electrode to record the static voltage during walking. The general test setup and walking pattern, appear in Figure 2. To control the environmental conditions (Table 1), additional steps were taken to maintain low humidity. The participant wore a breathing mask that was connected to small bottles of desiccant to absorb moisture in the breath. Also, at high temperature and low humidity (e.g., 38 ˚C and 8% RH), a ventilated overall clothing reduced the chamber's moisture intake. Table 2 lists the floor and shoe types used in this experiment. Rubber1 and Rubber2 are conductive, low resistance rubber floors, which we refer to as "ESD floor" herein. The specific high-pressure laminate floor (HPLF) used is a high resistance floor, referred to herein as "Non-ESD" floor. Also, Vinyl1 and Vinyl2 are low dissipative range floors, which can be considered medium-ESD floors. Other researchers have shown a strong correlation between the shoe-floor resistivity and the charge voltage [9] and [10]. However, certain wax-like materials can reduce the tribo-charging strongly, although they do not exhibit conductive properties. We selected a wide range of popular shoes for our investigations.

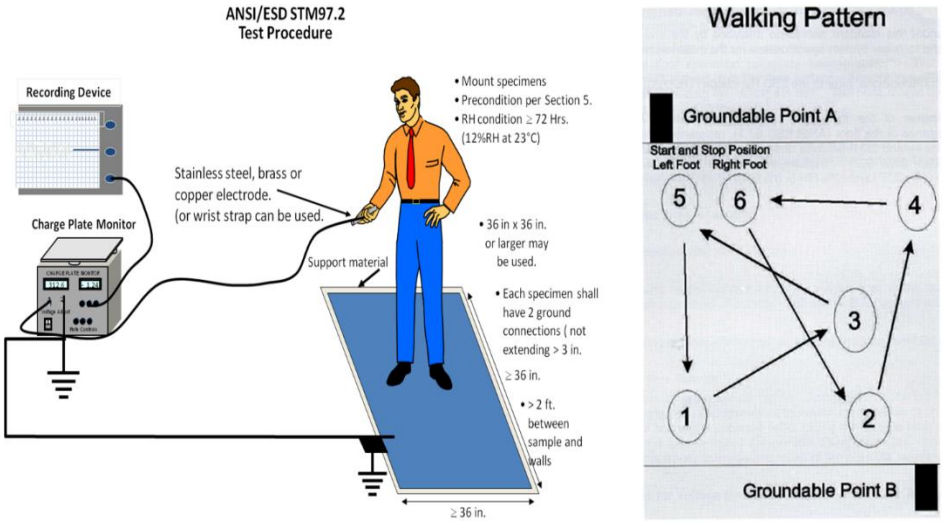

Figure 2 - (a) well-defined walking experiment setup, (b) well-defined walking pattern ([5] and [6]).

Table 2 - Floor and shoes type.

Shoes	Floorings	ESD-description
1) Low-range dissipative ESD 2) Mid-range dissipative ESD 3) Deck shoes #1 4) Deck shoes #2 5) Deck shoes #3 6) Plastic shoes 7) Running shoes 8) Leather dress	1) Rubber #1 2) Rubber #2 3) Vinyl #1 4) Vinyl #2 5) High-pressure laminate (HPL)	ESD-mitigating Non-ESD mitigating

The shoe column includes two low resistance shoes, which served as the ESD shoes in this experiment. The other shoes are high resistance shoes not considered to have ESD-reducing properties. Further information about footwear and flooring resistance in relation to ESD protection can be found in [10] and [11].

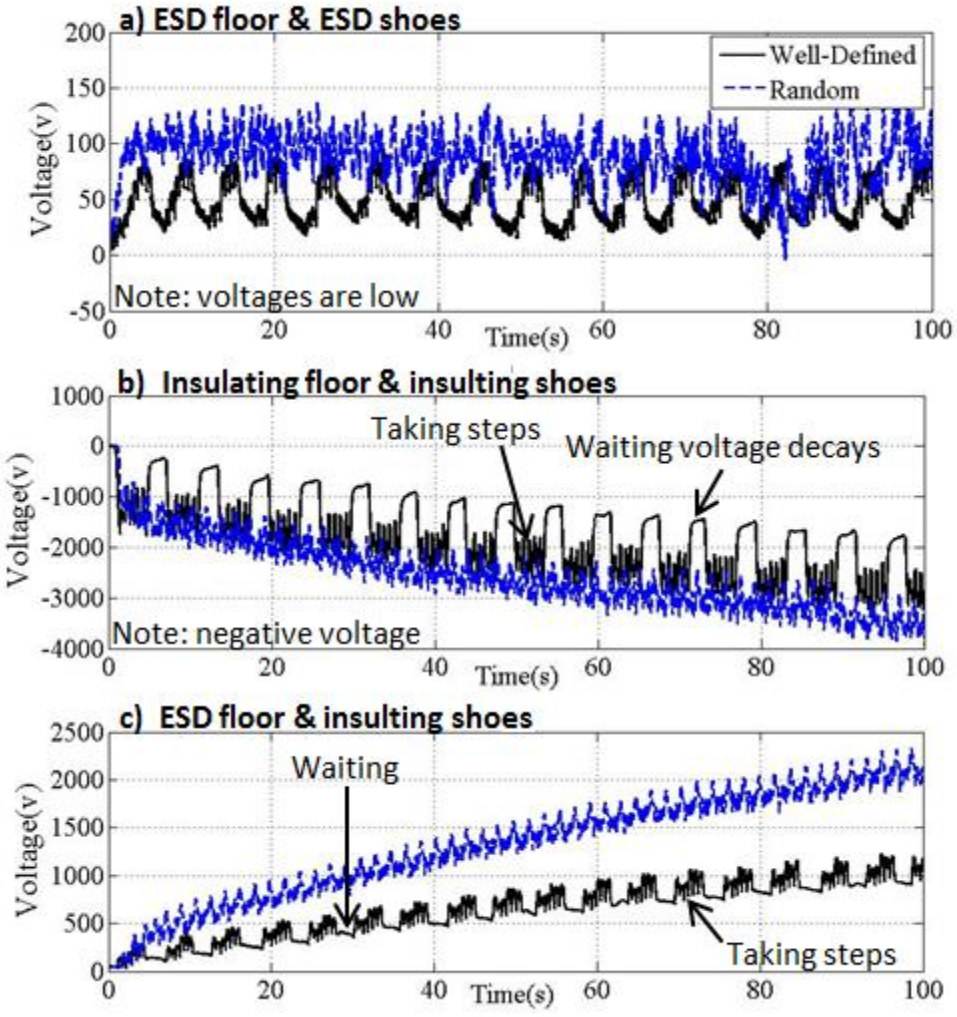

Figure 3 - Typical waveform of WDP (solid traces). (a) Rubber #2 floor, low-range dissipative ESD shoes, at 27°C & 8% RH, (b) HPLF floor, deck shoes 1, at 27°C & 8% RH, (c) Rubber #2 floor, plastic shoes, at 27°C & 8% RH.

Figure 3 illustrates examples of the voltages recorded during WDP (solid traces). Subfigure (a) was recorded for a person walking on an ESD floor (flexco rubber) while wearing a pair of ESD shoes (mid-range dissipative ESD shoes) at a temperature of 27 °C (80.6 °F) and relative humidity (RH) of 8%. In spite of the low humidity, only low voltages, less than 150 V, were recorded. This is a consequence of wearing ESD shoes on an ESD floor. Most charges created at the sole-floor interface were neutralized rapidly by the conductive path. The voltage increased every time the person walked along the defined pattern. However, in contrast, subfigure (b) shows the results for the case in which neither an ESD floor nor ESD shoes were used. The insulating properties of both allowed the build-up of much higher voltages. This material pairing created a negative voltage. In principle, the tribo-eletric series can be used to predict the voltage polarity; however, this is difficult given the unknown material properties and surface conditions. The voltage discharged more rapidly in case (a) than in case (b). Another phenomenon observed for some combinations of insulated flooring and footwear was that the voltage increased over the 100sec experiment, but returned to nearly zero between steps when using conductive surfaces. In the insulated case, the voltage finally reached a saturated value. The experiments were performed for 100sec, which was assumed to be the maximum walking time before an operator would either stand in one location long enough to discharge, or discharge by other means, such as touching a door.

2.1. WALKING AND STANDING VOLTAGES

To evaluate the recorded voltage waveform, three values were measured, the walking voltage, standing voltage, and maximal voltage magnitude. Figure 4 (a) and (b)

depicts two typical waveforms of WDP walking. For subfigure (a), the positive voltage was measured as the person lost electrons, while for subfigure (b), the person received a negative charge. According to ANSI/ESD STM97.2 [8], the walking voltage is the average of all local peaks of the voltage magnitude. In the figure, the circles represent the local peaks. In contrast, the standing voltage is the average of local minimums of the voltage magnitude, as indicated by the squares in the figure. The definition is based on two underlying assumptions: 1) using the average stabilizes the measurement, which is helpful in comparing different test conditions, and 2) how long a person will walk before touching a server is unknown.

Comparing the maximal voltage during 100 s of walking to the walking voltage for a wide range of test conditions provides insight into the usefulness of the definition of walking voltage. The results of two selected sets of materials are presented. These sets represent the most and least ESD-reducing configurations. The first column in Table 3 lists the set of ESD-reducing materials, which includes two ESD shoes (low-range dissipative ESD shoes and mid-range dissipative ESD shoes) and two ESD floors (rubber 1 and rubber 2). The second column lists the non-ESD materials, which includes six non-ESD shoes and one non-ESD floor (HPLF). Figure 5 shows the average voltage for each of these two sets of materials.

Figure 5 shows the voltages as a function of the dew point for the maximal voltage magnitude, walking, and standing voltage. Sub-figure (a) presents data for a case in which ESD was suppressed by using ESD shoes on a conductive rubber floor, while sub-figure (b) presents data for non-ESD-reducing floor and shoes. The following conclusions can be drawn from this dataset:

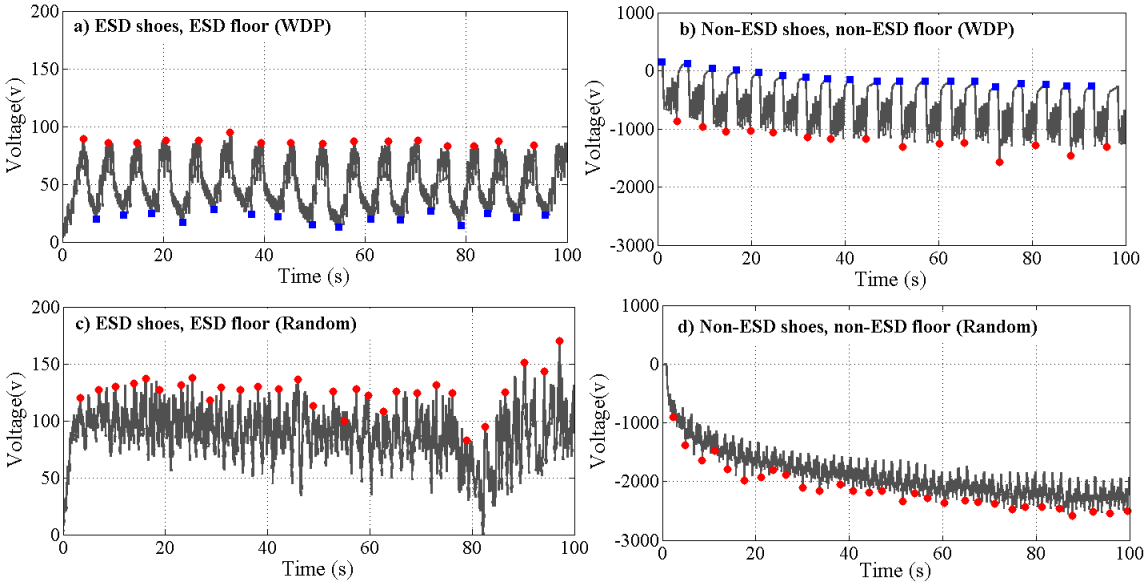

Figure 4 - Determining walking and standing voltage. (a) WDP walking at 27°C & 8% RH, (b) WDP walking at 18°C & 15% RH, (c) random walking at 27 °C & 8% RH, (d) random walking at 18°C & 15% RH.

- ESD suppression was very successful, reducing the maximal voltage by 10x or more,
- The maximal voltage magnitude was consistently a factor of approximately 1.3 above the walking voltage. This indicates that the experiments were consistent and not governed by momentarily high voltage peaks,

The standing voltage was much lower than the walking voltage. However, the ratio was not constant; it varied across environmental conditions and flooring / footwear selection. The ratio between the walking and standing voltage ranged from 0.8 to 3. The standing voltage is important because most operators will stand still before they touch a server. Especially for the more critical non-ESD controlled situation, a voltage maximum was indicated around a dew point just below 0 °C. This was most visible when the temperature reached 38 °C. This condition combined a high dew point with low relative

humidity. At lower temperatures, the maximum was more visible under environmental conditions of 18 °C and 15% RH.

Table 3 - ESD reducing and non-ESD reducing material combinations.

ESD Material (Floor, Shoe)	Non-ESD Material (Floor, Shoe)
(Rubber #1, Low-range dissipative ESD shoes)	(HPLF, Deck #2)
(Rubber #1, Mid-range dissipative ESD shoes)	(HPLF, Deck #1)
(Rubber #2, Low-range dissipative ESD shoes)	(HPLF, Deck #3)
(Rubber #2, Mid-range dissipative ESD shoes)	(HPLF, Leather dress)
	(HPLF, Running)
	(HPLF, Plastic dress)

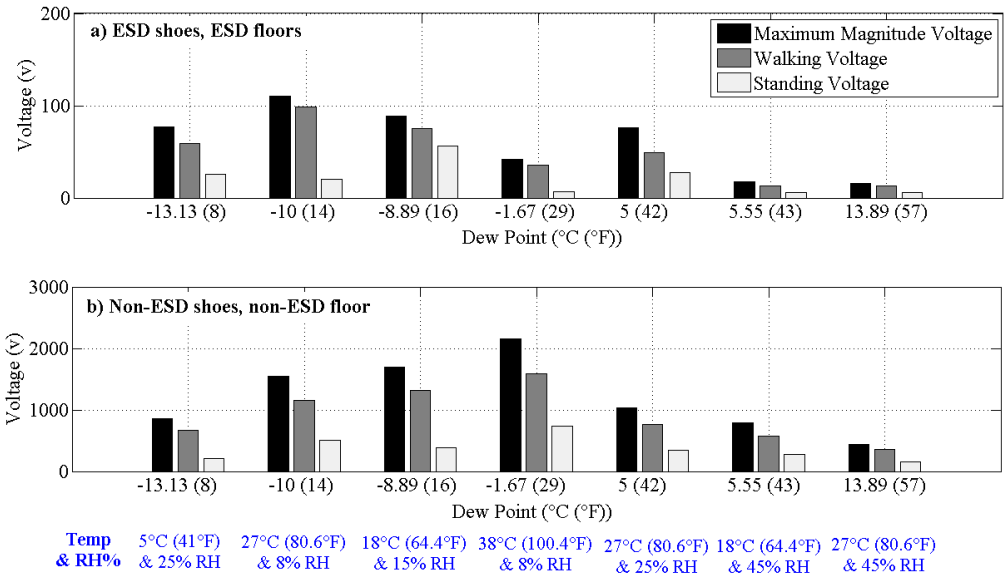

Figure 5 - Comparison of the maximum magnitude voltage, walking voltage, and standing voltage for WDP walking. (a) ESD material set, (b) non-ESD material set.

2.2. RANDOM WALKING EXPERIMENT

In the random walking experiments, the participant sometimes walked faster, or occasionally moved his or her shoes sideways. There was no requirement to walk a defined pattern with short stops in between. The random walking voltages were somewhat higher (30% higher) than in the case of the WDP and they did not exhibit a regular pattern. This somewhat contrasts the data from Ryser [11], which indicates a ratio of approximately 1:2 between walking and scraping. However, Ryser also noted that his walking voltages were rather low. It is not clear how the scraping action was performed. In our random walking, fast walking with some slippage was part of the procedure; however, strong sideways or large dragging movements were not considered common for walking in a data center and therefore were not included in our random walking pattern. This might explain the different ratios between walking in a pattern and random walking. In contrast to the WDP, during random walking, there were no brief stops, so no pronounced voltage minima were created by discharge. Therefore, it was only possible to extract two measurement values from every random walking experiment: 1) the maximal voltage magnitude, and 2) the walking voltage. The walking voltage was derived from the average of the local maxima. Figure 4 (c) and (d) illustrate typical random walking voltage waveforms and their processing. For the insulated floor and shoe combination (subfigure (d)), the voltage reached approximately -2500 V, while it only reached 150 V for the ESD-reducing footwear/floor combination. The individual steps produced short local maxima. These were identified, and their average was used to calculate a walking voltage. Figure 6 compares the maximal voltage magnitude, and walking voltage as a function of dew point for random walking. Subfigure (a) shows the average of voltages if ESD mitigating shoes and floors are used,

while subfigure (b) shows the average of voltages for a set of non-ESD materials. Similar to the WDP, the walking voltage is about 30% below the maximal voltage magnitude. For ESD mitigating materials the voltages are low. The more critical situation of non-ESD mitigating materials leads to voltages in the kV range. The measurements at a rather high temperature of 38 °C (100.4 °F) and 8% RH led to the highest voltages. A drop in voltages at lower dew points has been observed.

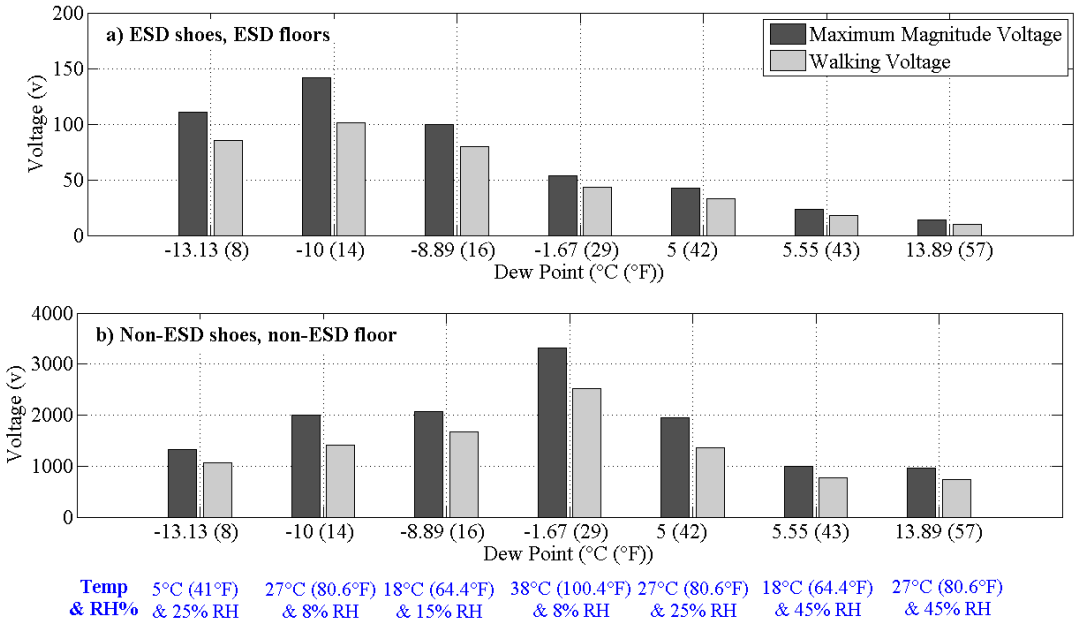

Figure 6 - Comparison of the maximum magnitude voltage, and walking voltage for random walking. (a) ESD material set, (b) non-ESD material set.

3. SITTING UP FROM A CHAIR EXPERIMENT

In addition to walking, a variety of other operator actions can cause considerable charges [13] and [14], such as moving carts removing a garment and dropping it in [15],

unwrapping plastic foil, and sitting up from an office chair [16]. Also, this study included sitting up from a chair and removing a garment. In this experiment, the participant sat down on a chair for three seconds and then stood up while holding an electrode to record the voltage. Then, the participant waited approximately five seconds before sitting down again, repeating this cycle a minimum of 10 times, so the length of each recorded voltage waveform would be around 50 seconds. During this experiment, the participants' shoes always remained on the ground, and their backs touched the entire back of the chair while sitting.

Figure 7 (a) shows the general setup for this experiment and the results. Three different, randomly selected, non-ESD-compliant office chairs were used. Subfigure (b) shows the recorded voltage waveform for all three chairs when the participant wore non-ESD deck shoes 1 on a non-ESD floor, HPLF. The chamber was set to 27 °C at 8% RH. For all chair experiments, the same outer garment was worn. Similar to the walking experiment, a mask was worn to help maintain a low RH.

When the participant's hips touched the chair (subfigure (b)), the person received electrons and charged to a negative voltage. When the participant completely sat down and leaned against the back of the chair, a positive voltage was acquired. The moment the person stood up, the voltage increased strongly. When the floor/shoe combination was well insulated, the participant did not discharge while standing. When the participant sat down again, the effect of the charges on the chair and on the person were compensated for partially, reducing the voltages until the participant stood up again. As the person does not discharge between repeated sit-down, stand-up cycles, the voltage may increase in each cycle if the flooring system does not provide a sufficient path to the ground. In analyzing

the maximal voltage, it should be noted that the data from chair 1 (solid trace) and chair 2 (dotted trace), subfigure (b), was measured for a shorter period of time. This was caused by sparking. This does not affect the voltage increase obtained by each cycle of sitting down and standing up, however, a higher maximal voltage would have been reached.

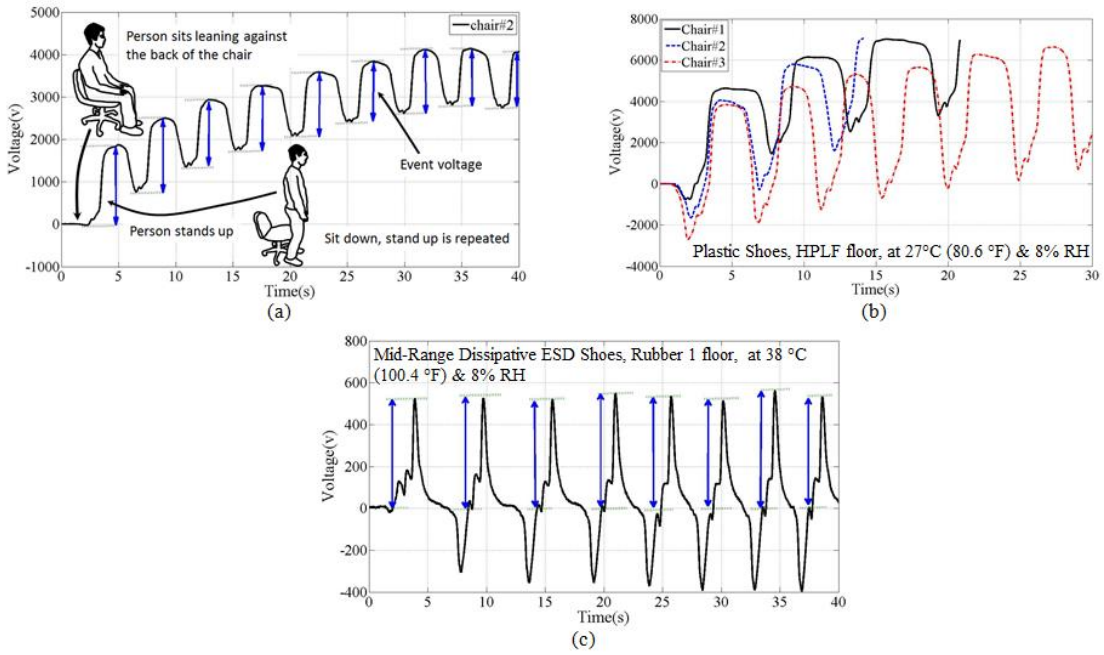

Figure 7 - Chair experiment. (a) Illustrating sitting up process, (b) example of typical waveforms, (c) chair event voltage for cases in which the shoe/floor system discharges rapidly from the person.

3.1. CHAIR EVENT VOLTAGE

To analyze the data, we defined an "event voltage" for both the chair and the garment experiments. The event voltage describes the average change in voltage when the person stands up from the chair or drops a sweater. Figure 7 illustrates the data. When standing up, the voltage rises. After standing up, the voltage may drop slowly Figure 7 (b)

or rapidly Figure 7 (c) depending on the shoe/floor resistance. The person stands for a few seconds and then sits down again, repeating this process ten times.

In many cases, it is easy to read a meaningful event voltage from the waveform. However, in cases in which the shoe/floor resistance is low, the charges will dissipate quickly Figure 7 (c). Further, the person may acquire a voltage of the other polarity for a moment upon sitting down. This voltage would dissipate to zero if the person were to sit for a longer period of time, so we defined the event voltage as the increase in voltage from zero to the highest voltage reached, as illustrated in Figure 7 (c). Figure 8 indicates that all three chairs followed a similar pattern with respect to the voltage magnitude. In most cases, Chair #3 showed the highest charge voltage; however, no large differences between the chairs existed.

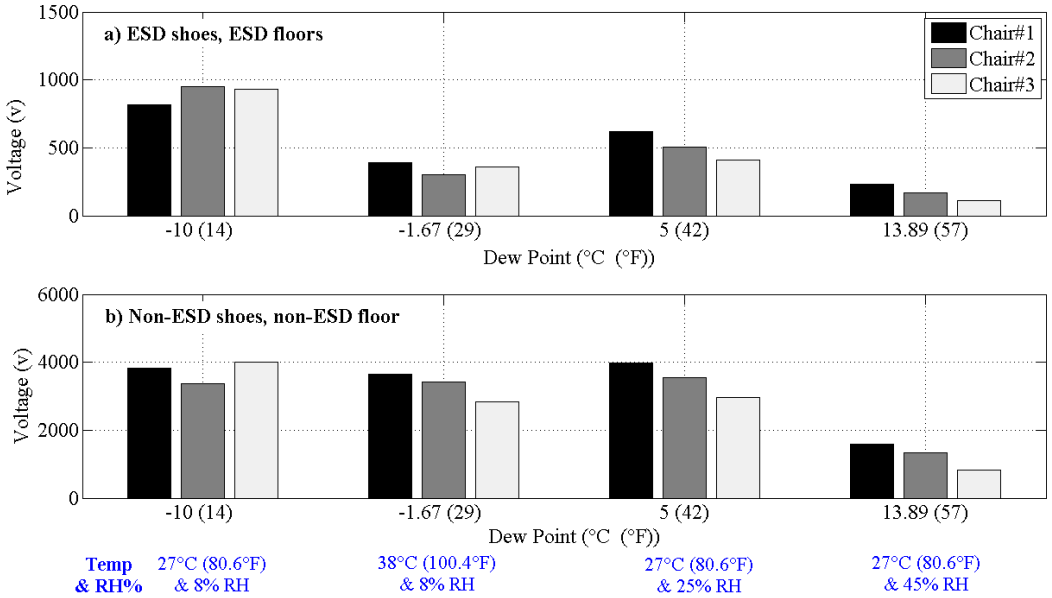

Figure 8 - Comparison of event voltage for different chairs. (a) ESD material set, (b) non-ESD material set.

This indicates that the samples of chairs selected did not contain an outliner, i.e., the data likely represent typical office chairs. Even when using ESD-reducing footwear (subfigure (a)) and flooring, an average event voltage of 1000V was recorded at a dew point of -10 °C (14°F). This voltage would not be sufficient to damage or upset servers that fulfill the IEC 61000-4-2 requirements of 4000/8000V ESD test levels; however, they would certainly endanger data center equipment during conditions in which the normal shielding has been removed, i.e., during service that requires accessing internal points. When no ESD-reducing footwear and flooring were used, the average event voltage reached 4000V at only -5 °C (42 °F). This value equals the ESD test levels. Other types of chairs, garments, or individual events will certainly surpass the 4kV limit, which clearly indicates the need to use only ESD-reducing chairs in data centers.

4. TAKING OFF A SWEATER EXPERIMENT

Many researchers have noted that removing a sweater can cause large voltages [15]. As the temperature in a data center can vary locally, it is reasonable to assume that operators may remove a sweater and drop it. The charge separation occurs when the sweater rubs on the underlying layer of clothing. However, that will not create a large voltage on the person, as the effects of the separated charge are compensated for by the short distance between them. However, the moment the operator removes and drops the garment, the effects of the charges are no longer compensated for, and the voltage will change rapidly. In this experiment, the participant always wore the same underlying garment but one of three different sweaters. Figure 9 (a) illustrates this process. After putting on the sweater, the participant discharged himself and began the recording. Next,

he removed the sweater and dropped it. Then, he waited 20 to 30 seconds to monitor the slow discharge via the footwear. After that, he discharged himself by touching the ground. The process was repeated three times. Figure 9 (b) shows waveforms for the case in which the user wore Non-ESD shoes (deck shoes 1) on a Non-ESD floor (vinyl #2) at a temperature of 27°C set to 8% RH. All three sweaters produced similar results. Again, this indicates that the random selection of sweaters did not contain an outliner, i.e., it is reasonable to generalize the results with caution, although the number of sweaters was low. These rather dry conditions yielded a voltage of close to 4 kV, high enough to endanger data center equipment.

4.1. SWEATER EVENT VOLTAGE

The event voltage describes the voltage change that occurred when the sweater was dropped. Figure 9 (c) illustrates this change for Non-ESD-controlled conditions. In the definition of the event voltage for the sweater experiment, considerations must be made similar to those in the chair experiment. Figure 9 (c) illustrates that dropping the sweater lead to a sudden voltage increase. Then, the voltage level dropped very slowly because the shoe/flooring system had a high resistance. However, for cases in which the shoe/flooring system provided a lower resistance path (Figure 10), the event voltage was not as easily recognized, as the voltage level was only maintained for a few seconds or less. This lead to some uncertainty in reading the event voltage, especially if the quick voltage fluctuation during the phase in which the person removed the sweater (before dropping) produced voltage of the opposite polarity. In these cases, the event voltage was defined as the voltage between zero and the maximal voltage reached when the sweater was dropped.

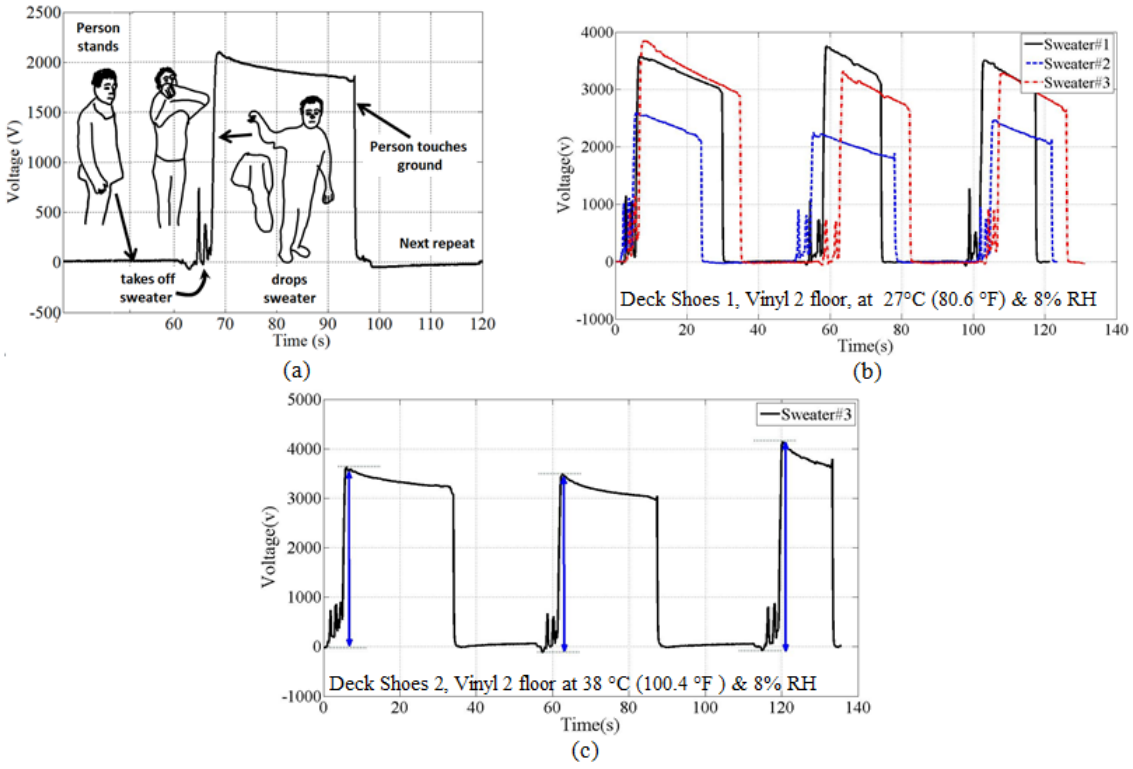

Figure 9 - Sweater experiment. (a) Illustration of removing a sweater, (b) examples of typical waveforms, (c) sweater event voltage for cases in which the shoe/floor system discharges rapidly from the person.

The voltage was low and brief, so this ambiguity will not influence the conclusions of this study strongly; this only occurred for cases in which the ESD precautions lead to low charge voltages. Both the low voltage levels and fast discharge strengthen the argument that good ESD control from footwear, flooring, or ground straps is very effective in controlling the risk of ESD damage. The sweater experiment produced similar trends across repetitions, as indicated by the small difference between the average event voltage and the maximal event voltage. In general, the ratio was less than 1.2. Figure 11 presents the average event voltages for the sweater experiments at different dew points. The three types of sweaters created different voltages, varying much more widely than in the chair

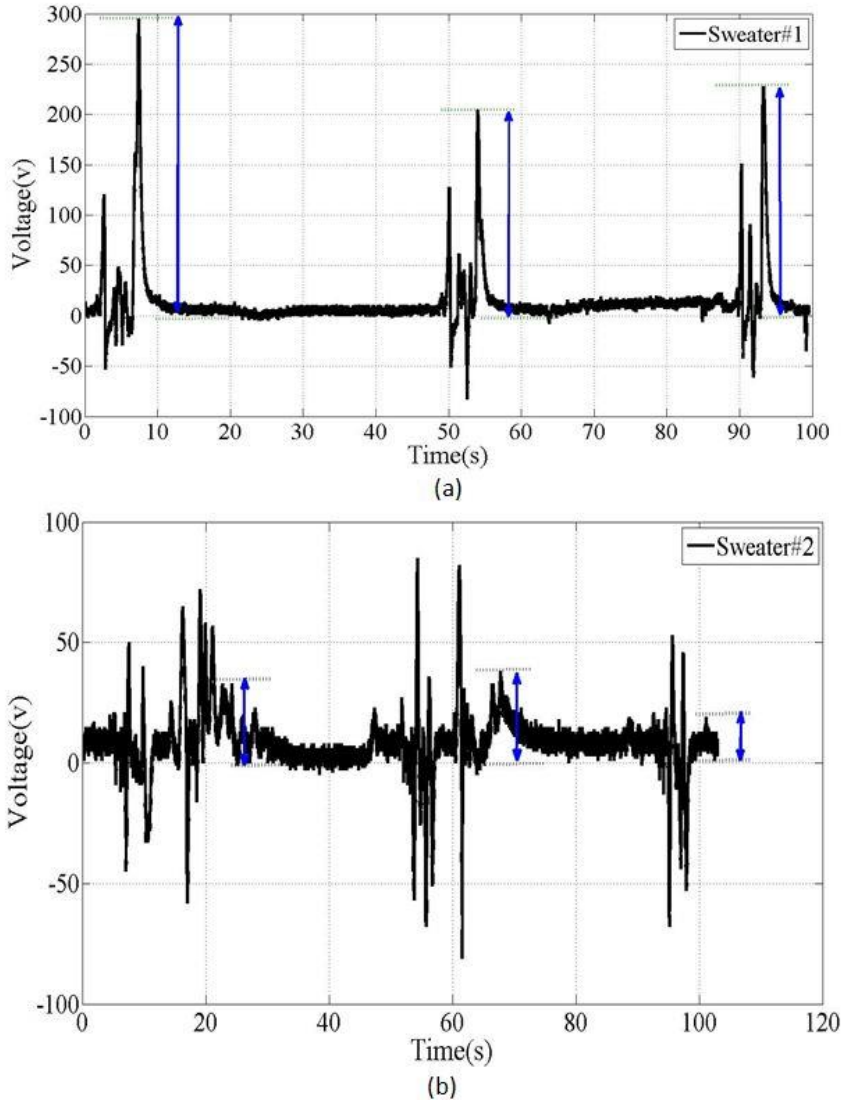

Figure 10 - Definition of event voltage. (a) mid-range dissipative ESD shoes and rubber #1 floor at 38˚C and 8%RH, (b) low-range dissipative ESD shoes and rubber #1 floor at 27˚C and 8% RH.

experiment. Subfigure (a) presents results for ESD-reducing flooring and shoes. The voltages still reached 500 V, a value well below the damage or upset threshold for servers; however, it is close to the robustness level that we assume to be the threshold for service (500 V). As shown in Figure 10, the voltage will remain on the operator only for a brief moment due to the shoe/floor discharge path. In addition to having a low voltage, the

likelihood of the operator touching a sensitive part during this brief moment is low. However, if we consider the voltage level and the possibility of other charge-inducing events, such as standing up from a chair, and remind ourselves that this dataset represents only a small set of possible sweaters and underlying garments, we believe the data indicate that it is advisable to use a ground strap during service, even if ESD-controlling footwear and flooring is used. Subfigure (b) of Figure 11 presents the average event voltages for the non-ESD-controlled setting. The voltage levels were 8-10 times larger, reaching levels that could damage data center equipment. If we further consider that the voltage remained on the operator for a long time (see Figure 9 (c)), we can easily conclude that operators must be aware of the ESD dangers imposed by the removal of a sweater. In Figure 11, both sub-figures (a) and (b) indicate that there was not a strong tendency for the voltage to increase as the dew point decreased. This was generally observed in all data and is discussed in greater detail in the second article.

5. VOLTAGE LEVELS

Table 4 compares the maximal walking voltages (i.e. WDP and random walking) and maximal event voltages (i.e. removal of sweater and dropping it, and sitting and getting up) for four different environmental conditions: (1) 27°C & 8%RH, (2) 38°C (100.4 °F) & 8%RH, (3) 27°C & 25%RH, and (4) 27°C & 45%RH including all floors and shoes. Core findings from the table are as below:

- The WDP leads to the lowest peak voltages. This is a consequence of the defined walking pattern which was conceived to define a well reproducible method for comparing conditions. The maximal voltages measured in random

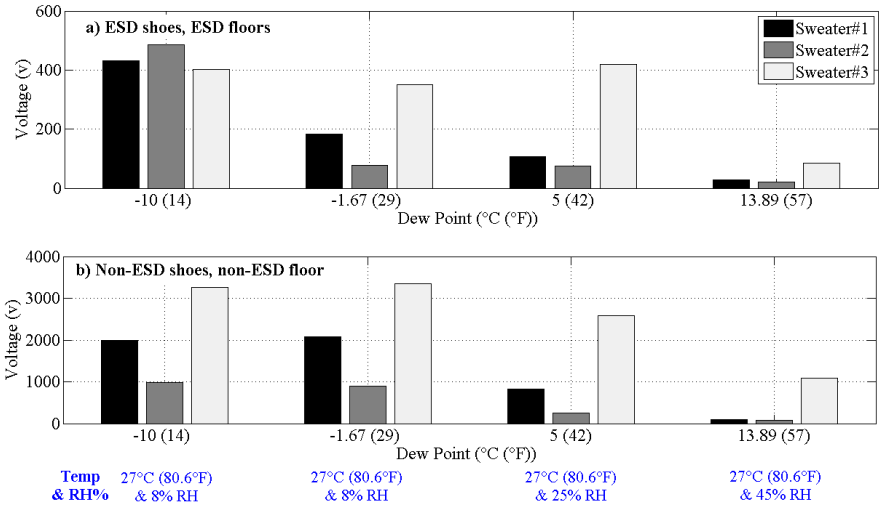

Figure 11 - Comparison of event voltage for different sweaters. (a) ESD material set, (b) non-ESD material set.

- walking are about 50% larger, while they are in average about 30% larger.For the assessment of risk to the data center one needs to further consider that most operators will stand for a moment before touching equipment. This would lead to a reduction in voltage,
- The highest voltages have been obtained during the chair and sweater experiment,
- For walking experiments the highest voltages have been recorded for non-ESD flooring and non-ESD mitigating footwear. However, during the sweater and chair experiment high voltages can occur also for other floor combination, as the charge separation is not occurring at the shoe-floor interface. From a risk point of view any discharge path to ground will reduce the time the operator is charged to this voltage. Thus, even a moderately conductive path to ground will reduce the risk.

Table 4 - Maximal voltage at each experiment.

Test	Conditions	Maximal Voltage (v)	Floor/shoes	Garment	Chair
WDP	27°C & 8%RH	2,570.0	HPLF/ Deck #1	-	-
Random	27°C & 8%RH	2,904.0	HPLF/ Deck #1	-	-
Sweater	27°C & 8%RH	8,688.0	HPLF/ Plastic	3	-
Chair	27°C & 8%RH	5,419.0	Rubber#2/ Deck #2	-	2
WDP	38°C & 8%RH	2,820.0	HPLF/ Deck #1	-	-
Random	38°C & 8%RH	4,220.0	HPLF/ Deck #1	-	-
Sweater	38°C & 8%RH	4,965.0	Vinyl #2/ Deck #1	1	-
Chair	38°C & 8%RH	4,502.0	Rubber#1/ Deck #2	-	3
WDP	27°C & 25%RH	2,0183.0	HPLF/ Deck #1	-	-
Random	27°C & 25%RH	3,214.0	HPLF/ Deck #1	-	-
Sweater	27°C & 25%RH	5,402.0	HPLF/ Deck #2	1	
Chair	27°C & 25%RH	3,388.0	Viny1/ Plastic	-	3
WDP	27°C & 45%RH	927.5	HPLF/ Deck #1	-	-
Random	27°C & 45%RH	2,547.0	HPLF/ Deck #1	-	-
Sweater	27°C & 45%RH	2,298.0	HPLF/ Plastic	1	-
Chair	27°C & 45%RH	2,570.0	HPLF/ Plastic	-	3

6. CONCLUSION

Allowing a larger range of humidity in data centers saves energy. However, lower humidity may increase the risk of damage by ESD. To obtain data for estimating the risk increase, a set of electrostatic charging experiments was conducted under a wide range of environmental conditions. The experiments included well-defined pattern walking, random walking, dropping a sweater after removing it, and sitting up from office chairs. The experimental motivation, setup, and initial data analysis were described. The results

showed the effectiveness of ESD flooring and footwear, indicating that a lower dew point will not necessarily lead to a higher charge voltage. The results also showed that charge does not only build up during walking; critical voltage levels can be reached simply by standing up from a non-ESD certified chair, or by removing and dropping a sweater. The second part of this article will provide a deeper analysis of the voltage change with respect to the relative and absolute humidity, as well as the effectiveness of ESD precaution measures, such as conductive floors. Part II of the paper analysis the data set in greater detail.

REFERENCES

[1] Mardiguian, Michel 2011. Electro Static Discharge: Understand, Simulate, and Fix ESD Problems. John Wiley & Sons.

[2] Simonic, R, 1982 . "ESD event rates for metallic covered floor standing information processing machines." In IEEE EMC Symp, pp. 191-198.

[3] Swenson, D. and J. Kinnear. 2009. The role of relative humidity and dew point on electrostatic charge generation and electrostatic discharge (ESD).The Green Grid - White paper.

[4] ASHRAE. 2011. Thermal guidelines for data processing environments. Atlanta: ASHRAE.

[5] Fayu, W., et al. 2013. The effect of humidity on static electricity induced reliability issues of ICT equipment in data centers —Motivation and setup of the study. ASHRAE Transaction 119(2): DE-13-031.

[6] Moradian, M., et al. 2014. Determination of the effect of humidity on the probability of ESD failure or upset in data centers. ASHRAE Transaction 120(2): SE-14 .

[7] J. Klein, L., H.F. Hamann, 2011. Humidity control and dew point management. Proceeding of the ASME 2011 Pacific Rim technical Conference & Exposition in packaging and Integrating of Electronic and Photonic Systems InterPACK2011, Portland, Oregon, USA, IPACK2011-52211.

[8] ANSI/ESD S20.20 -2007. 2007. Protection of Electrical and Electronic Part, Assemblies and Equipment (Excluding Electrically Initiated Explosive Device). Washington, DC: American National Standards Institute.

[9] Lim, S., 2000. Conductive floor and footwear system as primary protection against human body model ESD event. Electronics Packaging Manufacturing, IEEE Transactions 23(4): 255-258

[10] Swenson, D.E., J.P.Weidendorf , D.Pakin, E.Gillard. 1995. Resistance to ground and tribocharging of personnel, as influenced by relative humidity. In Electrical Overstress/Electrostatic Discharge Symposium Proceedings IEEE:141-153.

[11] Gaertner, R., K.H.Helling, G.Biermann, E.Brazada. 1997. Grounding personnel via the floor/footwear system. Electrical Overstress Electrostatic Discharge Symposium Proceedings: 170-175.

[12] Ryser, H. 1990. The relationship between ESD test voltage and personnel charge voltage. In proceeding of: EOS/ESD Symposium Orlando: Session2-paper1.

[13] Smith, D.C., 1999. Unusual forms of ESD and their effects. Electrical Overstress Electrostatic Discharge Symposium Proceedings: 329-333.

[14] Pommerenke, D. 1995.ESD: Transient field, arc simulation and rise time limit.J. Electrostatics, 36(1): 31–54.

[15] Vinson, J.E., J.C.Bernier, G.D.Croft, J.J.Liou. 2003. ESD Design and analysis handbook. 1st ed, Springer.

[16] Tonoya ,Y., K.Watanabe, M.Honda. 1993. Impulsive ESD noise occurred from an office chair. EOS/ESD Symposium Proceedings: EOS-15.

II. DEPENDENCE OF ESD CHARGE VOLTAGE ON HUMIDITY IN DATA CENTERS (PART 2 - DATA ANALYSIS)

ABSTRACT

This is Part 2 of a three-part paper investigating the dependence of charge voltage generated by human activity on humidity in data centers. The first paper described the experimental methods, while this paper is devoted to the analysis of the electrostatic charge voltage levels along the following parameters: relative humidity, absolute humidity, footwear, flooring, and type of activity. The human activities studied included well-defined walking, random walking, taking off and dropping a sweater, and standing up from a chair. This study confirms the importance of footwear and flooring and quantifies their effectiveness. The results indicate that lower absolute humidity may not always lead to higher voltages, while reducing the relative humidity will cause the average voltages to increase. The high voltages created by removing and dropping a sweater and by standing up from a chair indicate that these types of user activities might pose a higher risk of generating voltages greater than 6 kV much larger than the walking activities. The analyses are based on the definition of walking, standing, chair event, and sweater event voltages, as presented in Part 1.

1. INTRODUCTION

Typically, triboelectric charging caused by friction between non-conducting objects or between one conducting and one insulating object creates the charges that may cause an electrostatic discharge (ESD). Various researchers have studied the effect of the relative humidity (RH) on tribo-charge generation. Simonic investigated ESD discharges

in different carpeted rooms, confirming the known strong correlation between the RH and the peak discharge current [1]. For a range of 15% to 55% RH, a relationship has been derived between the probability of an ESD event occurring at a given current level and the RH; this relationship states that the probability of an ESD event occurring at a given magnitude increases by (RH)-3.39. Based on this equation, a reduction in the RH from 45% to 15% increases the probability of ESD event occurrence by a factor of 41[2]. Simonic's study dates back to the late 1980s and investigated carpeted floors, which are no longer used in data centers. Another report [3] presented a table of voltages measured during various activities, such as walking across vinyl and synthetic carpet floors, and sliding a styrene box on a carpet. The data from that table have been cited by other authors [4] and [5] as well. According to [4], the data, which were measured at 20% and 80% RH at 20℃, indicates that for walking across a vinyl floor, decreasing the RH from 80% to 20% increased the voltage by 48 times (from 250 V at 80% RH to 12 kV at 20% RH). Another study in [6] presented the voltage results for walking with different shoes and floor materials under different RH values. For most of the materials, the charge voltages increased at lower RH values. However, the rate of increase varied greatly, and some materials yielded no increase. [7] showed the effect of the RH on the charge generation at different temperatures by rolling a metallic ball through different plastic tubes and measuring the charge accumulated on the ball. The results indicated that for a given temperature, reducing the RH increased the amount of charge generated. [8] focused on removing charge from insulators and also presented data on the effect of humidity on the charge generation on insulated flooring. [9] studied the number of electrostatic shocks that people experienced while walking, rising from a seat, or wearing clothes in outdoor and

indoor environments. In dry weather (RH lower than 30%), people complained about the frequency of electrostatic shocks. In [10], the effect of sitting up from various car seats under different environmental conditions was discussed. However, each measurement was performed at a specific RH value, which did not allow for an analysis of the effect of the RH on any one seat/garment combination. Another study related to automobile seats [11] analyzed the voltages accumulated inside a car and when a person exited a car. The data indicated that the maximum voltage was reached at a dew point of approximately 0˚C. In [12], Sharmaet observed that the charge-to-mass ratio increased for polymer powder deposited on an aluminum panel as a result of reduced RH. Although the paper focused on the deposition of powder coating, it provided additional data pertaining to the effect of the RH on charge generation. However, [13] suggested that the dew point is more important for charge generation; his data indicated that the RH had no effect. The following two reasons generally are cited for the increase in voltage with reduced RH: 1) reduced conductivity leads to less charge neutralization by the current, and 2) the charge separation is more effective in dry air. This complex picture is caused by the multitude of possible material combinations, the type of surface to surface movement and the fact that some data pertaining to ESD caused by human activity is more anecdotal data rather than the result of well-documented studies. As all surface effects, triboelectricity depends on not only the material, but also the atomic surface properties and the environmental conditions. Therefore, it is not surprising to see so many conflicting conclusions from different experiments. For the study presented in this paper, 3596 experiments were conducted, having a total of 5645 minutes of recorded time-domain data. The materials were selected to be as similar as possible to materials used in data centers.

Table 1 shows the environmental conditions under which the measurements were taken. The following activities were considered: (a) well-defined walking pattern (WDP), (b) random walking, (c) taking off and dropping a sweater, and (d) standing up from a chair. Other parameters included the flooring and footwear used.

The results and discussions attempt to answer the following relevant questions of interest:

- By how much will the random walking voltage exceed the WDP walking voltage?
- By how many times does the voltage in each experiment surpass the threshold, e.g., 1kV?
- By what factor will the voltages increase, on average, if the RH value decreases?
- How can the effectiveness of ESD-controlling footwear and flooring be quantified?
- What is the effect of standing up from a chair or taking off a sweater on the charge voltage level at different dew points?
- How does the control effectiveness vary with the human activity?
- Which experiment yields the highest voltage?

2. DATA PROCESSING WELL-DEFINED PATTERN AND RANDOM WALKING EXPERIMENT

The WDP experiment, which as explained in [14], provides a walking voltage and

a standing voltage. The random walking pattern (as defined in Part1 of this three-part series of papers) provides a walking voltage but no standing voltage, as the operator walks continuously. As discussed in Part1, three voltages were compared for three different types of experiments. The WDP had been developed and standardized to allow for the best reproducibility, the random walking pattern better reflects actual walking behavior, and the standing voltage is the voltage on an operator after he or she stops walking for about 2 seconds. Figure 1 and Figure 2 present a comparison of the voltages for these three types of experiments for the following six categories of floors and shoes:

1. ESD shoes with ESD floors
2. ESD shoes with medium ESD floors
3. ESD shoes with non-ESD floor
4. Non-ESD shoes with ESD floors
5. Non-ESD shoes with medium ESD floors
6. Non-ESD shoes with non-ESD floor

Table 1 - List of selected environmental conditions.

Temperature (℃)	RH (%)	Dew Point (℃)
5	25	-13.13
27	8	-10
18	15	-8.89
38	8	-1.67
27	25	5
18	45	5.55
27	45	13.89

Table 2 and Table 3 present the available shoes and floors for each category. These categories cover a large set of conditions in data centers and are based on using ESD or non-ESD floors and shoes.

Table 2 - ESD shoes with different types of floor.

ESD Shoes, ESD Floors	ESD Shoes, Medium ESD Floors	ESD Shoes, Non-ESD Floor
Mid-range dissipative ESD shoes, rubber #1	Mid-range dissipative ESD shoes, vinyl #1	Mid-range dissipative ESD shoes, HPL
Mid-range dissipative ESD shoes, rubber #2	Mid-range dissipative ESD shoes, vinyl 2	Low-range dissipative ESD shoes, HPL
Low-range dissipative ESD shoes, rubber #1	Low-range dissipative ESD shoes, vinyl #1	-
Low-range dissipative ESD shoes, rubber #2	Low-range dissipative ESD shoes, vinyl 2	-

Figure 1 shows the voltages as a function of the dew point for the case in which the operator is wearing ESD-mitigating shoes. The data in Figure 1 (a) were collected by selecting voltages from the test results for the category "ESD shoes and ESD floors," and then taking the average of the voltages. Moreover, (b) and (c) show the average voltage for the categories "ESD shoes and medium ESD floors" and "ESD shoes and non-ESD floors," respectively. The data show that random walking produced the highest voltage in most cases, and standing produced the lowest voltage. For the best combination of materials (ESD shoes and ESD floors), as shown in Figure 1(a), the voltages remained below 100V.

If the judgment of the ESD risk were based solely on the walking voltages obtained during the 100 s experiment, one may conclude that using ESD shoes is sufficient to avoid voltages > 500V, a voltage threshold in [15]. However, the voltages shown are the average walking voltages generated while stepping for 100 sec. Especially on the non-ESD floor, this average gives no assurance that the voltage threshold was not surpassed during the 100 seconds of the experiment, nor does it exclude this voltage from being surpassed under slightly different conditions or a longer period of walking time. The third paper in this series discusses using the probability density function of the measured voltage values to estimate the probability of a voltage exceeding a limit.

Table 3 - List of non-ESD shoes with different types of floors.

Non-ESD Shoes, ESD Floors	Non-ESD Shoes, Medium-ESD Floors	Non-ESD Shoes, Non-ESD Floor
Deck #2, Rubber #1	Deck #1, Vinyl #1	Deck #1, HPL
Deck #2, Rubber #2	Deck #1, Vinyl #2	Deck #2, HPL
Deck #1, Rubber #1	Deck #2, Vinyl #1	Plastic shoes, HPL
Deck #1, Rubber #2	Deck #2, Vinyl #2	Leather dress shoes, HPL
Plastic shoes, Rubber #1	Plastic shoes, Vinyl #1	Running shoes, HPL
Plastic shoes, Rubber #2	Plastic shoes, Vinyl #2	Deck #3, HPL
Leather dress, Rubber #1	Leather dress, Vinyl #1	-
Leather dress, Rubber #2	Leather dress, Vinyl #2	-
Running shoes, Rubber #1	Running shoes, Vinyl #1	-
Running shoes, Rubber #2	Running shoes, Vinyl #2	-
Deck #3, Rubber #1	Deck #3, Vinyl #1	-
Deck #3, Rubber #2	Deck #3, Vinyl #2	-

Figure 2 presents the voltage for the cases in which non-ESD-mitigating shoes were worn during testing. The data are presented for ESD-mitigating floors, medium floors and non-ESD-mitigating floors. Figure 2 (a), (b) and (c) present the average voltages for "non-ESD shoes and ESD floors," "non-ESD shoes and medium ESD floors" and "non-ESD shoes and non-ESD floors," respectively. Similar to the data in Figure 1, the random walking voltage values were approximately30% higher than the well-defined walking voltages. The standing voltage was much lower, having a more complex variation than the ratio between the random and well-defined walking voltages. Not surprisingly, using no ESD mitigation methods yielded the highest voltages, as shown in Figure 2.

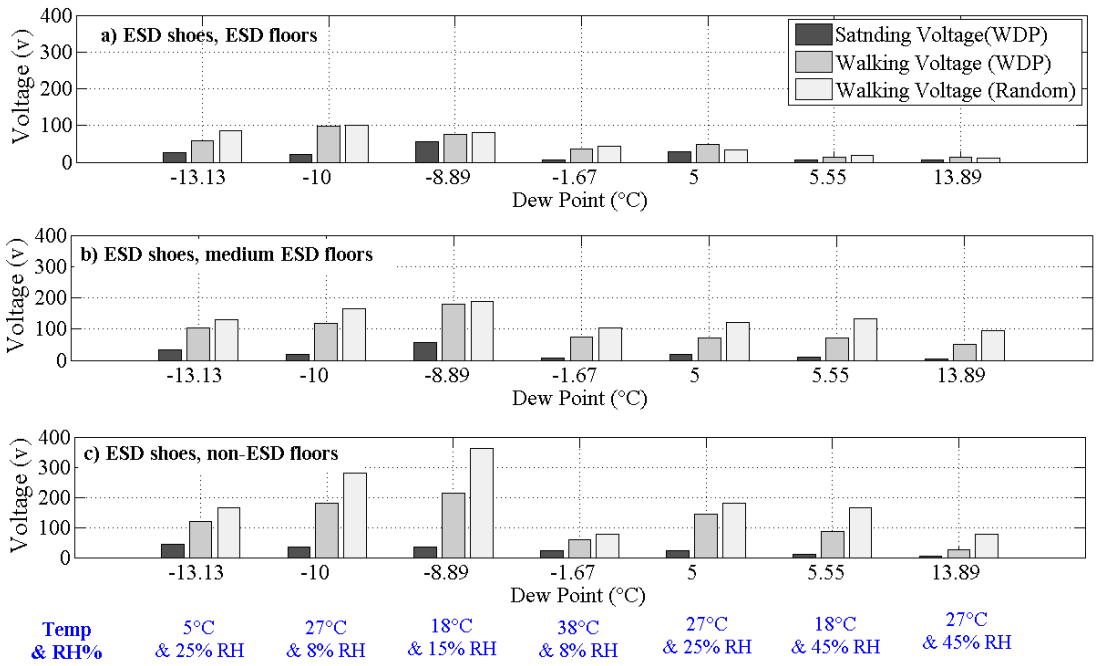

Figure 1 - Comparison between WDP walking voltage, standing voltage, and random walking voltage for ESD shoes. (a) ESD floors, (b) medium ESD floors, and (c) non-ESD floor.

The highest voltages were measured at 38°C with a dew point of -1.67 °C, as shown in Figure 2 (c). This result indicates that low RH will promote charge build-up and cause it to remain; however, highly polar water molecules are needed to create tribo-charging between certain materials. The distribution of charge voltages versus the dew point is represented by the dotted, curved line in Figure 2 (c). Similar behavior was observed in [11]. As noted previously, WDP walking was considered for its reproducibility. However, operators do not follow a WDP, which motivated the authors to introduce the random walking pattern. However, operators are not likely to touch instruments while walking; they are more likely to stop first and stand still for a moment before touching any instruments. This likelihood is reflected in the standing voltage. Consequently, while an analysis using WDP offers better reproducibility and allows for a better comparison between experiments performed under different environmental conditions, it may overestimate the voltages compared to the standing voltage and underestimate the voltages relative to random walking. This effect can be analyzed by comparing the average voltages of random walking, WDP walking, and standing.

Figure 3 illustrates the observed ratio between the random walking voltage and WDP walking voltage for the six categories of shoes and floors based on approximately 280 experiments each for WDP walking and random walking (8 shoes, 5 floors and 7 environmental conditions). The random walking voltage was greater than the WDP walking voltage at almost all dew points (ratio greater than 1). The ratio varied between 1 and 2. This was the result of the higher walking speeds during random walking, further enhanced by shoe dragging and scraping during walking. As shown previously in Figure 2 (c), the voltage decreased at lower dew points (dotted, curved line). The next step was to

analyze the effect of the RH, as shown in. Two categories were selected: ESD shoes with ESD floors (Figure 4 (a)), and non-ESD shoes with non-ESD floors (Figure 4 (b)).In the figures, a dashed line connects the data obtained at 27 °C. Comparing (a) and (b) shows that the voltage level for the non-ESD material set was higher than for the ESD material set.

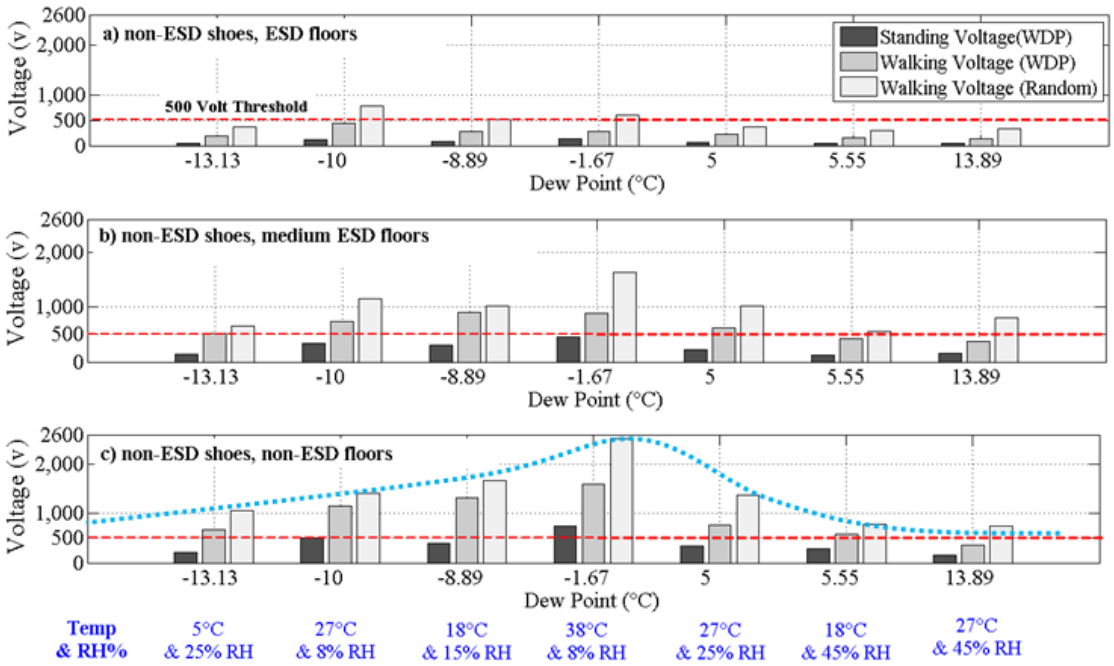

Figure 2 - Comparison between WDP walking voltage, standing voltage and random walking voltage for non-ESD shoes. (a) ESD floors, (b) medium ESD floors, (c) non-ESD material.

The voltages increased as the humidity decreased. To quantify this increase, a relative humidity voltage (RHV) factor was defined by normalizing the voltages at a lower humidity to the voltages at reference humidity. The factor indicates how much the voltage

would increase on average if a data center changed the humidity without changing the operator activities, flooring or footwear.

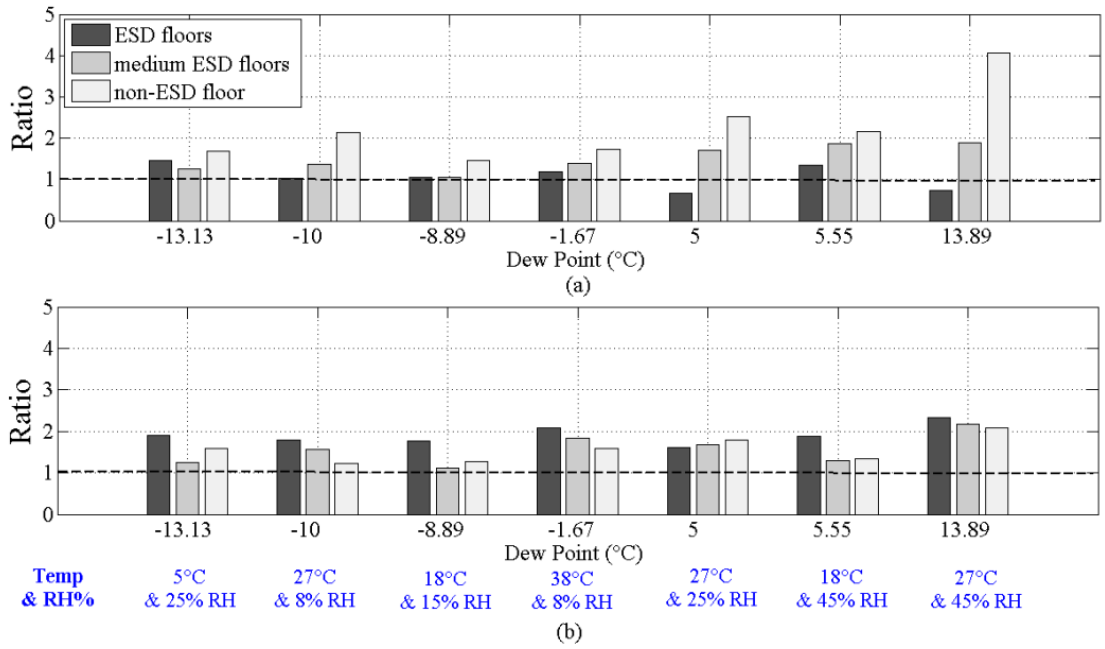

Figure 3 - Ratio between the average random walking voltage and WDP voltage for three different floors. (a) ESD shoes, (b) non-ESD shoes.

2.1. VOLTAGE DISTRIBUTION

In data centers, not only are the average voltages of interest, but so are the occurrences of high-voltage events, which might be under estimated when analyzing only the average voltage. The distribution of the observed voltages appears in Figure 5. The histogram was obtained using the following steps.

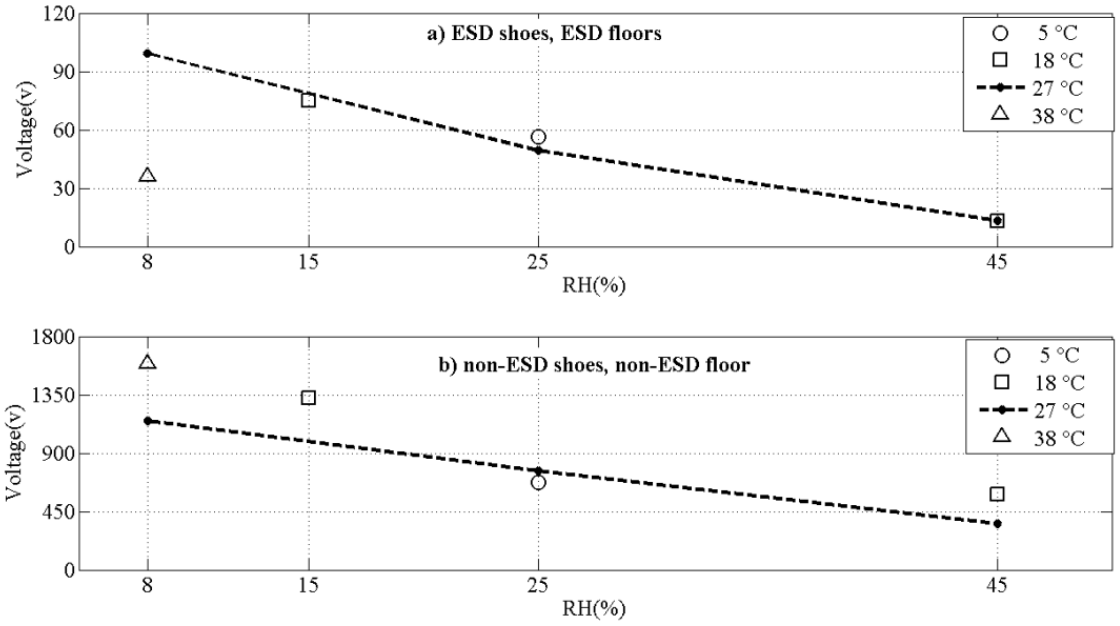

Figure 4 - WDP walking voltage versus RH reduction. (a) ESD shoes, ESD floors, (b) non-ESD shoes, non-ESD floor.

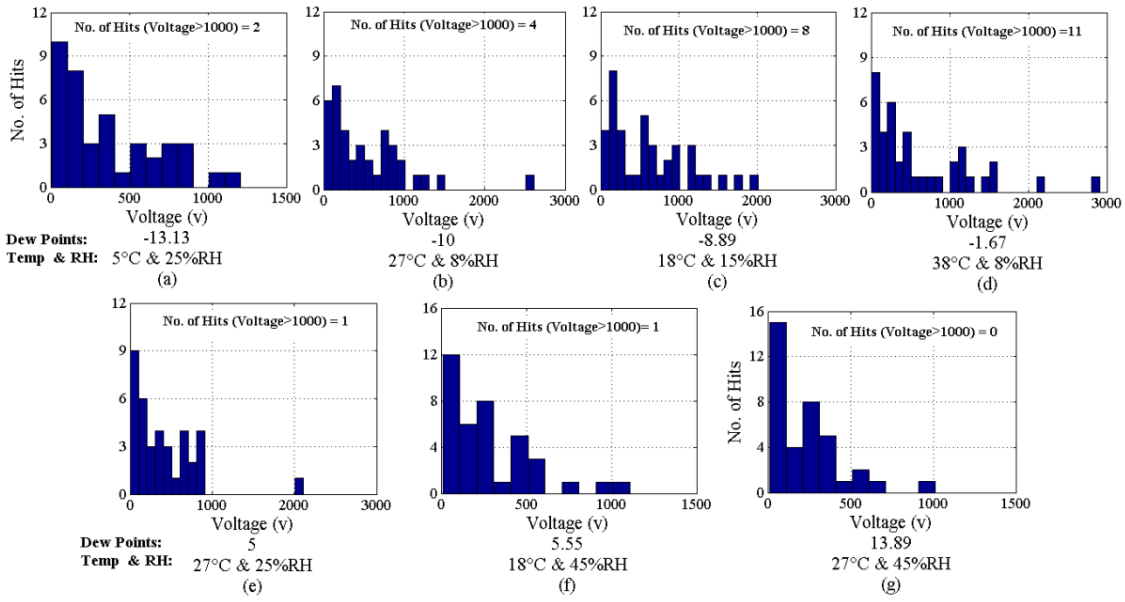

Figure 5 - Distribution of walking voltage versus the dew points for WDP walking experiment.

For each recorded voltage versus time waveform, the walking voltage was obtained (Part 1). This yielded 280 walking voltage values for 7 environmental conditions, 8 shoe types and 5 floor types. Each subfigure shows the distribution under one environmental condition. Furthermore, the number of occurrences of V > 1kV is indicated. For example, at a dew point of -1.67℃ (Figure 5 (d)), the WDP walking voltage exceeded 1kVeleven times. However, for the lowest and highest dew points (Figure 5 (a) and (g)), there were two and zero instances, respectively, where the voltage was higher than 1kV. Only considering 27℃, the voltage was greater than 1kV four times at 8% RH (Figure 5 (b)), while at 25% RH (Figure 5 (e)), only one WDP exceeded 1kV. No such instances occurred at 45%RH (Figure 5 (g)). Random walking yielded higher voltages; the distributions appear in Figure 6.At 27℃, a walking voltage > 1kV was observed in 16 experiments at 8% RH (Figure 6 (b)), and in 8 experiments at 25% RH (Figure 6 (b)).

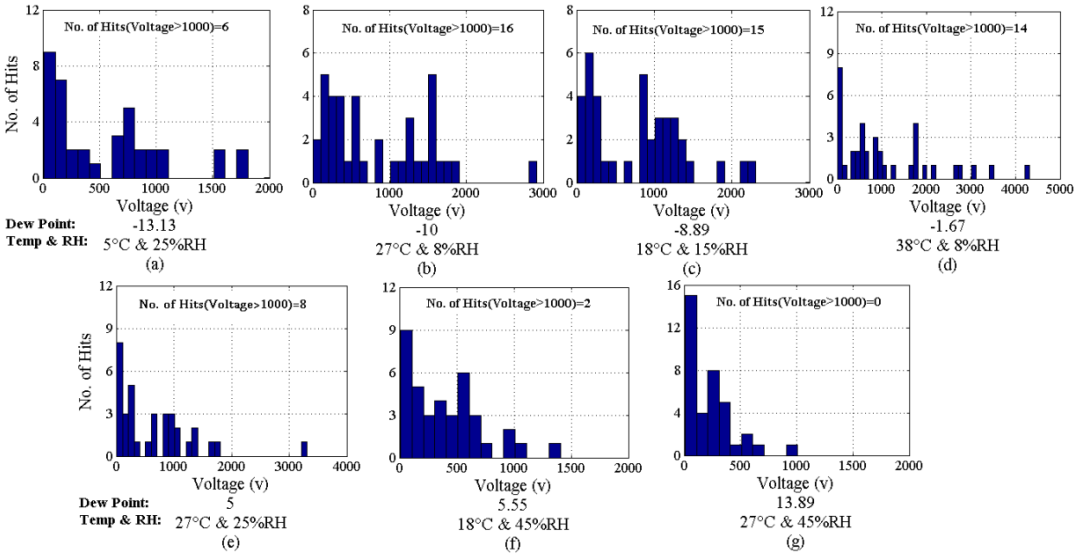

Figure 6 - Distribution of walking voltage versus dew points for the random walking experiment.

The voltages did not exceed 1kV at 45% RH (Figure 6 (g)). Figure 7 shows the number of experiments that recorded a walking voltage > 1kV for WDP and random walking at different dew points. The approximate overall behavior is indicated by a dashed line. The average voltages (Figure 2(c)) and the distributions (Figure 7(a)) follow the same trend.

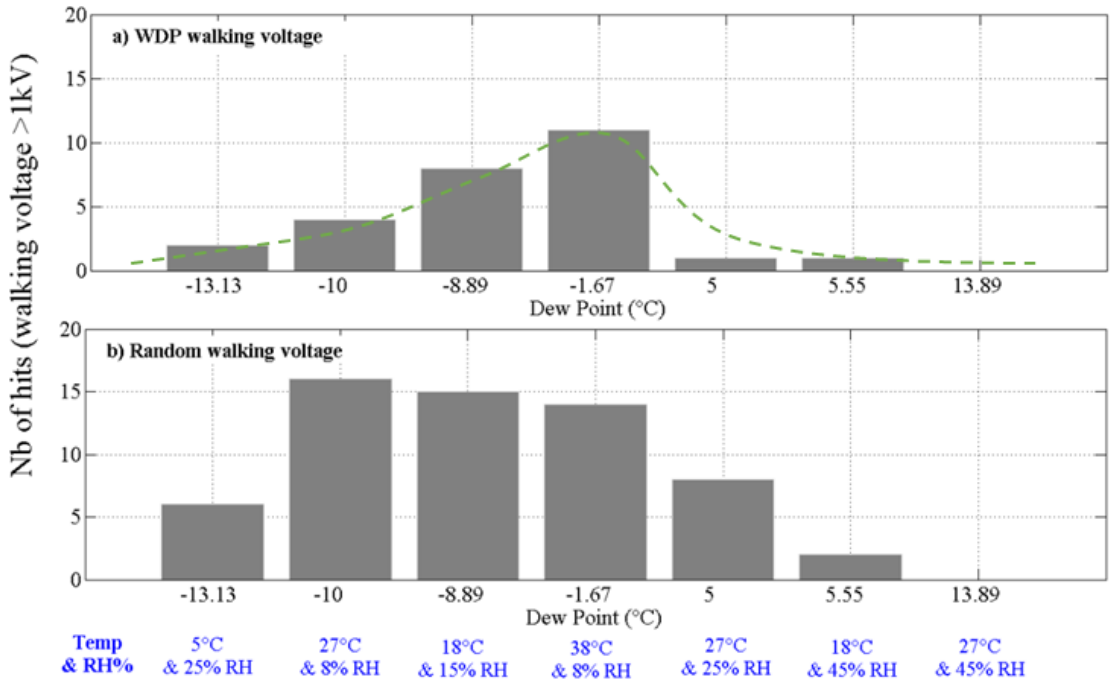

Figure 7 - Number of experiments that recorded a walking voltage > 1 kV. (a) WDP walking voltage, (b) random walking voltage.

2.2. RHV DEFINITION

The RHV factor is defined as the ratio of the walking voltage at a higher RH to the walking voltage at a lower RH. It expresses that the voltage increases as the humidity decreases. To calculate this factor, three dew points at 27℃ having a RH of 8%, 25% and

45% RH were selected. As discussed in the introduction, the data in the literature came from studying a wide range of materials, and the experimental setups often were not documented well. The data from the literature were processed and compared to data from the two sets of experiments performed in the present study. First, the voltage data were normalized to voltages at a high RH. Next, a function was fitted to the data points and extrapolated to 8% RH. Due to the varying experimental conditions and the uncertainty introduced by the extrapolation, the resulting data were only able to provide a qualitative impression. In the data from the literature, an average 3.5-fold voltage increase occurred when the humidity decreased from 45% RH to 8% RH, as shown in Figure 8. Different setups and material pairings may explain this wide spread. Table 4 summarizes the resulting factors. For the combination that yielded the highest voltages (non-ESD shoes and non- ESD floor), this previous study predicted a factor of 2.3, and a much larger factor

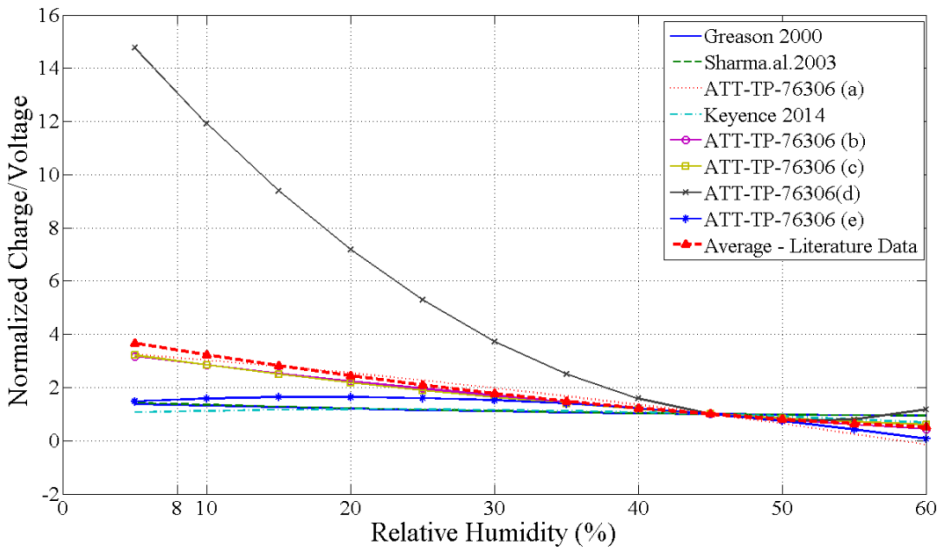

Figure 8 - Prediction of the normalized voltage increase with reduced humidity based on the studies in [15] and [16] for WDP walking.

Table 4 - Prediction of RHV factor based on Figure 9.

Category	Predicted RHV factor (45% to 8%RH)
ESD shoes, ESD floors	16
ESD shoes, Medium-ESD floors	3.8
ESD shoes, Non-ESD floor	2.9
Non-ESD shoes, ESD floors	19
Non-ESD shoes, Medium-ESD floors	2.85
Non-ESD shoes, Non-ESD floor	2.3
All shoes, All floors	3.2

16 for the ESD shoes and ESD floors category, which posed no risk due to the low voltage levels. The measurements from the current study verified those previous predictions. The relative voltage increase was analyzed at three RH conditions, i.e., 45% RH, 25% RH and 8% RH, at 27℃ (Table 5). The extrapolation results also appear in the table of WDP walking voltages (Table 5). Figure 9 illustrates the normalized voltages for random and WDP walking. The same methodology was used to process these data. For each category, the average walking voltage was calculated, and then the value was normalized at 45% RH. Figure 9 (a) indicates a voltage increase of 2.87 for the group of all shoes and all floors when the RH decreased from 45% to 8% during WDP walking. Random walking yielded an increase of 1.93 under the same conditions, as shown in Figure 9 (b).

The following conclusions can be drawn from the data obtained from the walking experiments:

- Reducing the RH from 45% to 8% and having no ESD mitigation will increase the voltage levels by a factor of 2-3, while reducing the RH from 25% to 8%

will increase the voltage by a factor of 1-2.

- The RHV is much larger in settings with good ESD mitigation. The larger increase poses no risk because the voltage remains low.

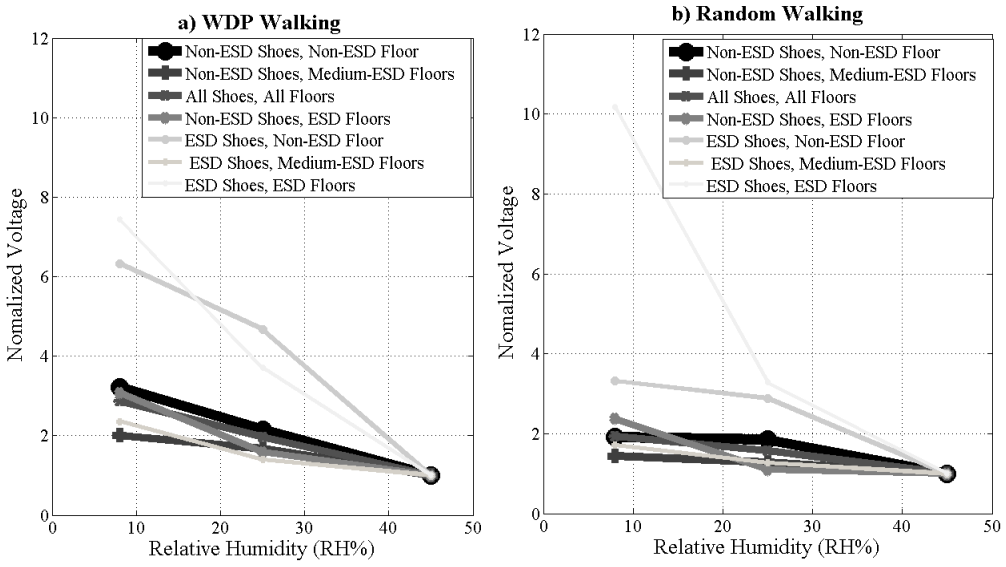

Figure 9 - Increasing the average voltage normalized to voltages observed at 45% RH for different categories. (a) WDP walking, (b) random walking.

3. ANALYSIS OF TWO OPERATOR ACTIONS: (1) SITTING UP FROM A CHAIR AND (2) DROPPING A SWEATER

Part1 of this series defined the event voltage. The following two unrelated operator actions were considered: 1) sitting up from a non-ESD-mitigating chair and 2) taking off and dropping a sweater. Three chairs and three sweaters were used in the experiment, and the average event voltages were considered. Figure 10 compares the average voltages generated during five different actions: random walking, WDP walking, standing, taking off and dropping a sweater and sitting up from a chair. Sitting up from a chair caused the

highest recorded event voltages. ESD shoes worn on ESD-mitigating flooring produced only 900V, as shown in Figure 10 (a)), at a dew point of10 °C (27 °C & 8% RH).The figure indicates the tendency of ESD-mitigating flooring and shoes to have less of an effect on the chair and sweater event voltages than on the walking voltages. The last section of this article investigates the effectiveness of ESD-mitigating conditions in detail. Figure 11 presents the results of five experiments conducted at the same dew points for three categories, including non-ESD shoes with different types of floors (ESD, medium ESD and non-ESD). The event voltages when wearing non-ESD shoes (Figure 11) were approximately 3-5 times greater than when wearing ESD mitigating shoes (Figure 10). Moreover, the capacitance of the participant changed during the sitting and standing experiment, so the voltage changed significantly just due to the capacitance changes (V=Q/C). Table 6 presents the measured capacitance between three used chair and participant. The measurement was done by a LCR meter at 100 kHz.

3.1. EVENT VOLTAGE DISTRIBUTION DIAGRAM

Figure 11 shows the distribution of the average event voltages for 3 chairs and 3 sweaters among 40 combinations of floors and shoes at 27°C and 8%, 25% and 45% RH. The total number of voltages > 1kV is indicated for each condition. The histogram in Figure 11 (a) indicates that the sweater event produced 29 such voltages at 27 °C and 8% RH (-10°C dew point). The chair event produced 32 such voltages (Figure 11 (b)). These results are comparable with the walking voltage results (i.e., 4 for WDP walking and 16 for random walking), which were shown in Figure 5 (b) and Figure 6 (b).

Table 5 - RHV value for different RH and categories. (Based on [16] and [17])

Test	shoes/floors	45% to 8% (Predicted from Table 4)	45% to 25%	25% to 8%
WDP	ESD shoes/ESD floors	7.43 / 16	3.70	2.01
WDP	ESD shoes/ medium-ESD floors	2.36 / 3.8	1.40	1.68
WDP	ESD shoes/ non-ESD floors	6.33 /2.9	4.68	1.35
WDP	Non-ESD shoes/ ESD floors	3.08 / 16	1.58	1.95
WDP	Non-ESD shoes/ medium-ESD floors	2.00 / 2.85	1.67	1.2
WDP	Non-ESD shoes/ non-ESD floors	3.23 / 2.3	2.14	1.5
WDP	All shoes/ all floors	2.87 / 3.2	1.96	1.46
Random	ESD shoes/ ESD floors	10.2	3.27	3.11
Random	ESD shoes/ medium-ESD floors	1.72	1.27	1.35
Random	ESD shoes/ non-ESD floors	3.32	2.89	1.15
Random	Non-ESD shoes, ESD floors	2.37	1.09	2.17
Random	Non-ESD shoes/ medium-ESD Floors	1.44	1.28	1.13
Random	Non-ESD shoes/ non-ESD Floors	1.91	1.85	1.03
Random	All shoes, all floors	1.93	1.57	1.23

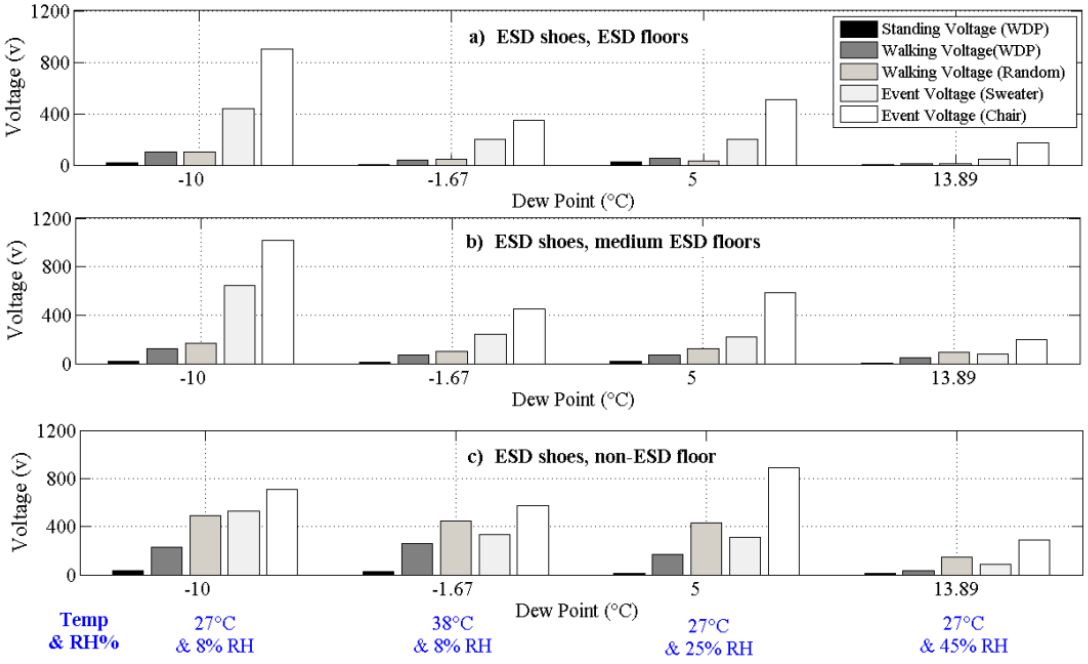

Figure 10 - Average voltages as a function of dew point for ESD shoes. (a) ESD floors, (b) medium ESD floors, (c) non-ESD floors.

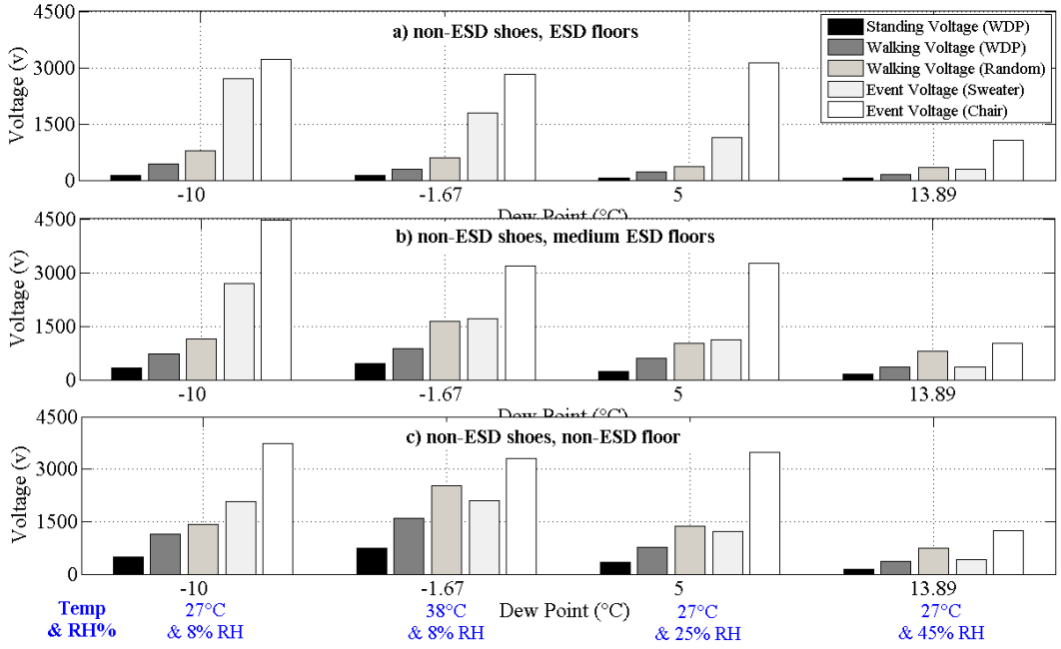

Figure 11 - Comparison of all four experiments based on walking, standing, and event voltages for non-ESD shoes. (a) ESD flooring, (b) medium ESD flooring (c) non-ESD flooring.

Table 6 - Capacitance between chair and participant.

Chair	Standing Mode	Sitting Mode
Chair #1	16.5 pF	78 pF
Chair #2	20 pF	137 pF
Chair #3	16 pF	43.4 pF

These numbers indicate that the event voltage distribution occurred at a higher voltage level than the walking voltage. Furthermore, the sweater event voltage varied between 1-4kV at 27 °C and 8% RH, while the chair event voltage distribution ranged from

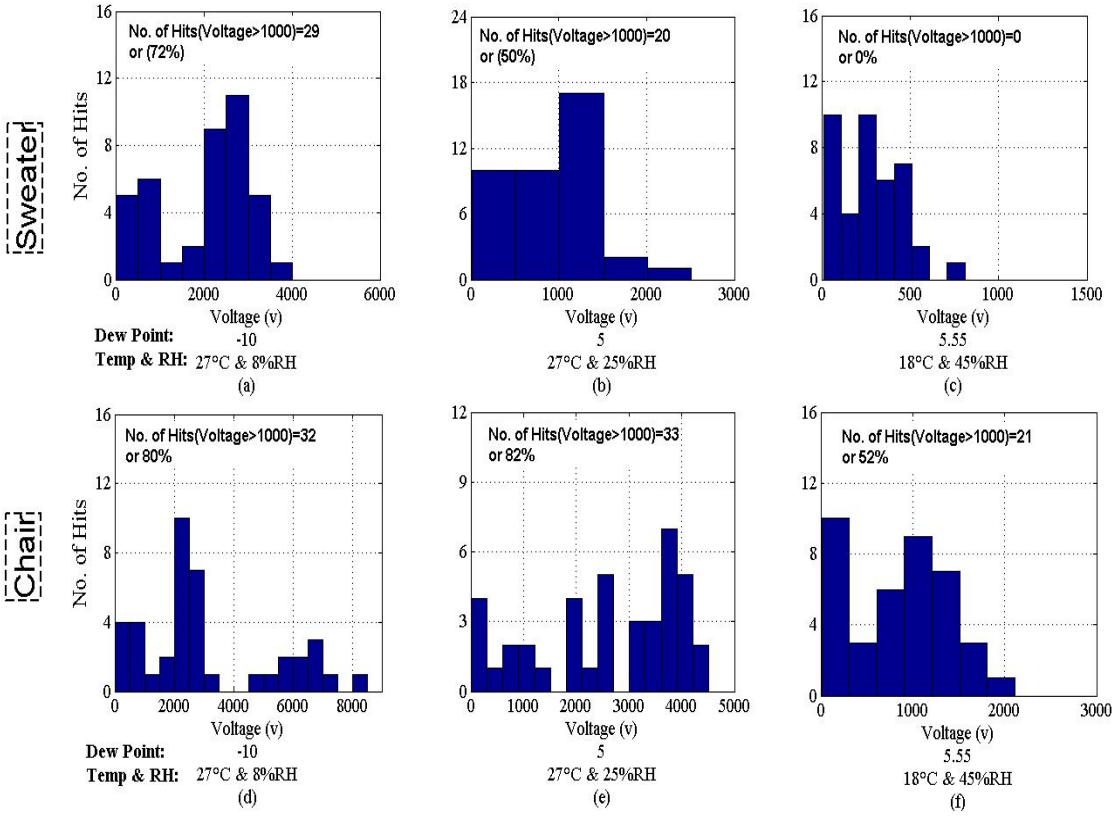

Figure 12 - Distribution of event voltages for different dew points. The three top subfigures are related to sweater event voltages and three bottom subfigures are related to chair event voltages.

1-8.5 kV. This voltage distribution shows that standing up from a chair yielded higher event voltage than taking off and dropping a sweater. Moreover, the lower RH value (8% RH) had more experiments with an event voltage > 1 kV than the higher RH value (8% RH).

3.2. RHV FACTORS FOR CHAIR AND SWEATER EVENTS

Figure 13 shows the average event voltages of three chair events and three sweater events for each of six shoe and floor categories. The RHV factor for the event voltages can be derived in a way similar to that for the walking voltage. Table 7 summarizes each category. For example, the RHV factors for the chair event voltage (considering all shoes and all floors) were 4 (45% RH reduced to 8% RH) and 1.18 (25% RH reduced to 8% RH). The RHV factors for the sweater event voltage were 7 and 2.07 before and after the RH

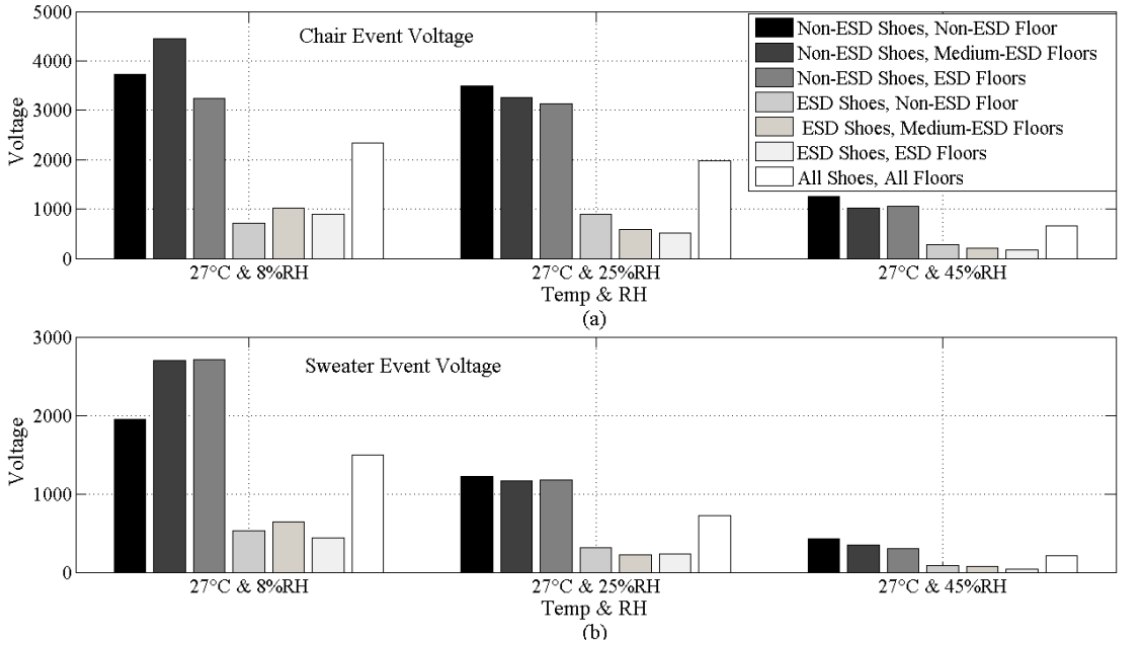

Figure 13 - Average of event voltages for seven categories of shoes and floors. (a) chair event, (b) sweater event.

reduction, respectively. Furthermore, the average RHV values for all user actions (i.e., event voltages, random walking and WDP walking) were 3.8 (45% RH reduced to 8% RH) and 1.5 (25% RH reduced to 8% RH).

4. ESD EFFECTIVENESS

To quantify the effect of ESD-mitigating floors and shoes, ESD effectiveness must be defined. ESD effectiveness is the ratio between the voltage measured using non-ESD-mitigating floors and shoes, and the voltage measured using ESD-mitigating floors and shoes. Figure 14 presents the ESD effectiveness for the dew points measured, and Table 8 presents the values.

The maximum ESD effectiveness was 116, calculated for the standing voltage at the critical conditions of 38°C and 8% RH. It remains unclear whether the walking, random or standing voltage yielded higher ESD effectiveness, no systematic trend was observed. However, the ESD effectiveness clearly was much lower for the sweater and chair event voltages, dropping below 10 in some cases.

This finding, together with the high event voltages measured for the chair and sweater events, emphasizes the need to avoid standard office chairs and to educate personnel about this risk. However, one must remember that the event voltage only represents the increase at the moment of the event. If the floor and shoes are conductive, the voltage will decay within a few seconds.

This quick discharge is not reflected in the definition of ESD effectiveness, which only takes the momentary voltages into account.

Table 7 - RHV value for different RH and categories.

Experiment	Category of Shoes/Floors	RHV 8%RH per 45%RH	RHV25%RH per 45%RH	RHV8%RH per 25%RH
Chair	ESD shoes, ESD floors	5.21	2.95	1.77
Chair	ESD shoes, medium-ESD floors	5.11	2.95	1.73
Chair	ESD shoes, non-ESD floors	2.49	3.12	0.796
Chair	Non-ESD shoes, ESD floors	3.05	2.94	1.04
Chair	Non-ESD shoes, medium-ESD floors	4.34	3.17	1.37
Chair	Non-ESD shoes, non-ESD floors	2.98	2.79	1.07
Chair	All shoes, all floors	3.52	2.97	1.18
Sweater	ESD shoes, ESD floors	9.86	5.29	1.87
Sweater	ESD shoes, medium-ESD floors	8.17	2.82	2.9
Sweater	ESD shoes, non-ESD floors	6.34	3.71	1.71
Sweater	Non-ESD shoes, ESD floors	9.06	3.94	2.3
Sweater	Non-ESD shoes, medium-ESD floors	7.74	3.36	2.3
Sweater	Non-ESD shoes, non-ESD floors	4.61	2.88	1.6
Sweater	All shoes, all floors	7.02	3.39	2.07

Table 8 - ESD effectiveness. (Ratio between ESD material and non-ESD material)

Voltages	27 °C 8%RH	38 °C 8%RH	27°C 25%RH	27°C 45%RH
WDP standing	24.31	116.38	12.55	25.92
WDP walking	11.59	44.21	15.49	26.71
Random walking	13.94	58.6	41.98	74.37
Sweater event	4.42	10.36	5.16	9.46
Chair event	4.15	9.97	6.85	7.24

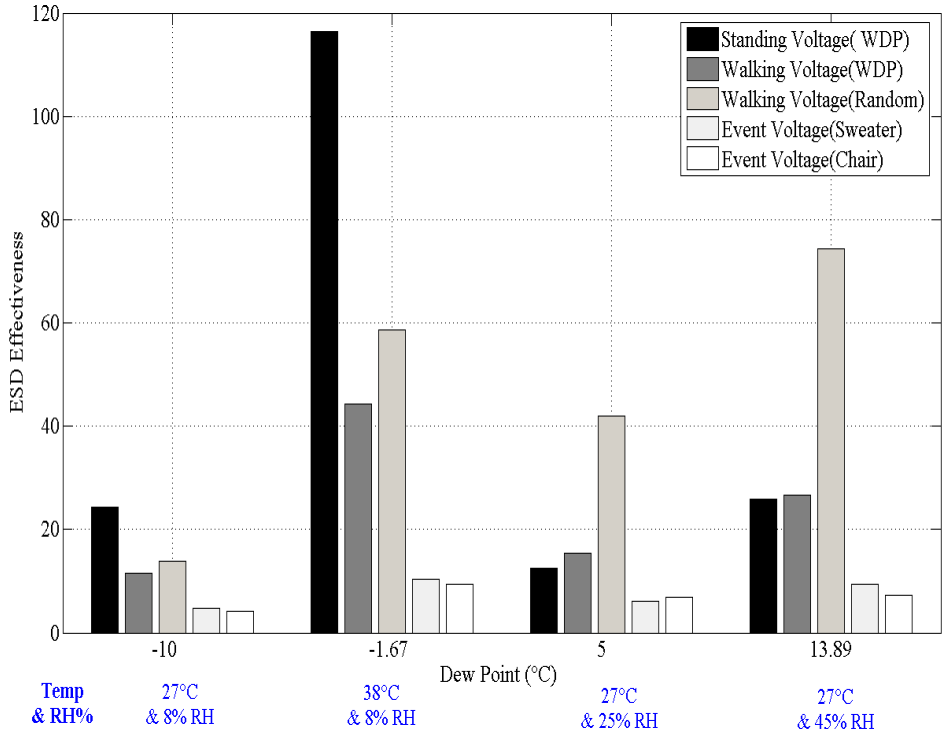

Figure 14 - ESD effectiveness as a function of environmental conditions.

5. CONCLUSION

This paper analyzed the charge voltages measured for walking and other experiments for dew points from -13.13 to 13.89 °C using RH values between 8% and

45%. Different ESD-mitigating and non-ESD mitigating flooring systems and shoes were used. The following five types of user activities were considered: WDP walking, random walking, standing, sitting up from a chair and removing and dropping a sweater. The data suggest that:

- Reducing the RH increases the average voltages.
- Decreasing the RH from 45% to 8% at 27°C leads to an average voltage increase between 3 and 4.
- Reducing the RH from 25% to 8% at 27°C leads to an average voltage increase between 2 and 3.
- As the dew point decreases, the voltages initially increase; however, if the dew point falls below -10°C, the voltages decrease.
- The effectiveness of ESD mitigating methods is very high for walking. However, for sitting up from a chair or dropping a sweater, ESD footwear and ESD flooring is less effective at reducing the charge voltages. However, they still provide a fast discharge path.
- The high voltages created by removing and dropping a sweater or standing up from a chair indicate that these types of user activities might pose a higher risk of inducing voltages greater than 2 kV in comparison with walking.
- Standing up from a chair produced the highest event voltage. Therefore, using an ESD-mitigating chair could be a reasonable requirement in data centers.

REFERENCES

[1] Simonic, R. 1981.Personal ESD statistics. IEEE/EMC Symposium. Boulder, CO.

[2] Mardiguian, M. 2009.Electrostatic discharge: Understand, simulate and fix ESD problems. 3rd Edition.Wiley-IEEE Press.

[3] McFarland, W.Y. 1981. The economic benefits of an effective ESD awareness and control program-an empirical analysis. Electrical Overstress/Electrostatic Discharge Symposium Proceedings,EOS 3:28.

[4] Kolyer, J. M., D. Watson. 1996. ESD from A to Z. Springer.

[5] Allen, R. C. 1998. Humidity and ESD control. ESD Systems. Desco Industries, Inc.

[6] http://esdsystems.descoindustries.com/whitepapers/wp_humidity.html

[7] Ryser, H. 1990. The relationship between ESD test voltage and personnel charge voltage. In Proceedings of EOS/ESD Symposium Orlando: Session2 – paper1.

[8] Greason, W. D. 1999. Investigation of a test methodology for triboelectrification. Electrical Overstress/ Electrostatic Discharge Symposium Proceedings, Orlando, FL, USA, 344-5.

[9] Keyence. 2014. Static electricity and static eliminator resource site. Static electricity solution for insulators.

http://www.keyence.com/ss/products/static/resource/solution/insulator.jsp.

[10] Clements-Croome, D. 2004. Electromagnetic environments and health in buildings. Taylor & Francis.

[11] Andersson, B., L. Fast, P. Holdstock, D. Pirici. 2008. Charging of a person exiting a car seat. In Journal of Physics: Conference Series. IOP Publishing, (142)1.

[12] Katrak, K. 1995.Human body electrostatic charge (ESC) levels: Are they limited by corona bleed off or environmental conditions? Electrical Overstress/Electrostatic Discharge Symposium Proceedings,Milford, MI, USA, 73-12.

[13] Sharma, R., S.Trigwell, A.S.Biris, R.A.Sims, M.K.Mazumder. 2003. Effect of ambient relative humidity and surface modification on the charge decay properties of polymer powders in powder coating. IEEE Transactions on Industry Applications (39).

[14] Montoya, A. 2002. Effect of dew point and relative humidity in electrostatic charge control. http://www.sematech.org/meetings/archives/esd/20021014/montoya.pdf

[15] ANSI/ESD STM97.2-2006. 2006. For the protection of electrostatic discharge susceptible items- Floor material and footwear-voltage measurement in combination with a person. Rome: American National Standards Institute.

[16] Moradian, M., F.Wan, A.Patnaik, D.Pommerenke, Y.Han, D.E.Swenson. 2014. Determination of the effect of humidity on the probability of ESD failure or upset in data centers. ASHRAE Transaction 120(2): SE-14.

[17] Fayu, W., D.E.Swenson, M.Hillstrom, D.Pommerenke, and C.Stayler. 2013. The effect of humidity on static electricity induced reliability issues of ICT equipment in data centers —Motivation and setup of the study. ASHRAE Transaction 119(2): DE-13-031.

III. EFFECT OF HUMAN ACTIVITIES AND ENVIRONMENTAL CONDITIONS ON ELECTROSTATIC CHARGING

ABSTRACT

The generation of electrostatic charge is considered for the cases of standing up from a chair and for taking off a sweater at dew points of -13.1°C (5°C-RH 25%), -10°C (27°C-RH 8%), -8.9°C (18°C-RH 15%), -1.7°C (38°C-RH 8%), 5°C (27°C-RH 25%), 5.6°C (18°C-RH 45%), and 13.9°C (27°C-RH 45%). Using ESD-mitigating shoes/floors rather than non-ESD can reduce the voltages by a factor of ~2-5 for garment removal and ~2-7 for sitting up from a chair. For the garment removal, the charge voltage will drop to 100 V within ~0.5-6 seconds and within ~1-30 min when ESD and non-ESD mitigating shoes/floors are used, respectively. For the standing up form a chair the corresponding times are ~0.5-3 sec and ~1-4 min, respectively. For the extreme case at 22°C-RH 5%, the voltage can surpass +/- 20 kV. Finally, it is shown that the voltages a person will charge up to may vary by +/- 30% just due to different capacitances to ground. Here residential home settings will lead to the highest voltages (60 pF test person to ground, US wood frame house), while standing on a concrete floor only half of the voltage may be reached (120 pF).

Index Terms—electrostatic charge; electrostatic discharge (ESD); environmental condition; ESD mitigating.

1. INTRODUCTION

Daily activities such as walking, standing up from a chair, and removing a garment can easily lead to electrostatic charge voltage of 10 kV or more in dry winter days. This can cause electrostatic discharge (ESD)-related upset or damage in electric equipment [1]-[2] . For data centers, the American Society of Heating, Refrigerating, and Air-Conditioning Engineers (ASHRAE) has introduced a recommended environmental envelope in 2008 [3] and four extended envelopes (A1 to A4 illustrated in Figure 1) in 2011 [4]. These new envelopes allow to reduce the power consumption of the air conditioning systems. At low humidity levels the risk of ESD increases [3]-[8], thus the high availability requirements of the data center services raised the need to understand the ESD risk increase at low humidity. This has been investigated in a series of studies focusing on the charge generated when people walk on typical data center floors [9]-[17]. The previous studies showed that walking on floors causes charges which are acceptable for most data center operations if ESD mitigation methods such as ESD shoes and floors are in place. However, only focusing on charges generated by walking will overlook operations which cause much higher voltages.

Standing up from a chair or taking off a garment are two examples of daily activities which can lead to a higher charge voltage than walking (2 to 3 times higher). In preliminarily study in [18], these two activities systematically were presented at four environmental conditions, data points 2, 4, 5 and 7 in Figure 1 and Table I.

In this extended study, the well-controlled experiments are expanded to seven dew point temperatures. Also, extreme case to overestimate worse condition was explored. The goal of this paper is to understand the ESD risk due to various human activities in data

centers at the extended environmental envelope in comparison with recommended envelope. The obtained results from standing up from a chair and garment removal along with results of walking can provide a good estimation of the ESD risk due to various human activities in data centers.

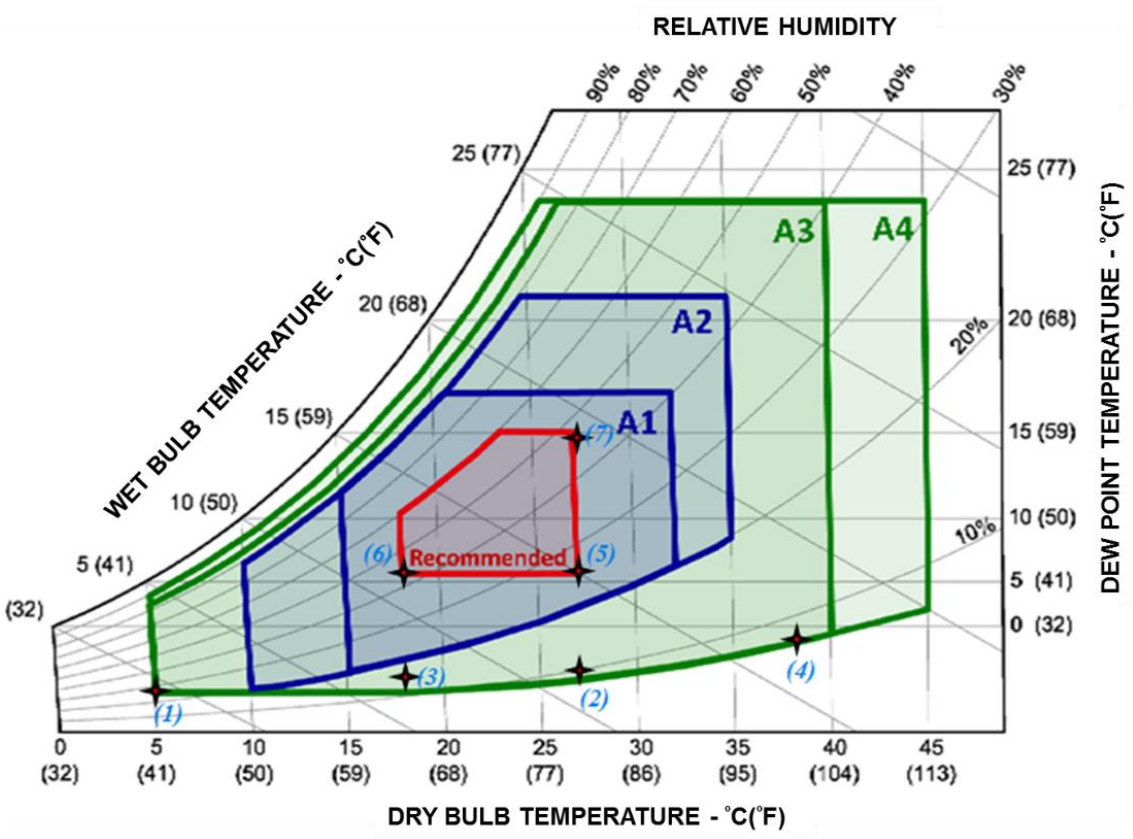

Figure 1 - ASHRAE psychrometric chart [9].

In order to investigate ESD severity at a dry environmental condition (referred to as extreme case studies), garment removal and standing from a chair were aggressively performed at 22°C-RH 5% (i.e., outside of extended envelopes suggested by ASHRAE).

Since sequence of human activities without grounding in between can occur in data centers, three sequences of random activities such as packing, unpacking, carrying and dropping a roll of plastic packaging foam, putting were aggressively performed under very dry conditions (22°C-RH 5%) to obtain electrostatic accumulation and dissipation histogram.

2. DATA PROCESSING

For well-controlled case study, totally 588 experiments varied with two categories of shoes and floors (given in Table 2), three office chairs, three typical sweaters, and seven dew points temperature (given in Table 1 and marked in Figure 1) were performed to analyze the event voltage and decay time. The results were discussed and compared for recommended and extended envelopes. For both experiments a PFM-711A electrostatic field meter with an isolated plate was used to record the transient voltage waveforms. To attain a higher accuracy in results, each activity was repeated 10 times for standing up from a chair experiment and 3 times for garment removal experiment.

Table 1 - List of selected environmental conditions.

Data Points	Temperature (°C)	RH (%)	Dew Point(°C)
1	5	25	-13.1
2	27	8	-10
3	18	15	-8.9
4	38	8	-1.7
5	27	25	5
6	18	45	5.6
7	27	45	13.9

Table 2 - ESD mitigating features for shoes and floorings.

Shoes	Floorings	ESD-description
9) Low-range dissipative ESD 10) Mid-range dissipative ESD 11) Deck shoes #1 12) Deck shoes #2 13) Deck shoes #3 14) Plastic shoes 15) Running shoes 16) Leather dress shoes	6) Rubber #1 7) Rubber #2 8) Vinyl #1 9) Vinyl #2	ESD-mitigating
	10) High-pressure laminate (HPL)	Non-ESD mitigating

2.1. GARMENT REMOVAL EXPERIMENT

For the garment experiment, a person wore the sweater and grounded himself, as shown in Figure 2. Therefore, the voltage should be zero. When the person started to remove the sweater, there were some fluctuations in voltage due to the removal of the sweater. The voltage suddenly increased when the person dropped the sweater on the floor. After dropping the garment, the person waited about 20-30 sec before grounding himself. This experiment was repeated three times for each sweater (total of three different typical sweaters). The person used the same clothes underneath the sweater throughout all experiments, and all clothes, shoes, and floors remained in the climate chamber at the desired dew point. In Figure 2, two typical voltage waveforms for sweater #3 at 38°C-RH 8% are presented. The illustrated waveforms are for the case of ESD shoes (i.e., mid-range ESD shoes) and ESD floor (i.e., Rubber #1), and the case of non ESD shoes (i.e., leather dress shoes) and non-ESD floor (i.e., HPL). The measured voltage was caused by the

contact and separation of the sweater and the underlying layer of clothing. However, the voltage did not reach its peak until the person dropped the sweater. As long as the set of separated charges were all close to the operator, the observed net charge was small. However, the moment that the operator dropped the sweater, the two sets of opposite charges were no longer close enough together to cancel each other out and this lead to a measurable increased voltage on the test subject.

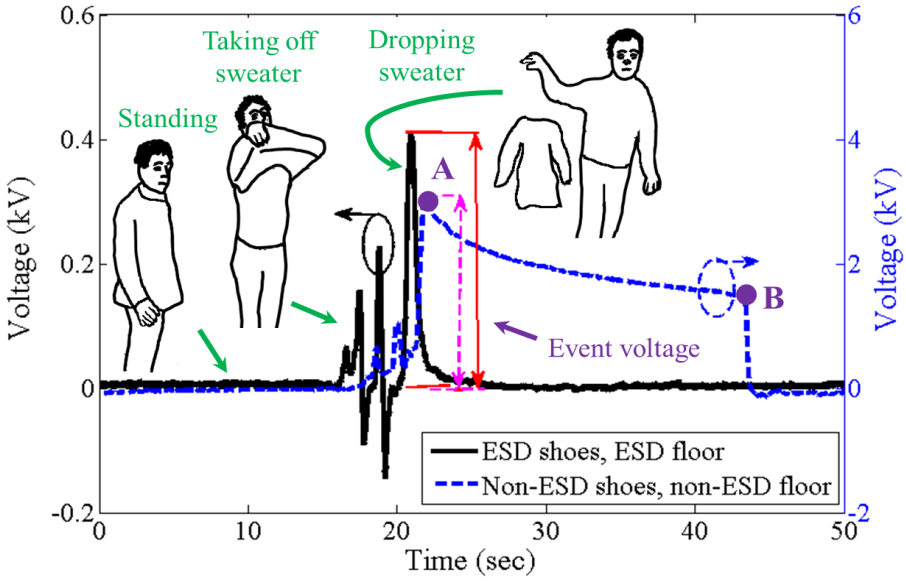

Figure 2 - Illustration of the garment removal experiment and its typical voltage waveforms for ESD and non-ESD mitigating materials.

To quantify the results, event voltage (see Figure 2) was calculated from the transient voltage waveform. The event voltage in the sweater experiment was defined based on the average change in voltage when the participant dropped a sweater. For these voltage waveforms, the event voltage is 0.487 kV for the case of ESD shoes/floor and 2.62 kV for the case of non-ESD shoes/floor. The event voltage for the case of the non ESD

combination is ~5 times greater than the case of the ESD mitigating combination. To illustrate how the decay times were extracted from a voltage waveform, which was based on a simple RC network, two points (A and B) from each action voltage waveform (see Figure 2) were selected. Then, the decay time constant was obtained as follows:

$$\frac{e^{\frac{-t_A}{\tau}}}{e^{\frac{-t_B}{\tau}}} = \frac{V_A}{V_B} \tag{1}$$

$$\tau = \frac{t_B - t_A}{\ln(\frac{V_A}{V_B})} \tag{2}$$

where, τ is the time constant, V_A and V_B are the voltage at points A and B, respectively; and t_A and t_B are the time at points A and B points, respectively. Then, the average was taken for each obtained τ. For this specific example, the decay time for the case of ESD shoes/floor is 1.2 sec, and for the case of non ESD shoes/floor is 30 sec.

By using decay time and event voltage, one can see the effectiveness of ESD shoes and ESD floors with respect to the elimination of ground strap. As reported in [19], a fast decay time of 0.2 sec for walking experiment when the person had ESD footwear on ESD flooring was sufficient to avoid using ground strap. Similarly, [20] investigated the possibility of elimination of the ground strap for walking and standing from a chair with ESD shoes on ESD flooring at RH 55%. It showed that the peak voltage of 58 V decreased to almost zero in less than 1.5 sec for standing up from a chair. The voltage limit of 100 V is chosen to guarantee the operation of devices without ESD failure or damage [19].

2.2. CHAIR EXPERIMENT

As shown in Figure 3, for the chair experiment the person sat down on a chair with their back touching the entire chair for three seconds. Then, the person stood up while holding an electrode to record the voltage waveform. Then, the person waited for ~5 sec before sitting down again and repeating the experiment 10 times. During these repetitions, the shoes remained on the floor. In addition, three typical office chairs were chosen for this experiment. In Figure 3, the voltage changes are shown by arrows in which the average of these values yielded the event voltage, as discussed above. The voltage waveforms for both cases of ESD shoes/floor and non-ESD shoes/floor combinations are presented for chair #1 at 38°C-RH 8 %. The illustrated voltage waveforms are for the case of ESD shoe (mid-range ESD shoes) and floor (Rubber#1), and non-ESD shoes (Deck shoes #1) and floor (HPL floor). For these voltage waveforms, the event voltage is 0.3 kV for the case of the ESD combination and 2.6 kV for the case of the non ESD combination. The event voltage for the non ESD combination case is ~8 times greater than that of the ESD combination case. The ESD decay time was also obtained for each action by using equation (1). Then, the average was taken for the experiment. For the illustrated results in Figure 3, the decay time is 0.4 sec for the case of the ESD combination and 27 sec for the case of the non-ESD combination.

3. RESULTS AND DISCUSSION

During the sweater experiment, the tribocharge was generated by the separation of the sweater and the underlying garment, while in the chair experiment the separation was

between the chair's surface and the garment. After charge separation, the voltage decays exponentially because of the shoe-floor current path.

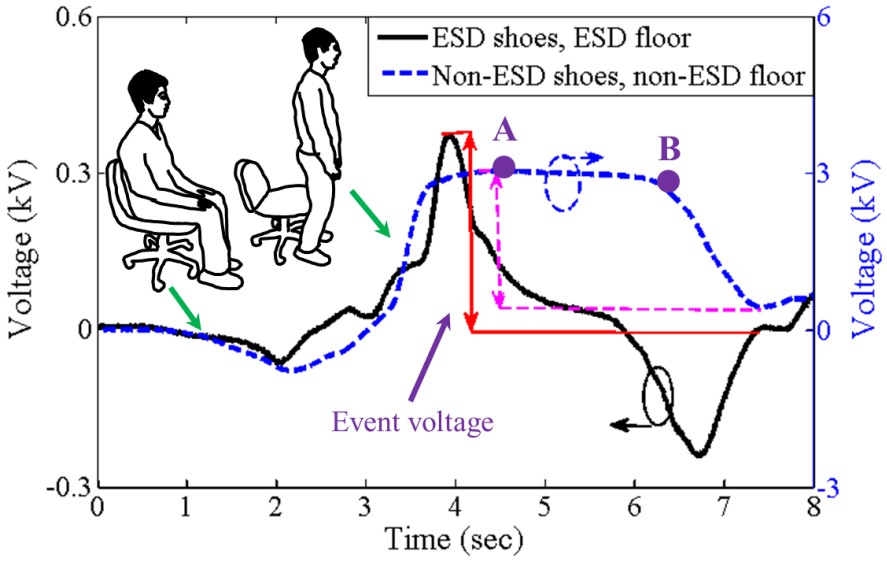

Figure 3 - Illustration of the chair experiment and its typical voltage waveform.

3.1. GARMENT REMOVAL EXPERIMENT

In Figure 4, the voltage waveform for the garment removal experiment, sweater#1 with leather dress shoes (i.e., non-ESD shoes) on HPL floor (non-ESD floor) is shown. The peak voltage varies from 2.8 kV at -8.9 ºC dew point (i.e., inside A3 envelope) to 0.03 kV at 13.9 ºC dew point (i.e., boundary of the recommended envelope).

In Figure 5, further analysis was performed to study the effect of RH and temperature separately. When the temperature was at 27°C, RH reduction from 45% to 25% resulted in an increase of the event voltage by a factor of ~4 for ESD shoes/floors, and by a factor of ~3 for non-ESD shoes/floors.

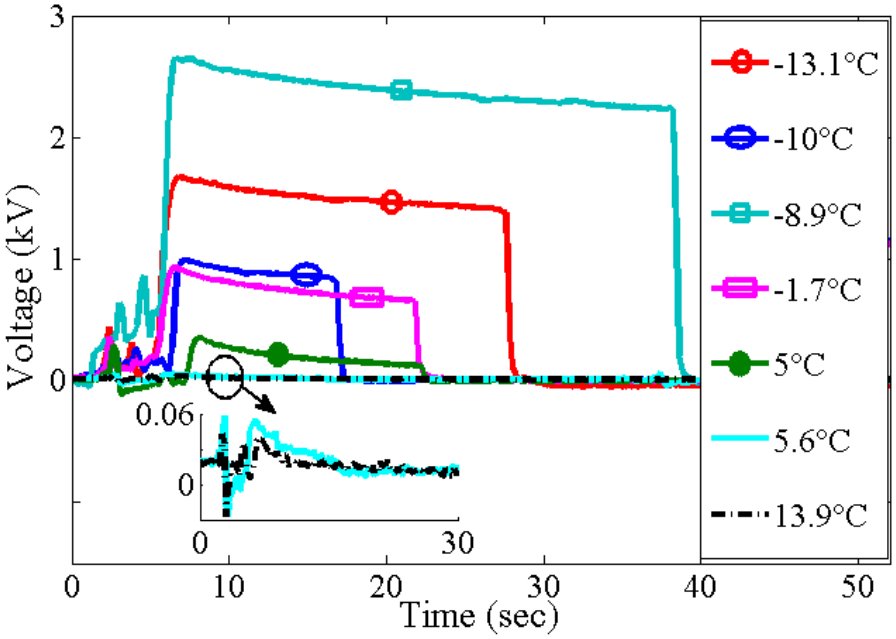

Figure 4 - Typical voltage waveforms for garment removal experiment.

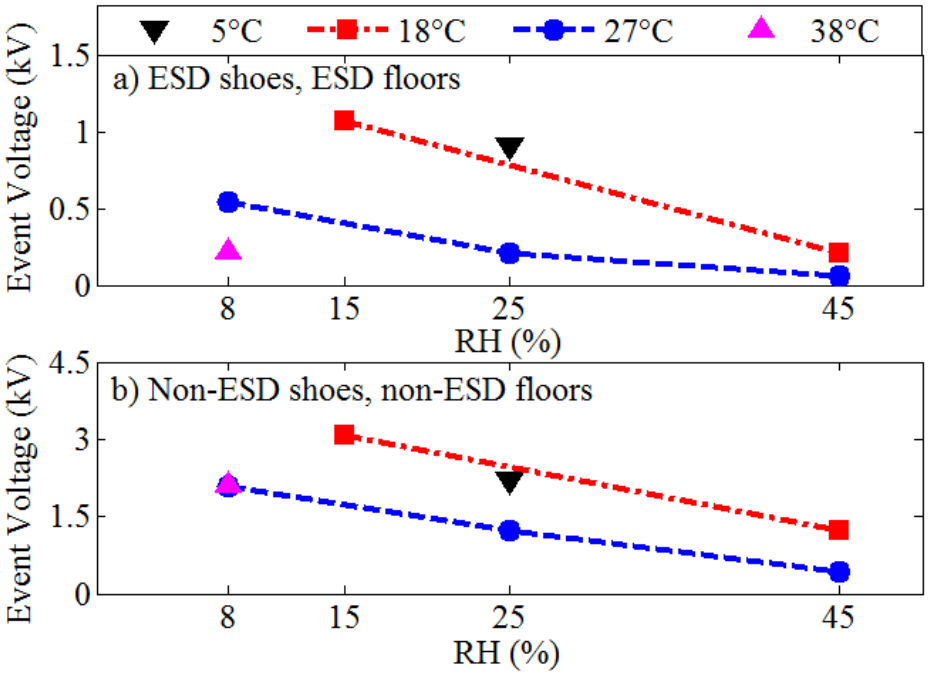

Figure 5 - Average event voltage for the garment removal experiment. It is a function of RH and temperature for ESD shoes/floors and non-ESD shoes/floors.

Additionally, by reducing the RH from 25% to 8% (at 27°C), the event voltage increased by a factor of ~2.5 for ESD shoes/floors, and by a factor of ~1.5 for non-ESD shoes/floors. By changing the RH from 45% to 15% at 18°C, the same trend was observed with a ratio of ~5.5 and ~3 for the case of ESD shoes/floors and non ESD shoes/floors, respectively. For a fixed RH point, raising temperature could result in a decrease in the event voltage value for the both cases.

Figure 6 shows the average event voltage among three sweaters. The standard deviation of event voltage among the three sweaters is also depicted, showing the range of the event voltage change for various dew points. Data points 1-4 given in Figure 1 that are outside of the recommended envelop represent greater event voltage than points 5-7 that are at the boundary of the recommended envelope. Data point 3 with dew point of -8.9 ºC has the highest and data point 7 with dew point of 13.9 ºC has the lowest event voltage. As seen, event voltages increased from 13.9°C to -8.9°C dew points and then decreased. Moreover, using ESD-mitigating materials instead of non-ESD-mitigating materials can reduce the event voltages by a factor of ~2-5, depending on the dew point.

The ESD decay time is depicted in Figure 7. From the results, the decay time constants based on Eq. (1) and (2) are ~0.1 sec (lowest value) and ~2 sec (highest value) at 13.9°C and -8.9°C dew point for the ESD shoes/floors, respectively. For the non-ESD shoes/floors, the corresponding values are ~40 sec and ~400 sec. These results indicate that utilizing ESD shoes/floors reduces the decay time constant in comparison with the case of non-ESD shoes/floors.The effectiveness of ESD vs. non-ESD shoes/floors on accumulation and dissipation of electrostatic charge with respect to elimination of the ground strap was of interest.

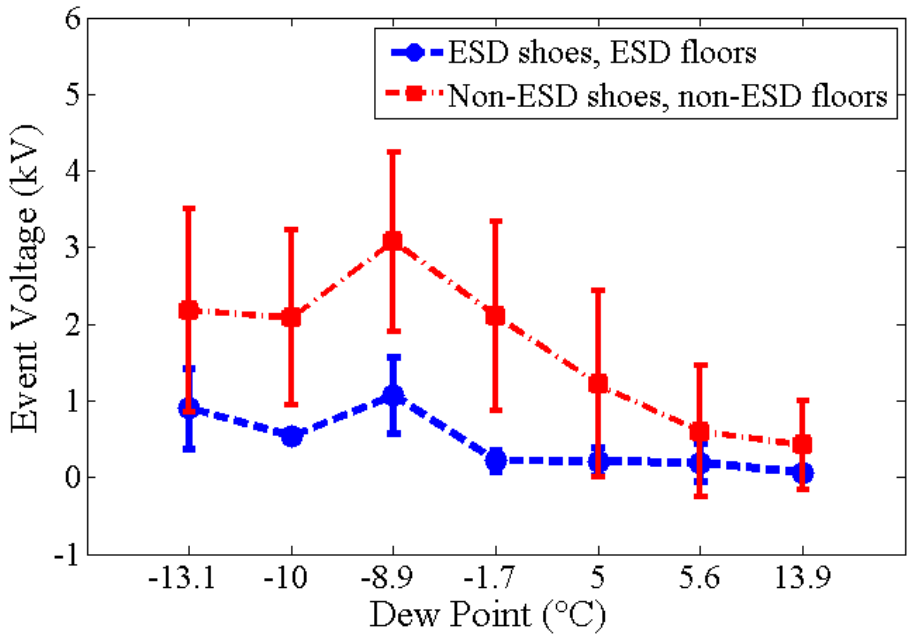

Figure 6 - Event voltage for the garment removal experiment.

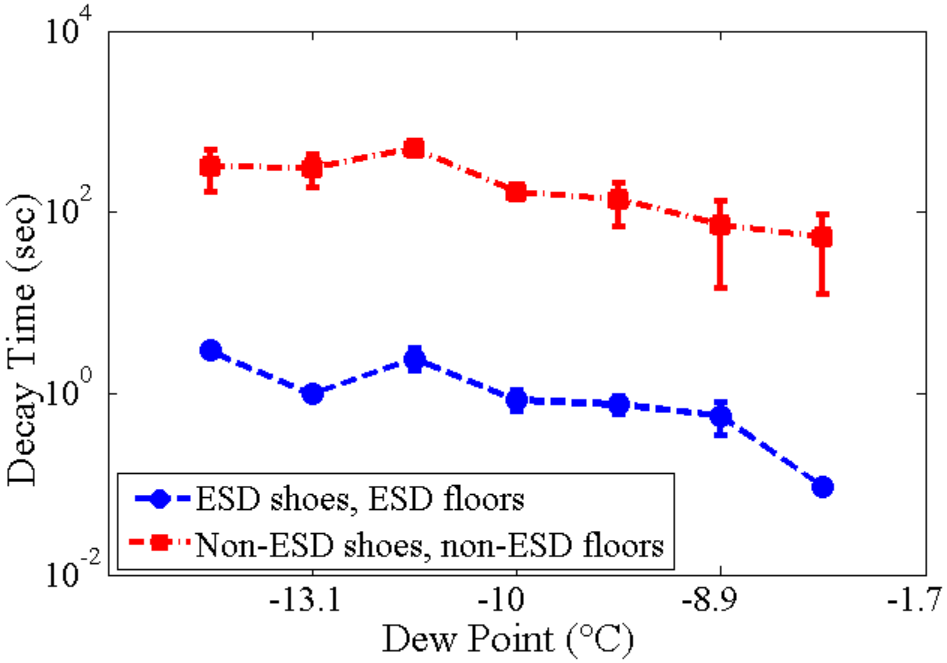

Figure 7 - Decay time constant for the garment removal experiment.

To do so, the voltage threshold of 100 V was chosen based on IEC 1340-5-1 standard. Then, the time a person needs to stand to discharge to 100 V was estimated by using the event voltage and decay time constant at each dew point temperature, as shown in Figure 8. The charge voltage generated during the garment removal when utilizing the ESD mitigating materials dropped to 100 V within 0.5 sec for data points at the recommended envelope (Figure 1, points 5-7). For data points taken inside A3 (Figure 1, points 1-4), a discharge time of up to ~7 sec was achieved.

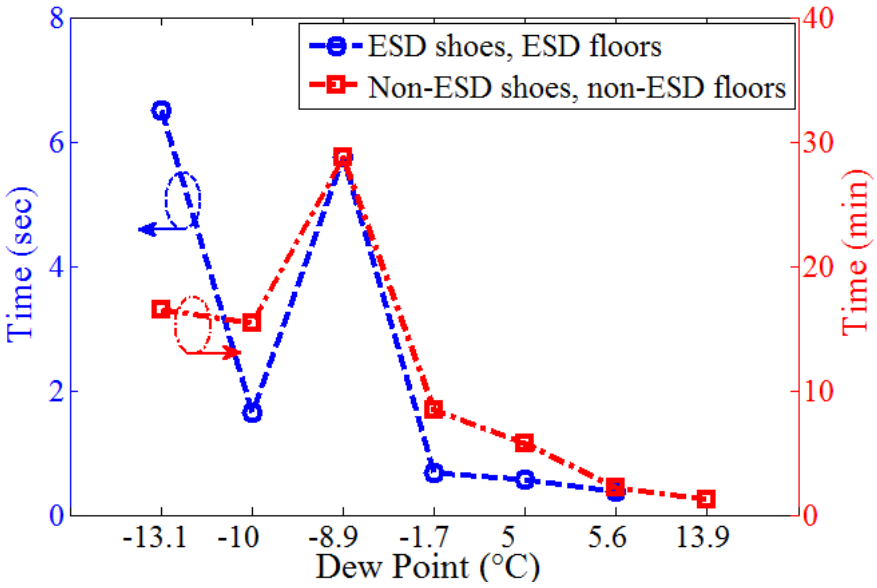

Figure 8 - Expected time to reach 100 V during discharge for the garment experiment.

As such, wearing the ground strap can be eliminated for recommended envelope when ESD mitigating materials are used. Outside of the recommended envelope, waiting for couple of second was required. When using non-ESD shoes/floors, the discharge time from charge voltage to 100 V were within ~30 min at dew point of -8.9°C (i.e., inside A3).

For data points in recommended envelope (Figure 1, data points 5-7), up to 8 min was required when non-ESD materials were used.

3.2. CHAIR EXPERIMENT

In Figure 9, the voltage waveform for the chair experiment, chair#1 with leather dress shoes (i.e., non-ESD shoes) on HPL floor (non-ESD floor) is presented. The peak voltage decreased from 5.2 kV at -8.9ºC dew point (i.e., inside A3 envelope) to 1.8 kV at 13.9ºC dew point (i.e., boundary of the recommended envelope). As shown in Figure 10, further analysis was performed to observe the effect of RH and temperature separately for chair experiments. When the temperature was at 27°C, RH reduction from 45% to 25% resulted in an increase in the event voltage by a factor of ~3 for the both the ESD and non-ESD combinations. In addition, the reduction of RH from 25% to 8% (at 27°C) resulted in an increase in the event voltage by a factor of ~3 for the case of ESD shoes/floors, and ~1.1 for the case of non-ESD shoes/floors. Changing RH from 45% to 15% at 18°C, the same increasing trend was observed with a ratio of ~2.5 and ~1.2 for the ESD and non-ESD combinations, respectively. For a fixed RH point, raising temperature could result in a decrease in the event voltage value for both cases. However, at very low temperature (5°C) with RH 25%, a decrease in voltage was observed for non-ESD case. Figure 11 shows the average event voltage among three chairs. The standard deviation of event voltage is also presented to show the change in the range of the event voltage. Data point 3 with a dew point of -8.9 ºC has the highest and data point 7 with a dew point of 13.9 ºC has the lowest event voltage. The event voltage increased by a factor of ~4 from 13.9°C to -8.9°C and then decreased.

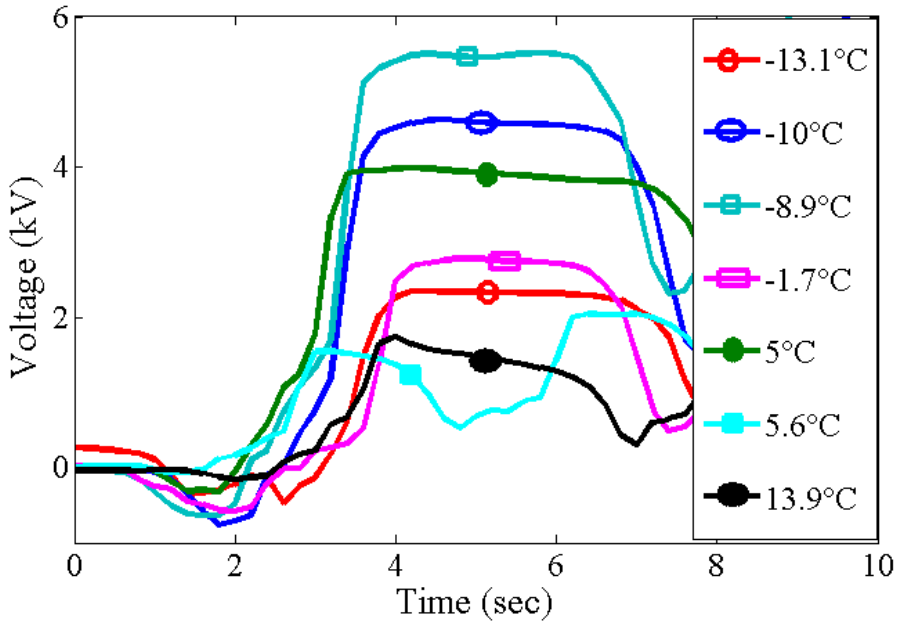

Figure 9 - Typical voltage waveforms for the chair experiment.

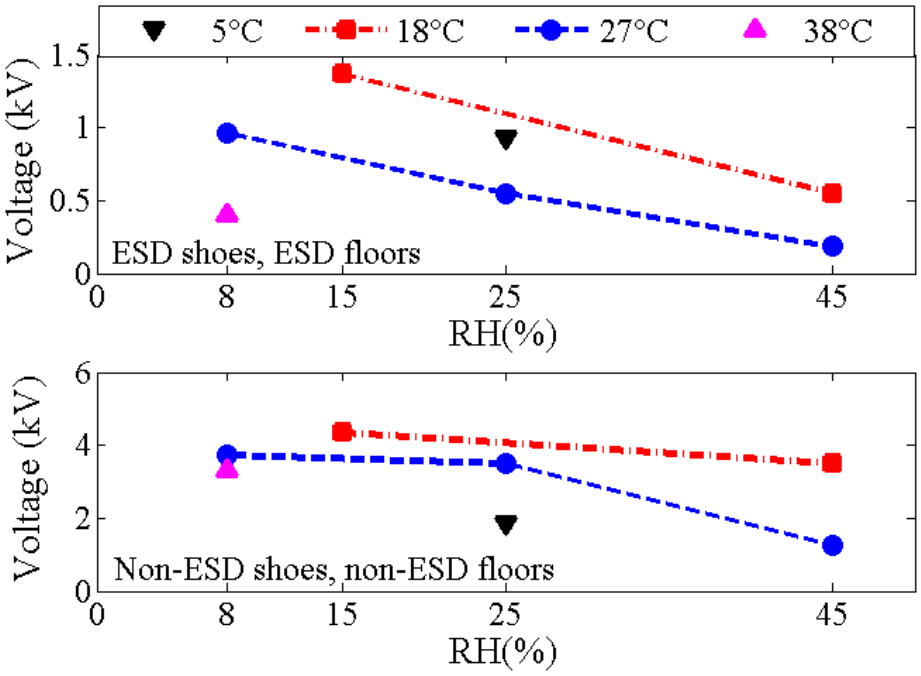

Figure 10 - Average event voltage for the chair experiment as a function of RH and temperature.

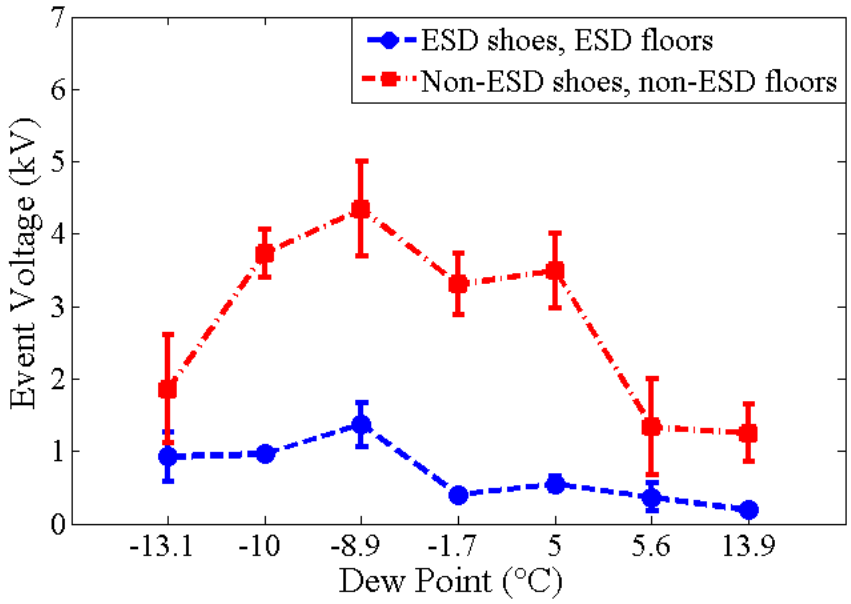

Figure 11 - Event voltage for the chair experiment.

For ESD shoes/floors, the decay time constant is around ~0.5 sec at 13.9°C and ~1 sec at -8.9°C. For the non-ESD case, these values are ~20 sec at 13.9°C and ~60 sec at -8.9°C. These results indicate that utilizing ESD shoes/floors reduces the decay time constant in comparison with the case of non-ESD shoes/floors. In Figure 13, the expected time that a person needs to stand to discharge to 100 V is presented. The charge voltage generated during the chair experiment when utilizing ESD mitigating materials (shoes/floor) dropped to 100 V within ~1.5 sec for recommended envelope data points 5-7 (marked in Figure 1), and within ~3 sec inside A3 envelope with data points 1-4. As such, wearing the ground strap can be eliminated for recommended envelope when ESD mitigating materials are used. Outside of the recommended envelope, waiting for few seconds is required. Using the ESD-mitigating materials instead of non-ESD-mitigating materials can reduce the event voltages by a factor of ~2-7, depending on the dew points.

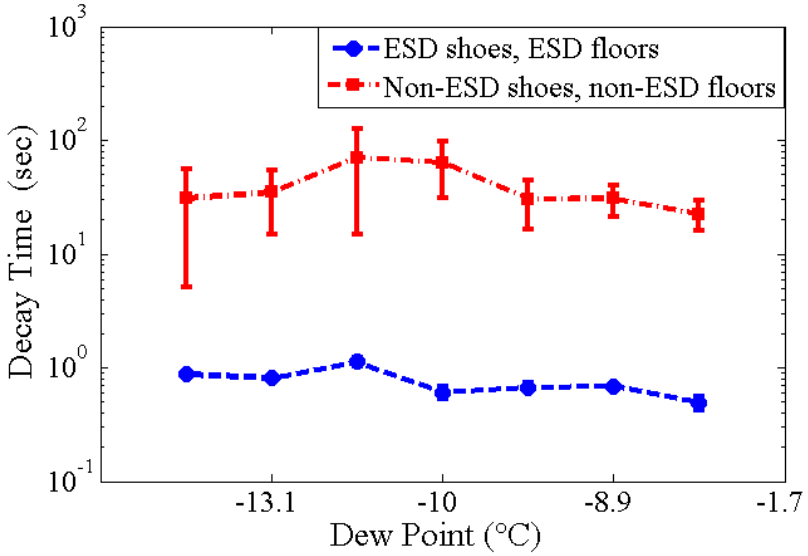

Figure 12 - Decay time constant for the chair experiment.

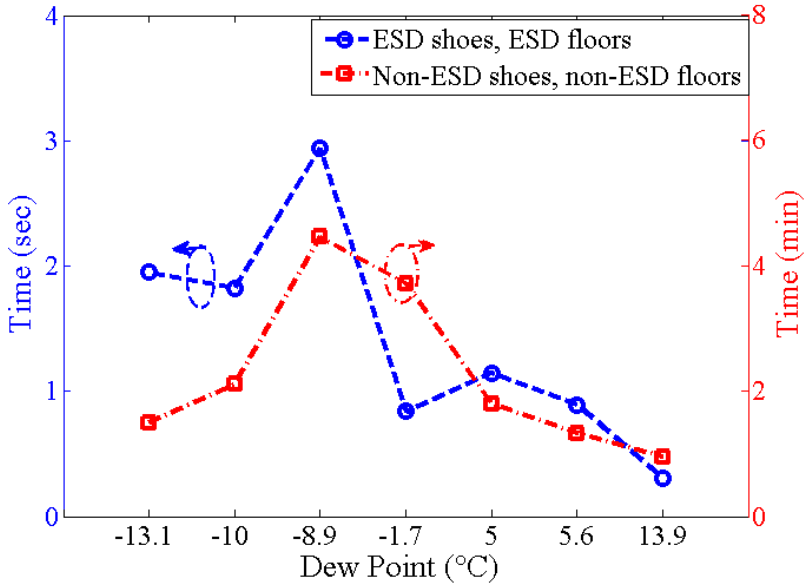

Figure 13 - Expected time to reach 100 V during discharge for the chair.

The ESD decay time is depicted in Figure 12. When non-ESD shoes/floors were utilized, the discharge voltage to 100 V is within 4 min at dew point of -8.9°C (i.e., inside A3). For data points 5-7, the discharge time to 100 V was within 2 min.

4. EXTREME CASE STUDY

The results shown in the preceding paragraphs were obtained under well-controlled conditions. Extreme case study serves as a reminder to be careful about voltage levels given in any triboelectric study as these values strongly depend on the materials, surface property, pressure, rubber type, etc. Based on our extensive experience, it is observed that the well-defined walking pattern experiments predict real voltages well. In the other experiments, the general tendencies with respect to the RH, capacitance, and decay times are good predictors for real situations. However, predicting the voltage levels over a large range of activities (walking, chair, garment removal, unspooling of plastic foil, etc.) is difficult. For an extreme case of environmental conditions which is outside of the A4 envelope, 22°C-RH 5% (multiple instruments showed values between 3% and 13%; the 5% is based on an instrument which specifies +/-3% error at RH 5%), both chair and garment experiments were conducted aggressively to explore the highest value. Three different flooring structures were investigated, including expanded polystyrene (foam) on wood, wood, and metal. These experiments were conducted wearing insulated standard street shoes. As the shoes are insulated, the effect of the flooring material is via their effect on the capacitance of the person. As an example, an illustration of the situation that occurs in a typical US residential building (i.e., made from dry wood and having rather thick polymeric or otherwise insulated flooring) is presented. In this case, the capacitance may be about 30% less relative to the same person standing on a reinforced concrete floor. As the tribocharging is a charge separation process, the voltage rise is by ~30% if the capacitance is reduced by the same amount.

To initiate the garment experiment, a person was discharged at first by contact with ground. The person rubbed the sweater against the next layer of clothing, then took it off and dropped it on the floor. The friction between the sweater and the next layer caused charge separation. However, this did not increase the voltage as both positive and negative charges are very close to the body of the person. Once the person dropped the sweater, one type of charge moved away from the person, and the voltage suddenly rose. The voltage was measured after garment removal. For this experiment, various types of sweaters were used. The highest voltages were measured using two-layer winter clothing. Here, the inner layer is a fleece sweater while the outer layer is a wind and waterproof jacket. As shown in Figure 14a, the charged voltage for the case of standing with insulated shoes on metal is the lowest and the foam is the highest which is due to the capacitance value between the person and the ground. The mean (μ) and standard deviation (σ) from the measured voltages are also presented showing the range of variation.

For the chair experiment, the person was discharged by touching ground at the beginning of the each experiment. For the experiment the person rubbed his back on the chair, then stood up and the voltage was measured. Various types of sweaters (three sweaters) were used with different types of chairs (three chairs) to investigate a wide range of variations. The data shown in Figure 14 for each case is sorted from low to high voltage value. Partially explainable due to the capacitance to ground the lowest voltages have been measured when standing with insulated shoes on grounded metal, while the setup which emulates a wood residential frame structure (foam on wood) reached the highest voltages. The mean and standard deviation from the measured voltages are also presented showing the range of variation in this experiment.

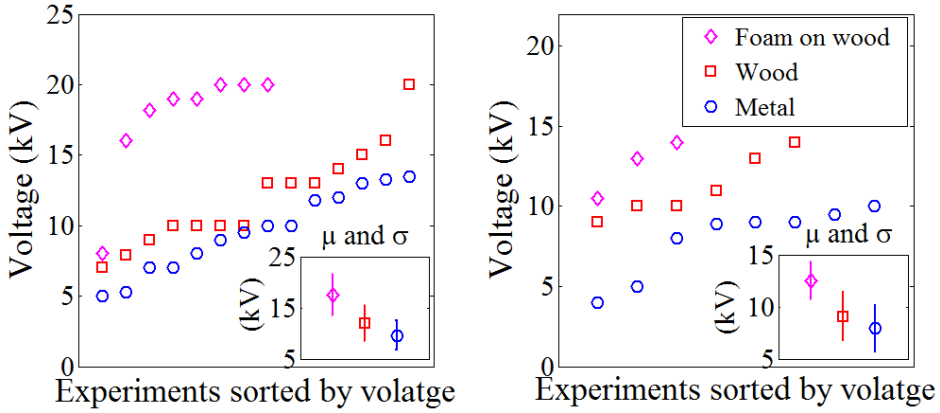

Figure 14 - Extreme case results of (a) garment removal, (b) chair experiment. The instrument saturated at 20 kV, thus, some voltage values may have surpassed 20 kV (the recorded values are sorted from low to high value).

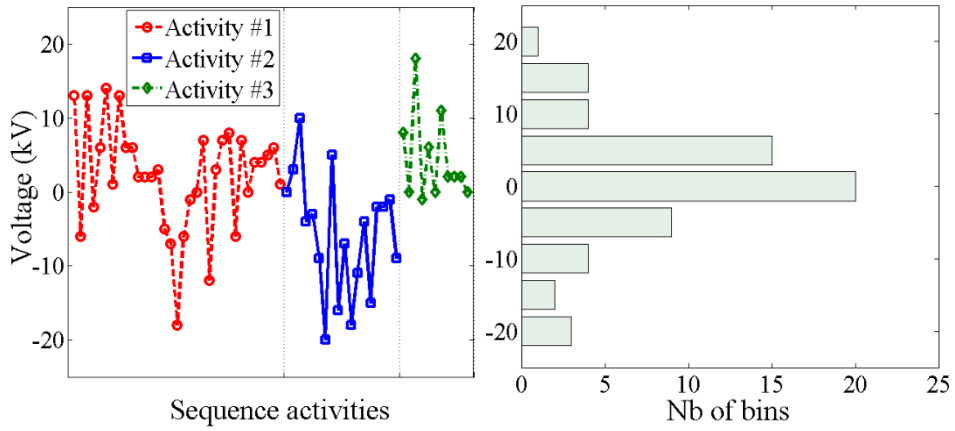

Figure 15 - Voltage waveform and histogram of three sequential activities.

The capacitance ratios have been 120pF (metal), 60pF and 50pF. They have the same tendency; however, we did not conduct the same experiments (same sweater, clothes, etc.) for each case. For the second extreme case study, a random sequence of activities was performed (22°C-RH 5%) on carpet including packing, unpacking, carrying and dropping a roll of plastic packaging foam (with diameter of 1 m and height of 1 m), putting on and

removing garments, sitting down and standing up from a chair, and walking. As the person is not grounded during these activities, charges can accumulate or cancel each other. These random activities were performed three times. As shown in Figure 15 (a), the recorded voltages (i.e., related to the accumulation and cancelation of charges) were measured after each activity. The voltage varies between -20 kV and 20 kV which are the upper and lower limit of our instrument. The histogram of all activities (Figure 15 (b)) shows that most voltage measurements occurred at -7.5 to 7.5 kV.

Table 3 - Measured capacitance between person and ground.

Capacitive Model	C value
Insulated shoes standing on wood flooring	65 pF
Insulated shoes on bamboo flooring above concrete	75 pF
Insulated shoes standing on kitchen tile	80 pF
Insulated shoes standing on carpet on wood flooring	60 pF
Insulated shoes sitting on a sofa	65 pF
Street shoes on basement concrete (both feet down)	120 pF
Street shoes on basement concrete (one feet down)	80 pF
Bedroom shoes on carpet	60 pF
Barefoot standing on thin PE foil on basement concrete	1200 pF
Barefoot standing on bamboo flooring	95 pF

As observed from these two extreme case studies, the voltage values can exceed 20 kV in dry winter conditions. It is possible to generate well-reproducible tribocharging

results if the materials and the movement are well controlled. The reader of every paper on ESD-related tribocharging should consider that the tendencies observed, e.g., with a change of humidity, are valid; however, the absolute voltage levels should be taken with care. The voltage levels in uncontrolled surroundings will vary strongly depending on the material selection, activity, and humidity. Flooring and shoes are additional influencing factors which can reduce the accumulated charges within seconds. The last, but sometimes overlooked factor, is the capacitance from the body to ground. It alone can change the voltages by +/-30%. A wide range of body-to-ground capacitance for different flooring in a residential home are presented in Table 3.

5. SUMMARY

If data centers can operate at the extended environmental conditions (introduced by ASHREA) safely, lots of energy can be saved. To end this, ESD severity must be studied for various human activities. Previous studies for walking showed that although the charge voltage due to walking will increase at lower RH (RH 25% to 8%) by a factor of ~2, but the probability of ESD-related failure due to walking is not strongly increased. Since garment removal and standing up from a chair are two common activities and lead to higher charge voltage (~2-4 times), the accumulation and dissipation of electrostatic charge from these two activities were presented, including well-controlled and extreme cases. Well-controlled systematic experiments were conducted at seven dew points (-13.1°C to 13.9°C) and in addition a less controlled extreme case outside the A4 envelope was analyzed. The total number of 588 well-controlled experiments varied the shoes and flooring and included three types of chairs and sweaters. The voltages generated, and the decay times have been

measured. The decay times tell how long an operator would have to wait until the voltage dropped to 100 V. Following is the summary of the main observations:

- Using ESD shoes/floors results in significant reduction in the average event voltage by a factor of ~2-5 (for garment) and ~2-7 (for chair) in comparison with non-ESD combinations, depending on the dew points.
- Decreasing the temperature at a fixed RH can increase the event voltage.
- Decreasing the RH at a fixed temperature leads to an increase in event voltage.
- The maxima of the voltages did not occur at the lowest dew point temperature (-13.1ºC dew point), but at a dew point of -8.9ºC.
- From three data points on the boundary of the recommended envelope, dew point 13.9°C shows the lowest event voltage and decay time for all experiments.
- For RH reduction from 25% to 8% at 27ºC, event voltage increases by a factor of ~1.5-2.5 for both garment removal and standing up from chair experiment.
- Utilizing ESD mitigating materials, for the garment removal the voltage dropped to 100 V within ~0.5 sec (1.5 sec for chair) at the recommended environmental envelope, and up to ~7 sec (3 sec for chair) inside A3 extended envelope. From these results, wearing ground strap can be eliminated in data centers for recommended range. For outside of the recommended range, it is required to wait for longer time or to educate the personnel about the risk.
- Utilizing non ESD mitigating materials, for the garment removal experiment the corresponding times are ~1-8 min (~1-2 min for chair) at recommended environmental envelope, and up to ~10-40 min (~2-4 min for chair) inside A3

envelope. As such, wearing ground strap is always inevitable when non-ESD mitigating materials used.

- Data center might potentially save lots of energy by reducing the relative humidity from 25% to 8% RH at 27ºC (i.e., from recommended environmental envelope to A3), but without strongly increasing probability of ESD-related failure due to human activities.

For the extreme case, which is conducted at 22°C-RH 5% (outside of the A4 envelope), two garment removal and chair experiments were done aggressively. These two activities along with three sequence of random activities such packing, unpacking, carrying and dropping a roll of plastic packaging foam, putting under very dry conditions shows that more than 20 kV electrostatic voltage can be generated. Reduced capacitance of the body, due to thick insulated floors such as wooden floors, can double the voltage for a given charge if a high capacitance situation (standing on concrete) is compared to a standing on a carpet in a dry wood frame home. The voltage levels in uncontrolled surroundings will vary strongly depending on the material selection and the action performed, making it difficult to predict these voltages. In spite of the difficulties to predict the voltages in uncontrolled environments, this study analyses the influence of humidity and ESD mitigating techniques. It indicates that ESD shoes/floors will not only reduce the voltages strongly, but also lead to very rapid and controlled discharge times.

REFERENCES

[1] A. Talebzadeh, Y. Gan, K. Kim, Y. Zhang, and D. Pommerenke, “Spark-less electrostatic discharge (ESD) on display screens,” In 2015 IEEE International Symposium on Electromagnetic Compatibility (EMC), pp. 1284-1289, 2015.

[2] T. S. McLeod, and G. Johnson, “Protection of data processing equipment against static electricity discharges,” Electronics and Power, vol. 24, no. 7, pp. 521-526, 1978.

[3] ASHRAE, TC, “ASHRAE Environmental guidelines for data com equipment,” Whitepaper by ASHRAE TC 9.9, 2008.

[4] ASHRAE, TC, “Thermal guidelines for data processing environments-expanded data center classes and usage guidance,” Whitepaper by ASHRAE TC 9, 2011.

[5] E. Helerea, B. Moasa, and A. Ciobanu, “Analysis of electrostatic environment and discharge models,” In 2012 International Conference on Applied and Theoretical Electricity (ICATE), pp. 1-4, 2012.

[6] S. Frei, and D. Pommerenke, “A study of the impulsive field occurrence rate and intensity." In 1997 IEEE International Symposium on Electromagnetic Compatibility, pp. 507-512, 1997.

[7] F. Wan, J. X. Ge, and D. Pommerenke, “Absolute humidity, relative humidity: which is more important in representing severity of electrostatic discharge,” Electronics Letters, vol. 49, no. 23, pp. 1451-1452, 2013.

[8] D. E. Swenson, “Humidity controls for data centers: Are they necessary?,” ASHRAE Journal, vol. 52, no. 3, pp. 48-55, 2010.

[9] F. Wan, M. Hillstrom, C. Stayer, D. E. Swenson, and D. Pommerenke, “The effect of humidity on static electricity induced reliability issues of ICT equipment in data centers-Motivation and setup of the study,” ASHRAE Transactions, vol. 119, pp. 341-357 2013.

[10] A. Talebzadeh, et al, "Dependence of ESD Charge Voltage on Humidity in Data Centers: Part I-Test Methods."ASHRAE Transactions, vol. 121, pp. 58-70, 2015.

[11] A. Talebzadeh, et al, “Dependence of ESD Charge Voltage on Humidity in Data Centers: Part II-Data Analysis,” ASHRAE Transactions, vol. 121, pp. 37-48, 2015.

[12] M. Moradian, A. Patnaik, Y. Han, F. Wan, X. Gao, D. Pommerenke, and D. E. Swenson, “Determination of the effect of humidity on the probability of ESD failure or upset in data centers,” ASHRAE Transactions, vol. 120, pp. 25-41, 2014.

[13] X. Gao, A. Talebzadeh, et al, “Dependence of ESD Charge Voltage on Humidity in Data Centers: Part III-Estimation of ESD-Related Risk in Data Centers Using Voltage Level Extrapolation and Chebyshev's Inequality,” ASHRAE Transactions, vol. 121, pp. 49-57, 2015.

[14] Greason, W. D. 1999. Investigation of a test methodology for triboelectrification. Electrical Overstress/ Electrostatic Discharge Symposium Proceedings, Orlando, FL, USA, 344-5.

[15] McFarland, W.Y. 1981. The economic benefits of an effective ESD awareness and control program-an empirical analysis. Electrical Overstress/Electrostatic Discharge Symposium Proceedings,EOS 3:28.

[16] Ryser, H. 1990. The relationship between ESD test voltage and personnel charge voltage. In Proceedings of EOS/ESD Symposium Orlando: Session2 – paper1.

[17] S. A. H. Rizvi, E. M. Crown, K. Osei-Ntiri, P. R. Smy, and J. A. Gonzalez. “Electrostatic characteristics of thermal-protective garments at low humidity,” Journal of The Textile Institute, vol. 86, no. 4, pp. 549-558, 1995.

[18] A. Talebzadeh, M. Moradian, Y. Han, D. E. Swenson, and D. Pommerenke, “Electrostatic charging caused by standing up from a chair and by garment removal,” In 2015 IEEE Symposium on Electromagnetic Compatibility and Signal Integrity, pp. 57-62, 2015.

[19] R. Gaertner, K-H. Helling, G. Biermann, E. Brazda, R. Haberhauer, W. Koehl, R. Mueller, W. Niggemeier, and B. Seder, “Grounding personnel via the floor/footwear system,” In 1997 Proceedings Electrical Overstress/Electrostatic Discharge Symposium, pp. 170-175, 1997.

[20] S. Lim, "Conductive floor and footwear system as primary protection against human body model ESD event." IEEE Transactions on Electronics Packaging Manufacturing, vol. 23, no. 4 pp. 255-258, 2000.

IV. TRIBOELECTRIC CHARGING BETWEEN DISPLAY GLASS PANELS AND DISSIPATIVE/INSULATIVE ROLLERS

ABSTRACT

The underlying cause of most Electrostatic discharge (ESD) is tribo-charging. Thus, understanding tribo-charging is essential to assess the likelihood of damages as they might occur in the production of LCD screens. In this paper a study of triboelectric charge build-up between the glass and rollers during the glass transfer process in display panel manufacturing is presented. A roller conveyor system was fabricated and two types of rollers materials, insulative and dissipative, with radiuses of 30 and 90 mm, were considered. To measure the triboelectric charge of the glass, a Faraday cup with elevator system was mounted on the apparatus. Various parameters including transfer velocity, acceleration/deceleration, and relative humidity (RH) were investigated. For instance, it is observed that the average saturated charge density on the glass is 0.324 nC/cm^2 after 320 m displacement if it transfers by small dissipative rollers with condition of 200 mm/s and 200 mm/s^2. In addition, a comprehensive study of the surface potential distribution on the glass and rollers by utilizing a 2D automated scanner is presented. The experiments pointed out that the amount of charge accumulated on the glass for the dissipative rollers was saturated faster with a smaller value than the insulative rollers.

Index Terms— electrostatic discharge (ESD); ESD-related failure, triboelectric charge; roller conveyor; glass; insulative; dissipative; relative humidity.

1. INTRODUCTION

The display panel manufacturing process includes photolithography, thin film transistor (TFT) fabrication, and a roller conveyor system. During the glass transfer for TFT fabrication, the static/dynamic friction force between the glass and the rollers results in triboelectric charging (or triboelectrification), which may lead to ESD failures including random short circuits and point defects in TFT driver array, damage to polarizer film and driver transistors, etc. might occur as a result of charge generated on the glass [1]. Thus, finding solutions to reduce the triboelectric charge generated during the glass transfer process can benefit manufacturing industries. To this end, at first the amount of charge generated and its parameter dependence needs to be known.

In [1]-[6], some aspects and parameters contributing to the triboelectric charging between the display panel and conveyor system were presented. In [1], the triboelectric charges at different stages of display manufacturing were reported and it was shown that the triboelectric voltage on the rollers during the glass transfer can build up to -2 kV. However, the effect of roller material and diameter, transfer velocity/acceleration and environmental conditions were not considered. In [2], triboelectric charges for a roller conveyor system were measured in display panel manufacturing. For dissipative rollers with a radius of 30 mm, a smaller static voltage in magnitude (-0.35 kV) was observed for the rollers compared to insulating rollers with a radius of 130 mm (-2.55 kV). Both experiments were performed with a similar transferring velocity of 116 mm/sec. Also, transfer velocities of 116 and 416 mm/sec for the insulative roller resulted in the roller's static charge voltage of -2.6 kV and -5.4 kV, respectively. In [3], various ionization technologies were compared for triboelectric charge reduction on the roller and glass in a

display panel manufacturing. In [4], the triboelectric charging was studied at different stages of a flat panel display manufacturing including vacuum stage, roller transferring system, and film detachment process. The study used only very limited experiments for a roller transferring system. In [5], a multi-physics model for triboelectric charging of a roller conveyor system was presented. For the measurement set-up, only insulative rollers with a radius of 30 mm, transfer velocity of 100 mm/sec, acceleration/deceleration of 100 mm/sec2, at 22°C and 30% relative humidity (RH) were studied. In [6], a static charge modeling and characterization of the glass was presented for the fabricated roller conveyor system. The triboelectric charge measurement was performed by Faraday cup. Further, only small diameter rollers (30 mm) were considered.

The main problem for the previous roller conveyor literature [1]-[4] was the lack of comprehensive comparison between parameters that contribute to the value of triboelectric charging during experiments in an actual display panel manufacturing setting. In [5] and [6], the study was conducted in a climate chamber with a fabricated roller conveyor system. However, some preliminary studies which also considered the triboelectric charging of the glass were only reported.

In this paper, a comprehensive study of the effect of roller material (insulative vs. dissipative), roller radius (small vs. large), transfer velocity (slow vs. fast), transfer acceleration (medium vs. high), traveling distance (200 m vs. 400 m) is presented. Moreover, the effect of RH (from 20% to 50%, all at fixed temperature of 22°C) is investigated. The triboelectric charge on the glass for different cases was measured by a Faraday cup. Further, the surface voltage on the glass and the rollers was studied with the 2D automated scanner system. Since it is not easy to achieve good repeatability in all

triboelectric charge experiments, three identically manufactured glass pieces were measured for the experiment to display the mean and standard deviation values. Moreover, the time decay of the insulting rollers was obtained and the surface potential on the rollers was assessed with a 2D automated scanner. The effect of using an ionizer also was presented. A comparison between previous literature and the present study is illustrated in Table 1.

2. RESEARCH METHODOLOGY

In order to assess the triboelectric charge on the glass and rollers, a bidirectional conveyor was fabricated as shown in Figure 1. The apparatus consists of an AC-DC power supply, a stepper motor to drive the rollers (transfer motor), 17 roller shafts, 11 rollers per shaft, three stepper motors to move the lift pins (lift-up motors), nine lift-up pins for the elevator, and four motor controllers. The apparatus is located inside a humidity chamber. Two RS485-USB converter cables were used to support the communication between the motor controllers and the computer (located outside of the humidity chamber). Two different types of rollers with insulating and dissipative properties were made. Ultra-high-molecular-weight (UHMW) polyethylene material was used for the insulative rollers, and the dissipative rollers were made of UHMW polyethylene containing carbon particles. The measured resistances of the insulative and dissipative rollers were 6.9×10^{11} and 2.7×10^{8} Ω, respectively. The ES 124, a digital high resistance and low current meter from ESDEMC Technology LLC, was used to measure the resistance of the insulating and dissipative materials. For each roller material two different sets of rollers were fabricated with the radius of R_R = 30 and 90 mm with the thickness of T_R = 10 mm.

Table 1 - Comparison between previous literature and the present study.

Ref.	Roller property	Velocity (mm/s)	Acceleration (mm/s^2)	Temp/ RH	Test Properties
[1]	-	-	-	-	-Performed in manufacturer -Ionizer effect and rollers were studied
[2]	Dissipative (rad = 30 mm) Insulative (rad = 130 mm)	116, 416	-	-	- Performed in manufacturer - Ionizer effect and rollers were studied
[3]	Dissipative (rad = 30 mm) Insulative (rad = 30 mm)	~115-200	-	-	- Performed in manufacturer -Ionizer effect and rollers were studied
[4]	Insulative (30 and 130 mm)	160, 320	-	22°C/55%	-Performed in manufacturer -Studied static voltage at different stages - A few experiments reported for roller
[5]	Insulative (rad = 30 mm)	100	100	22°C/ 30%	-Performed in a humidity chamber -Faraday cup -Glass studied
[6]	Dissipative (rad = 30) Insulative (rad = 30)	54, 100, 200, 300	54, 100, 200, 300	22°C/30% 22°C/50%	-Performed in a humidity chamber -Faraday cup -Glass studied -Steady state of triboelectric charge
This paper	Dissipative (rad = 30 and 90 mm) Insulative (rad = 30 and 90 mm)	100, 200, 300	200, 300	22°C/ 20% - 50%	-Performed in a humidity chamber -Studied ionizer -Faraday cup and 2D automated scanner -Glass and rollers studied

As seen in Figure 1, S_S = 200 mm was the spacing between two adjacent shafts, S_R = 50 mm was the spacing between two adjacent rollers mounted on the same shaft, L_G = 457 mm and W_G = 457 mm were the length and width of the glass with 0.5 mm thickness (i.e., Alkaline earth boroaluminosilicate glasses, which are typically used for display substrate).

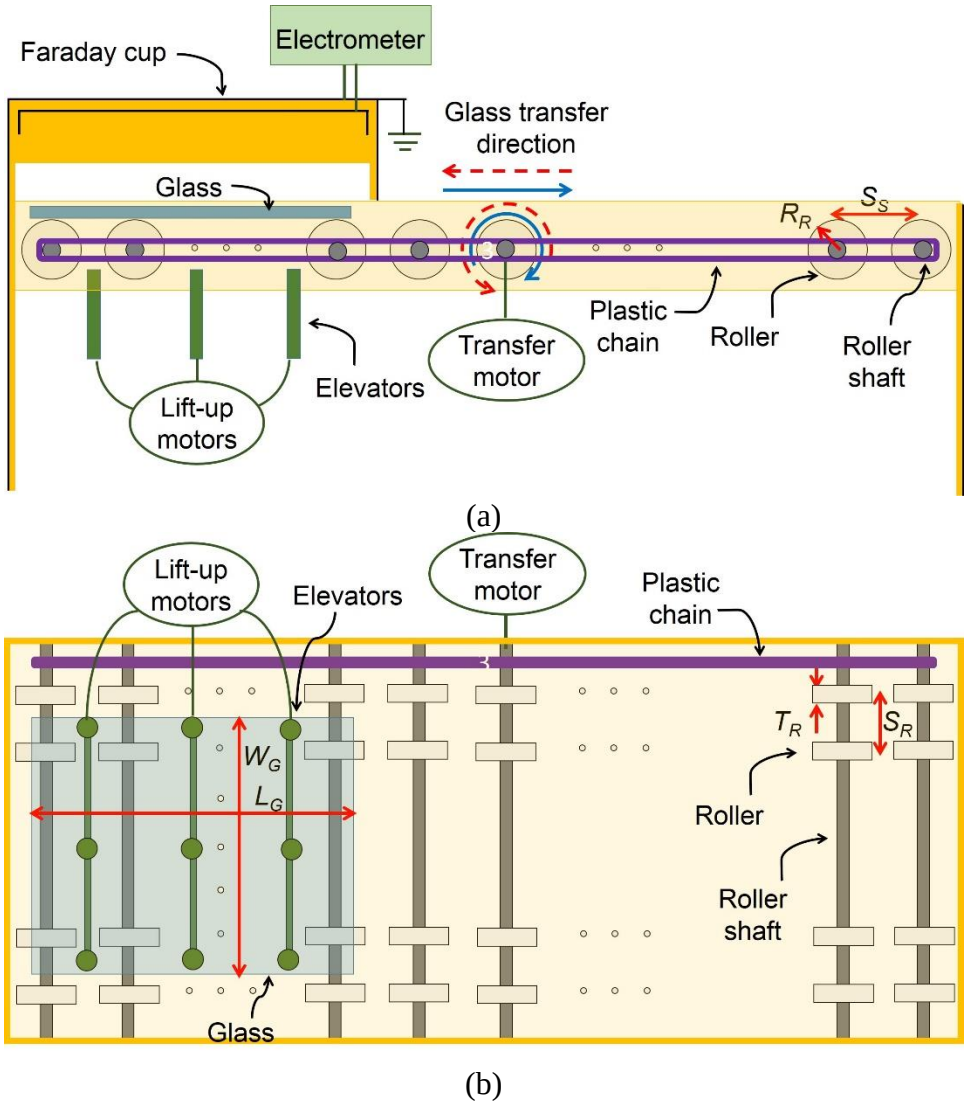

Figure 1 - Roller conveyor system schematic. (a) side view, (b) top view.

The research program undertaken in this investigation consisted of two phases. In the first phase, the effect of roller materials (insulative vs. dissipative), roller radius (small vs. large), transfer velocity (slow vs. fast), transfer acceleration (medium vs. high), traveling distance (200 m vs. 400 m), and RH variation (20% to 50%) on the amount of triboelectric charging on the glass was measured by the Faraday cup. In Figure 2a, the measurement set-up for the Faraday cup is depicted. To measure the total charge, the glass was lifted up toward the Faraday cup after the desired movements by utilizing an elevator system.

The voltage of the Faraday cup was recorded by an ES103 electrometer from ESDEMC Technology LLC. Table 2 presents the test conditions for the total charge measured by the Faraday cup. For all experiments, the glass lifted up toward the Faraday cup ten times, after each of twenty back-and-forth glass displacements. Two traveling distances (i.e., 1 and 0.5 m) for each back-and-forth movement were performed.

In the second phase, to study the triboelectric voltage distribution on the glass and rollers at different conditions (e.g., rollers with different material and radiuses) a 2D automated scanner (XY movement) was built and mounted on the roller conveyor. A non-contact TREK model 347 electrostatic voltmeter probe was used to measure the surface voltage. Figure 2b shows the scanner set-up for the glass. The top surface of the glass was scanned at the beginning, and after the first and the second back-and-forth movement of the glass (1 m traveling distance). Each back-or-forth movement includes 1 m displacement. The glass was lifted up by the elevator system and then the scanning initiated. Figure 2c shows the scanner set-up for the rollers. The middle part of the conveyor

was chosen to be scanned after 100 back-and-forth movements of the glass for 1 m traveling distance.

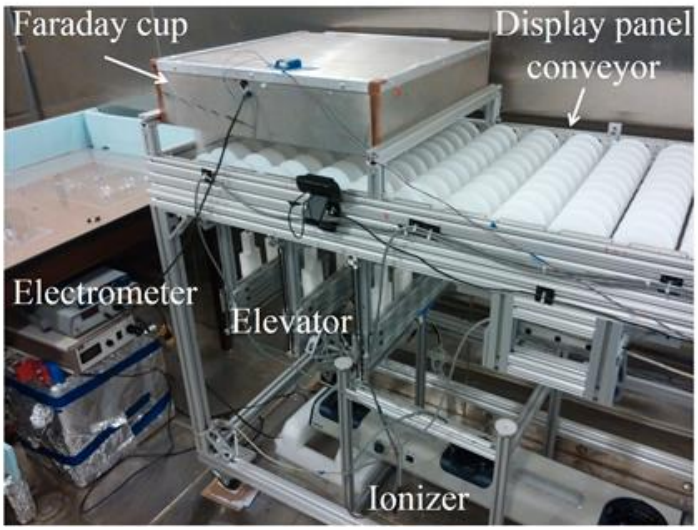

(a)

(b) (c)

Figure 2 - Measurement set-ups. (a) charge measurement of the glass by Faraday cup, (b) surface potential measurement of the glass by 2D scanner, (c) surface potential measurement of the rollers by 2D scanner.

In the second phase of the study, only the roller materials (insulative vs. dissipative), and roller radiuses (small vs. large) were investigated. In another word, the

transfer velocity (200 mm/s), the acceleration/deceleration (200 mm/s2), and the environmental condition (22°C and of 30% RH) kept consistent for all the experiments. At both phases of the study, a preconditioning procedure for the rollers and the glass was considered. As such, prior to each experiment, the glass was cleaned using a 91% Isopropyl Rubbing Alcohol (IPA) to remove the charges from previous experiments.

Table 2 - Test driving conditions.

Test	Acceleration/ Deceleration (mm/s^2)	Transfer velocity (mm/s)	Traveling Distance (m)	
I	200	100	1	0.5
II	200	200	1	0.5
III	200	300	1	0.5
IV	300	300	1	0.5

Moreover, a bar-type ionizer (BFN-803 overhead AC ionizing blower) located under the glass conveyor system was used for 30 sec in order to neutralize charges on the rollers. Subsequently, at least 30 min elapsed between using the ionizer/IPA and initiating the next experiment.

3. MEASUREMENT RESULTS AND DISCUSSIONS

3.1. TRIBOELECTRIC CHARGE MEASUREMENT BY FARADAY CUP

A comprehensive study of the effect of transfer velocity, transfer acceleration/deceleration, roller material and radius, transfer distance, and RH variation on

the triboelectric charging of the glass by the roller conveyor system was investigated. All experiments discussed in this section (except the RH variation) were performed at 22°C and 30% RH. Moreover, three glasses were used for the experiments and the mean and standard deviation values for each experiment were considered. The preconditioning of the Faraday cup experiment included using the ionizer and 91% IPA for the rollers and the glass, respectively.

3.1.1. Velocity. Transfer velocity of the glass, regardless of the roller's material or radius, will have an effect on the triboelectric charging on both the glass and rollers. Since faster transfer velocity might result in more friction force between the glass and rollers, a greater triboelectric charge can be expected. To illustrate the velocity variation on the transfer process, the transfer distance profile of a forward movement (for 1 m) of the glass with 100, 200, and 300 mm/s transfer velocities, but with the same acceleration and deceleration of 200 mm/s2 is depicted in Figure 3a. In the roller conveyor system, the glass moved with a transfer velocity of VT which is directly related to the roller's radius (RR) and angular velocity (ω) of the roller, expressed as follows:

$$V_T = R_R \times \omega \tag{1}$$

As such, in order to reach the desired transfer velocity (e.g., 200 mm/s), the angular velocity of the roller has to be determined based on the rollers' radius. In Figure 4a, the averaged total charge on the glass among three different glasses is shown after 20 back-and-forth movements with two traveling distances of 0.5 and 1 m, for 10 subsequent measurements.

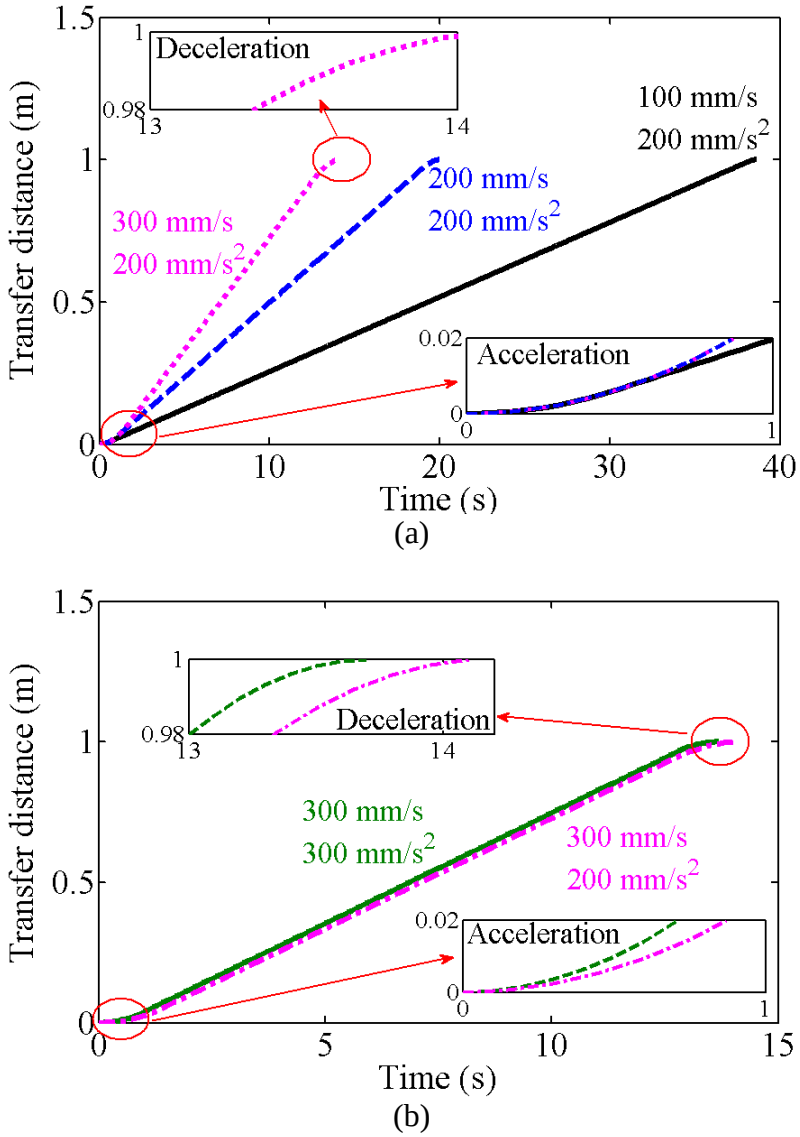

Figure 3 - Transfer distance profile comparison, (a) transfer velocity, (b) acceleration/deceleration.

For the transfer velocity study, the results for the small insulative rollers are presented. It was observed that other types of rollers presented a similar trend. As seen in Figure 4a, an increase in the glass transfer velocity from 100 to 300 mm/s resulted in greater triboelectric charge characterization of the glass. For instance, an increment from

0.38 µC to 0.49µC (~30% increment in total triboelectric charge) after 400 m displacement with 1 m back-and-forth movement can be observed for transfer velocities of 100 and 300 mm/s, respectively. The same trend observed for the transfer distance of 0.5m back-and-forth movement. However, the triboelectric charge characterization of the glass for 0.5 m back-and-forth movement is relatively lower than the 1 m back-and-forth movement. The reason could be that the glass with 0.5m back-and-forth movement was lifted up twice more than 1 m back-and-forth movement if the same overall displacement is considered. In another word, the experiment with 0.5 m back-and-forth movement included two times more lifting up action than the experiment with 1 m back-and-forth movement for the same transfer distance. However, because the difference between the charge for 1 m or 0.5 m back-and-forth is not significant, the effect of the separation from the roller by the lift-up elevator was eliminated in this paper.

3.1.2. Acceleration/deceleration. For each back-and-forth movement, the glass first accelerated to reach the desired transfer velocity from zero. Then, once the glass reached its desired transfer distance, the glass decelerated and ultimately stopped. The transfer profile for 200 mm/s^2 and 300 mm/s^2 with the same transfer velocity (300 mm/s) is depicted in Fig 3 (b), given as tests III and IV in Table 2. In an actual display manufacturing, the glass may experience only a few times of acceleration/deceleration during the transfer process by the roller conveyor system.However, each back-and-forth movement in this study resulted in a sequence of acceleration/deceleration for the glass transfer. Figure 4b presents the averaged value of the total charge measurement of the glass along with three different glasses with the same transfer velocity (300 mm/s) and acceleration/deceleration values (200 and 300 mm/s^2).

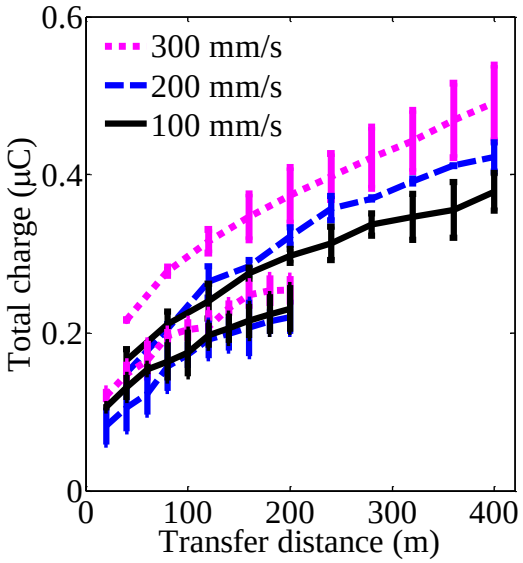

(a)

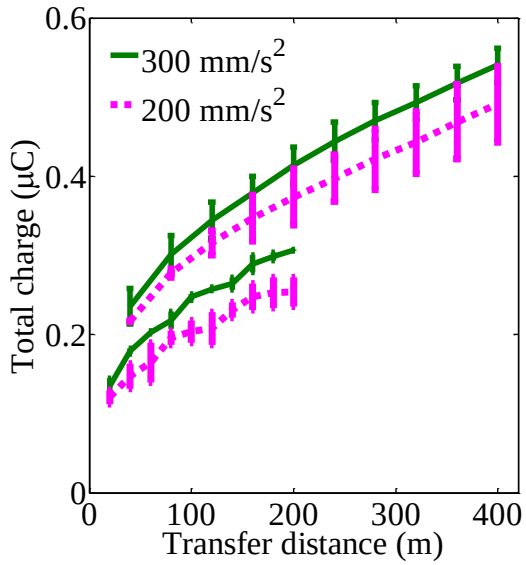

(b)

Figure 4 - Triboelectric characterization of glass for small insulative rollers. (a) transfer velocity, (b) acceleration /deceleration.

The greater acceleration and deceleration generates more friction including slipping and skidding between the glass and rollers and eventually leads to a greater triboelectric charge characterization. For instance, an increment from 0.49 μC to 0.55 μC (~12%

increment in total triboelectric charge) after 400 m displacement with 1 m back-and-forth movement can be observed for the acceleration/deceleration of 200 and 300 mm/s^2, respectively. In this figure, the results for small insulating rollers were presented while the other rollers also exposed a similar trend.

3.1.3. Material and Radius. Roller material and radius would have a major impact on the triboelectric charging on both the glass and the rollers. In electrostatic discharge (ESD) events, usually the dissipative materials are expected to reduce the triboelectric charging and also speed up the triboelectric discharge process [7]-[14]. As such, it is quite important to study the effect of material properties and the response to the triboelectric charge. Figure 5 illustrates a comparison between the averaged total measured charge of three various glasses for different roller materials and radiuses. Figure 5a to Figure 5d represent the results for four test conditions with various velocities and accelerations (see Table 2). For test conditions of velocity = 100 mm/s and acceleration/deceleration = 200 mm/s^2 (Figure 5(a)), by comparing large dissipative (LD) rollers with large insulative (LI) rollers, it was observed that the charge on the glass due to the insulative rollers was greater than the dissipative rollers after the first few movements. In addition, the triboelectric characteristic of the glass with LD rollers saturated quickly in comparison with the LI rollers. After 100 m, the triboelectric characterization of the glass due to the dissipative rollers was saturated at 0.18 μC (see solid black trace). Also, it was observed that the triboelectric characterization of the glass due to the insulative rollers has passed the triboelectric characterization of the glass due to the dissipative rollers after ~150 m transfer distance. The same trend can be observed for small insulative (SI) and small dissipative (SD) rollers. The triboelectric characteristic of the glass with SD rollers began

with the largest value and saturated quickly (e.g., at 300 m transfer distance) in comparison with the SI roller. However, the triboelectric characteristic of the insulative rollers has not saturated after 400 m transfer distance. From this plot, it can be estimated that triboelectric characterization of the glass due to the SI roller would saturate after ~800 m transfer distance. As a noticeable point, although the greatest triboelectric characterization among all types of rollers belongs to the SD rollers, if a longer distance is considered the triboelectric characterization of the glass due to the SI rollers will ultimately pass the SD trace. In other words, for a shorter distance the triboelectric charge of the glass due to dissipative rollers might be greater (compared to the charge at the first movements); however, for a longer transfer distance ultimately the glass would be saturated at a smaller value than using insulative rollers. Such a tendency may lead to a recommendation to use dissipative rollers for longer transfer distance (which is the most case at an actual display panel manufacturing) since they resulted in a smaller saturated charge. All above observations can be applied to the results of other test conditions (Figure 5 (b) to Figure 5 (d)).

In the roller conveyor system, the glass moved with a transfer velocity of VT which is directly related to the roller's radius (RR) and angular velocity (ω) of the roller, given in (1). In order to reach similar transfer velocity and acceleration/deceleration (e.g., 200 mm/s and 200 mm/s^2) for larger rollers in comparison with small rollers, the angular velocity (i.e., the number of revolutions per sec of the transfer motor) and the angular acceleration/deceleration had to decrease three times from small rollers to large rollers. As mentioned before, the radius of the large rollers was three times greater than the small rollers.

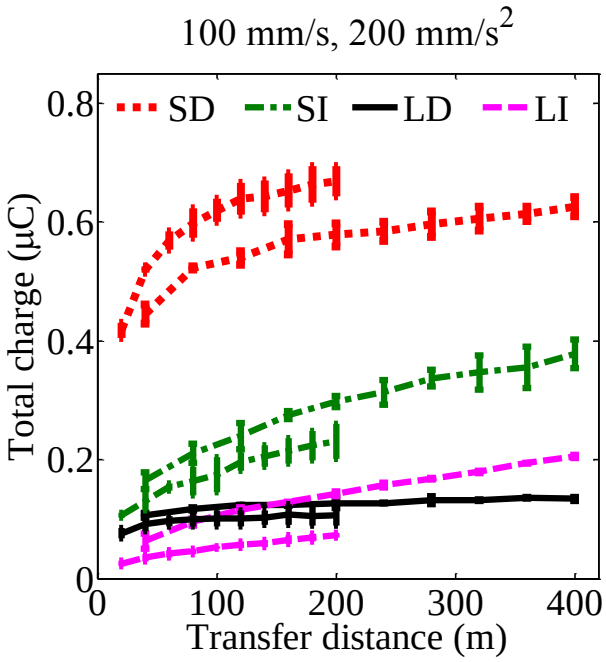

(a)

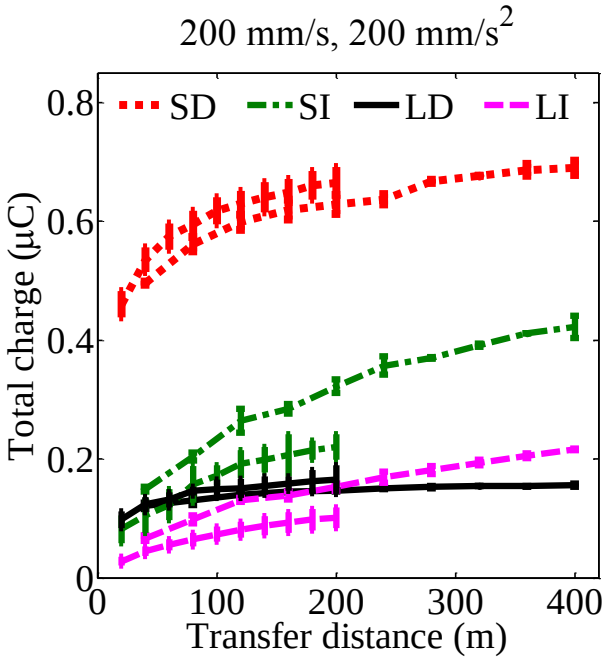

(b)

Figure 5 - Triboelectric characterization for various rollers material and diameter. (a) 100 mm/s, 200 mm/s^2, (b) 200 mm/s, 200 mm/s^2, (c) 300 mm/s, 200 mm/s^2, (d) 300 mm/s, 300 mm/s^2. (SD, SI, LD, and LI represent small dissipative, small insulative, large dissipative, and large insulative, respectively).

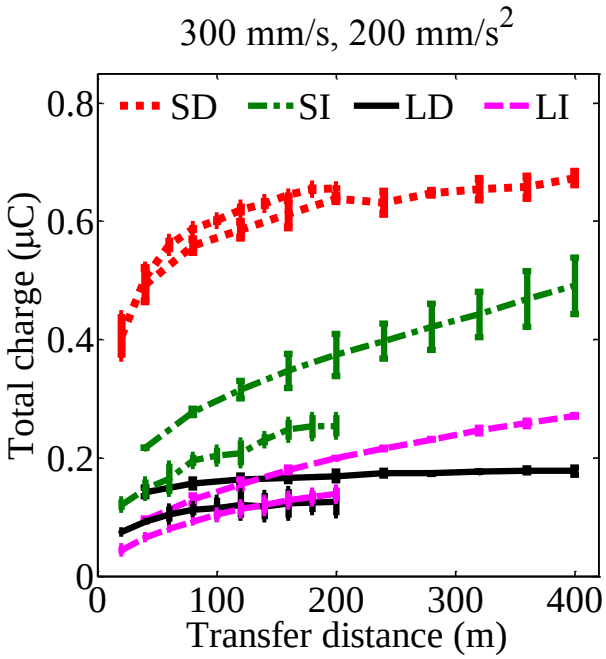

(c)

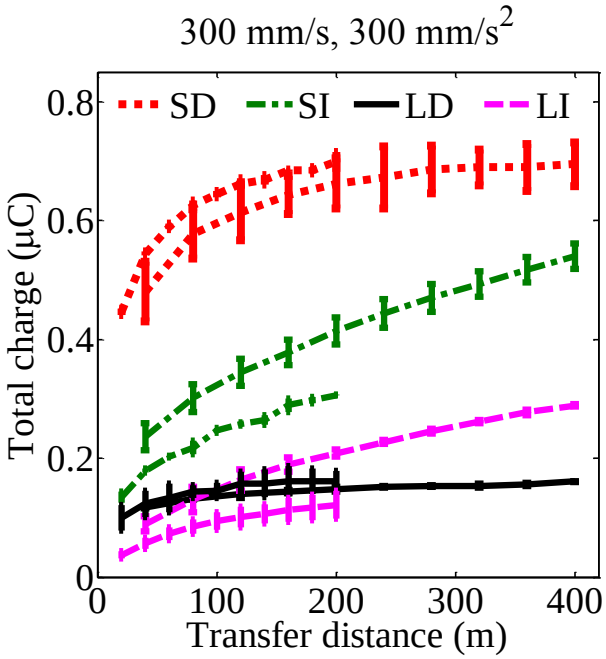

(d)

Figure 5 - Triboelectric characterization for various rollers material and diameter. (a) 100 mm/s, 200 mm/s^2, (b) 200 mm/s, 200 mm/s^2, (c) 300 mm/s, 200 mm/s^2, (d) 300 mm/s, 300 mm/s^2. (SD, SI, LD, and LI represent small dissipative, small insulative, large dissipative, and large insulative, respectively). (Cont.)

It can be observed from the comparison between the triboelectric characterization of the glass and different roller radiuses that large rollers led in a lower triboelectric characterization. The reason might be due to the fact that the angle at which the roller's surface meets the glass is smaller for larger rollers (see Figure 6 (a)), so the speed in which the roller is moved away from the glass is slower for larger rollers. In other words, the angle between the glass and the surface of the small rollers varies faster than larger rollers. This can be lead to more charge separation between the glass and smaller rollers. Moreover, slower angle variation between the glass and the larger rollers may enhance the charge neutralization between the glass and the large rollers. For the better comparison, Figure 6 (b) represents part of the result shown in Figure 5 (a). In Figure 6c, the triboelectric charge values of the larger rollers are multiplied by a constant coefficient (i.e., proportional to the radius ratio) to match the results of small rollers. In this figure the multiplication factor α_1 is set to 4.5 for LD and α_2 is set to 2.1 for LI. The reason that the coefficient, which leads to the best match, is not equal to three (i.e., radius ratio) might be that other factors such as surface roughness influence the charge build up. However, the ratio and the explanation using the surface separation speed indicate that the charging is anti-proportional to the radius. The conclusion from this observation could be applicable for display panel manufacturing, as for the same transfer velocity, larger rollers may be helpful for less triboelectric charging compared to small rollers.

3.1.4. Humidity. Some previous literature studied the effect of environmental conditions (such as RH and temperature) on the amount of triboelectric charging [7]-[16] and it was shown that increasing the RH can reduce the probability of triboelectric charge generation in data centers or in hospitals. These observations are all in line with most the

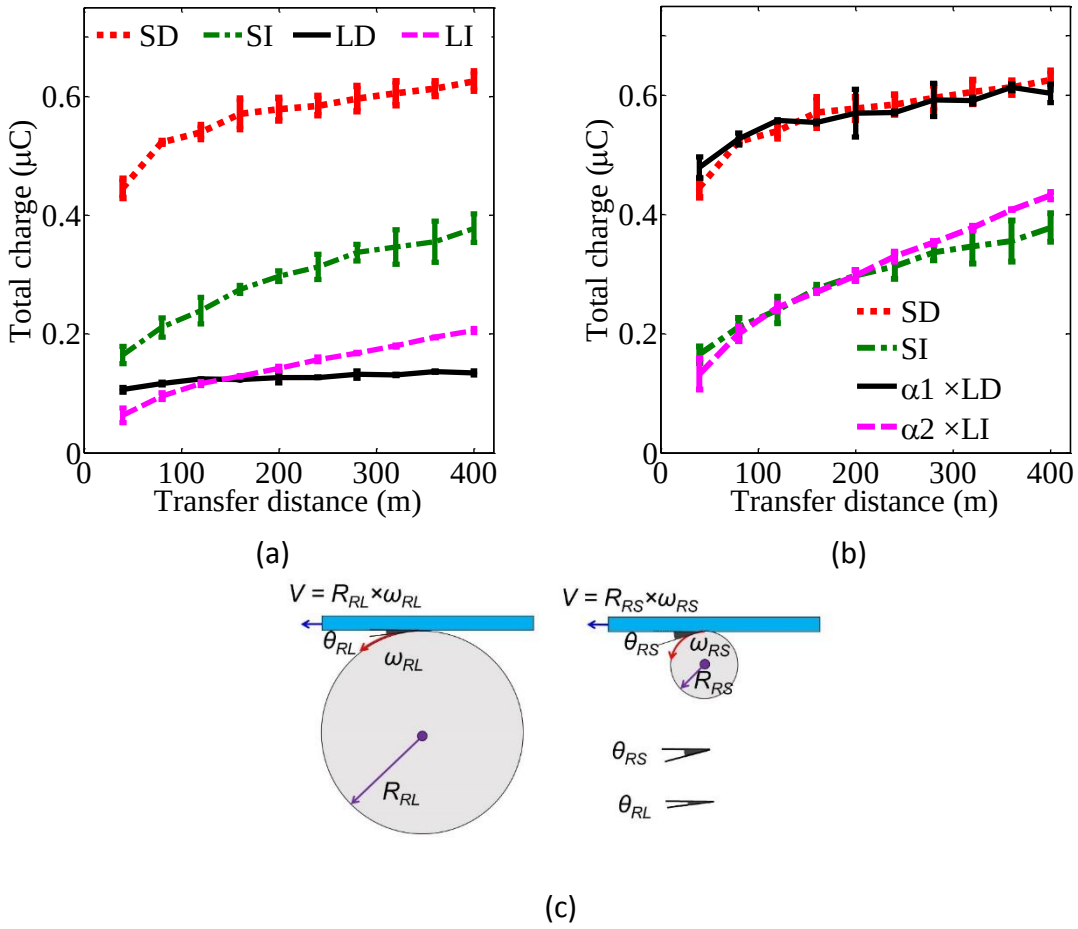

Figure 6 - (a) conceptual diagram of the effect of larger roller on the angle between the glass and roller, (b) before, (c) after multiplication.

often observed behavior in tribo-electrification. However, there are also papers e.g., [17]-[18] that contradict the most often observed behavior. Based on this knowledge, the effect of RH on triboelectric characterization for the roller conveyor system was investigated. For the RH test measurement, small dissipative rollers were considered since the glass was saturated faster (shown and discussed in Figure 5). For RH variation of 20% to 50%, shown in Figure 7, Test II and IV from Table 1 with 1 m traveling distance (total of 400 m transfer distance) were considered. From the results, it was observed that increasing RH from 30%

to 50% can reduce the saturated triboelectric charge about half. The outcome of this investigation can also be considered for display panel manufacturers.

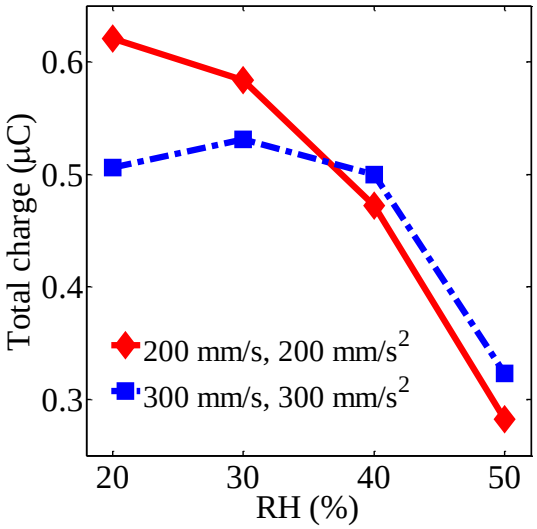

Figure 7 - Triboelectric characterization of glass at various humidity.

3.2. SURFACE VOLTAGE MEASUREMENT BY 2D SCANNER

In this section, the charge distribution on the glass and rollers are presented for rollers with different material and radiuses using a 2D automated scanner. The transfer velocity and acceleration/deceleration values for all results were 200 mm/s and 200 mm/s^2, respectively, with the ambient temperature of 22°C and 30% RH. The preconditioning of the scanning experiment included using an ionizer and 91% IPA for the rollers and the glass, respectively. Because the upper limit of our non-contact electrostatic voltmeter (TREK model 347 [24]) was 3.5 kV, the experiments were arranged based on this restriction.

3.2.1. Rollers. Rollers will charge up when glass travels on them, however, the amount of charge will vary based on the roller material and radius. In order to scan the rollers, the middle part of the conveyor system was scanned for an area of 400 mm × 400 mm, as shown in Figure 2 (b). Before the experiment, the rollers were scanned to ensure the voltage on the rollers is about zero after the preconditioning. To make sure that entire circumference of the rollers touched the glass, the glass was moved 100 times back-and-forth for 1 m traveling distance. Subsequently, the rollers were scanned. The measurement principle of the instrument is explained in .[24] Figure 8 indicates the different values measured by the instrument on the rollers after 100 glass movements and the initial condition for all types of the rollers. Rollers are located along the Y-direction and the roller shafts are separated along the X-direction. Since the shaft of the rollers was grounded, it was expected that for the dissipative rollers, represented in Figure 8 (a) and Figure 8 (b), the surface voltage (i.e., the measured value when the probe is on the rollers) was about 0 volts regardless of the roller radius. For the insulative rollers, the surface potential on the rollers should have a lower negative value (or greater absolute value), shown in Figure 8c and Figure 8 (d). As expected, the small insulative rollers exposed lower negative voltage value (or greater absolute value) than the large rollers. The results support the discussion in Section 3.1. for the triboelectric characterization of the roller with various radius.

From Figure 8 (d), the rather homogeneous voltage can be seen for the large insulative rollers and it indicates that large insulative rollers obtained less charge after 100 movements than small insulative rollers.

3.2.2. Glass. Scanning the surface voltage of the glass has to lead to the similar observation of the Faraday cup experiments. Scanning was performed before the

movement (to indicate the initial voltage), after 1 m back-and-forth movement, and after the second round of 1 m back-and-forth movement. The glass lifted up by the elevator, and the non-contact electrostatic voltmeter probe was adjusted with the lift-off distance of ~3 mm to the glass. The scanning area was for 400 mm × 400 mm. All scanning images were referenced to the initial scanning results (the voltage difference between the first movement

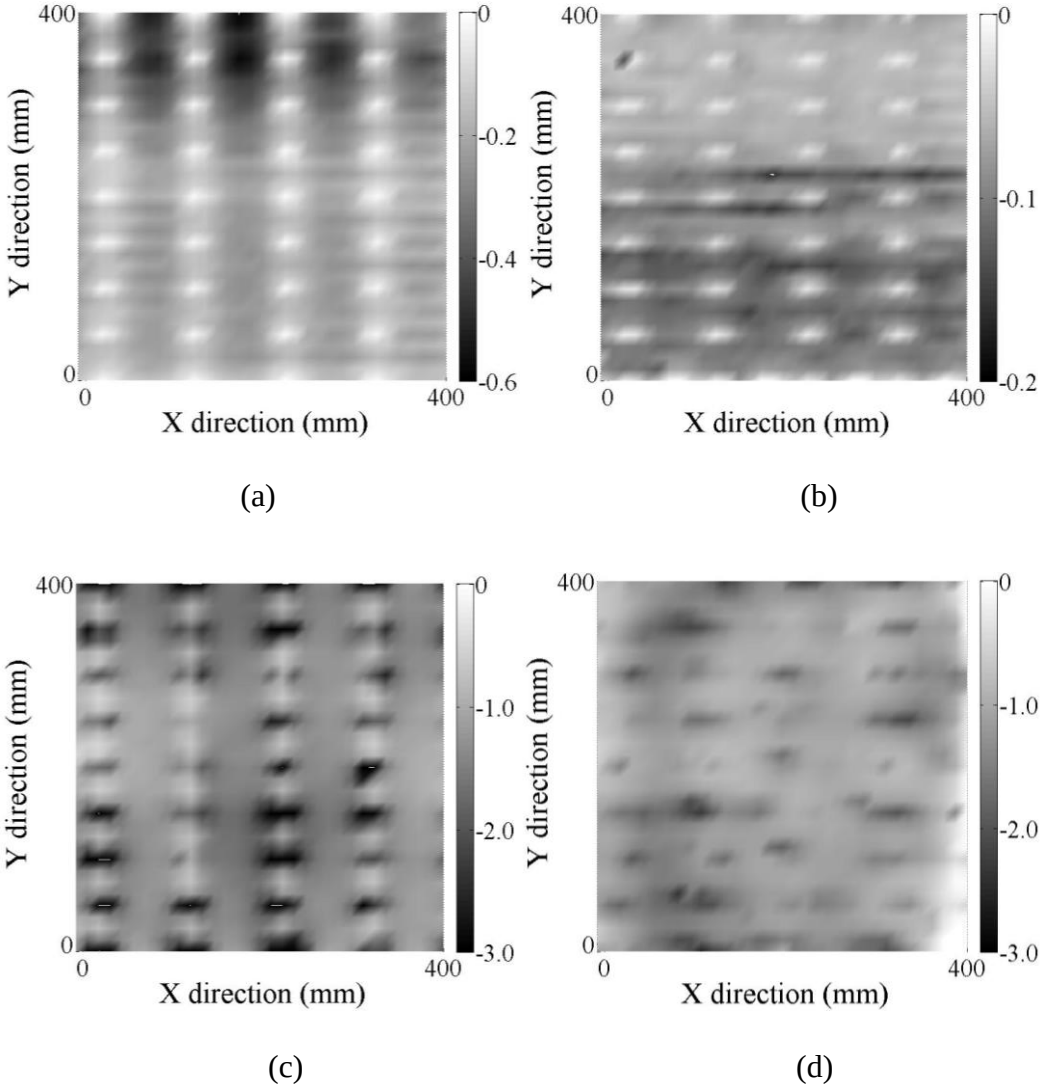

Figure 8 - Measured value by the instrument for the different rollers after 200 m glass transferred. (a) small dissipative, (b) large dissipative, (c) small insulative, (d) large insulative rollers (the color map indicates the voltage is in kV).

and the initial condition, or the second movement and the initial condition). The results of the scanned glass along with a histogram of the voltage difference distribution on the surface of the glass are depicted in Figure 9 for all types of roller conveyor system. The color map indicates the voltage in kV. As expected from the Faraday cup experiments, the glass moved by small dissipative rollers must expose greater voltage distribution. Moreover, large rollers have to lead to less voltage distribution on the glass than the small rollers.

A comparison between the first rows of Figure 9 for different rollers represents that utilizing small dissipative rollers resulted in the greatest charge on the surface of the glass. This observation is in agreement with the Faraday cup experiment. From the histogram, the average and standard deviation of the voltage distribution on the glass with small dissipative rollers was 2.20 kV and 0.3 kV, respectively. The corresponding values for small insulative rollers were 1.23 kV and 0.43 kV. Moreover, large insulative and dissipative rollers generated less voltage on the glass with an average value of 0.56 kV and 0.54 kV, respectively.

These low voltage values were also along with total charge measurement by the Faraday cup. After the second movement, the glass traveled by small dissipative roller gained more charge in comparison with small insulative rollers. It was observed that the glass transferred by the larger radius obtained less charge in comparison with small radius. In the fourth row, the voltage distributed histogram after the second round of 1 m traveling distance is presented. A comparison between the histogram of small insulative rollers and small dissipative rollers implied a wider histogram (greater σ) for small insulative rollers.

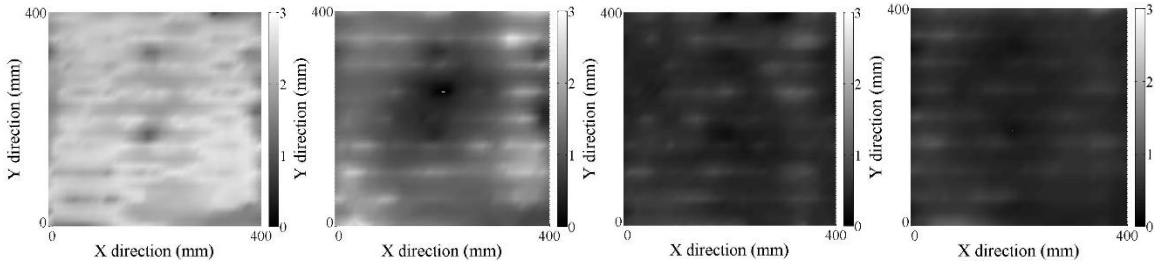

(a) Surface voltage distributed on the glass, after 1st movement

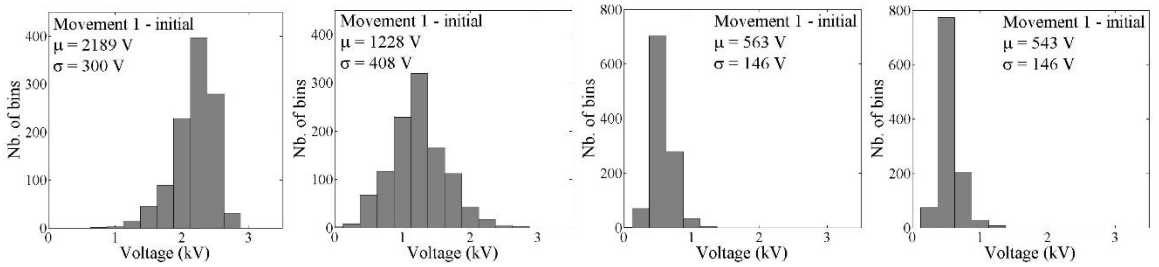

(b) Histogram of surface voltage distributed on the glass, after 1st movement

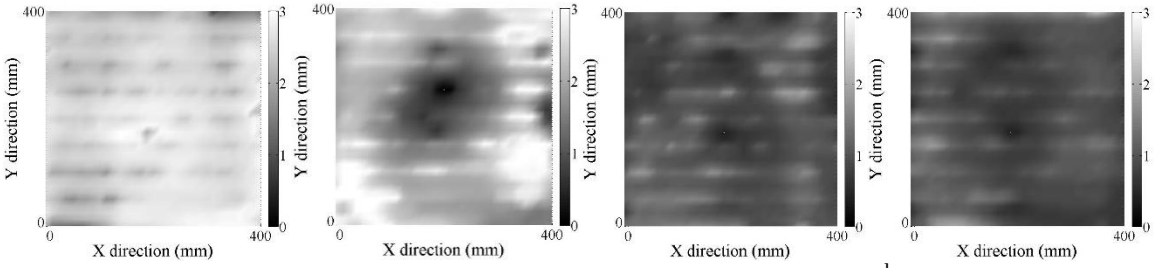

(c) Surface voltage distributed on the glass, after 2nd movement

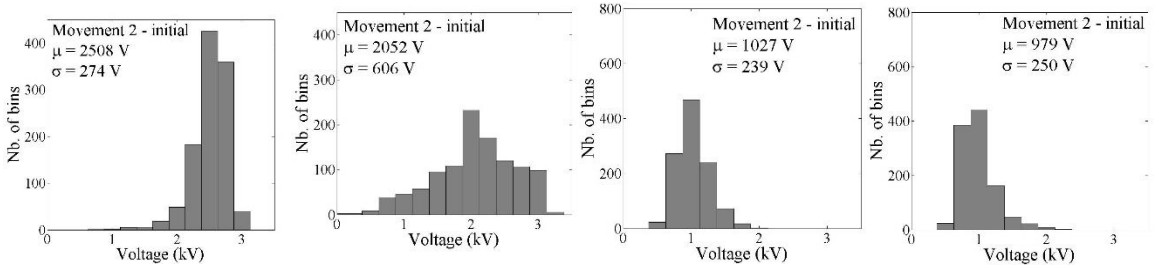

(d) Histogram of surface voltage distributed on the glass, after 2nd movement

Figure 9 - Surface potential results of the glass transferred by different rollers. 2D image and histogram (the color map voltage scale is in kV). μ and σ are the mean and standard deviation of the surface voltage distribution, respectively. [left to right: SD, SI, LD, LI].

3.2.3. Time Decay. Since the resistance of the dissipative roller is much smaller than an insulative roller, charge decay on the dissipative roller is much faster (e.g., by a

factor of ~10^4). Generally, the charge inside or on the surface of an insulating roller will leak away very slowly according to an approximately exponential function, given by:

$$Q = Q_0 \, \mathrm{e}^{-t/\tau} \tag{2}$$

where τ is the time decay constant [7]. In order to obtain the time decay constant of insulative rollers, an experiment was defined in such a way that the glass touches the circumference of the rollers continuously (back-and-forth). The diagram of the glass movement is shown in Figure 10a. As such, a point of the roller circumference was marked and the glass was located on top of that roller on that point. Then, the glass was transferred forward with a traveling distance of 282.7 mm (i.e., $2\pi R$, a full rotation/revolution of the roller), where R is the radius of the roller. The transfer velocity was 200 mm/s. Then, the glass was transferred backward with the same velocity and distance. This procedure was repeated 100 times to ensure that the whole circumference of the roller homogeneously touched the glass and obtained enough charge. Then, the glass moved away. The electrostatic probe moved to the marked position on the roller and measured the surface voltage at the marked position on the roller (Figure 10 (a)) after five seconds sec for one hour. In our case, the large insulative roller was investigated and it was found in practical terms that the decay time is at the range of $\tau = 1.5\times10^5$ sec. This value is practically large enough to indicate the charge on the insulative rollers will stay for a long time. This fact can illustrate the potential reason that the glass with insulative rollers has an exponential triboelectric characterisation and the glass is not saturated quickly in comparison with the dissipative rollers. The experimental data and the exponential are shown in Figure 10 (b).

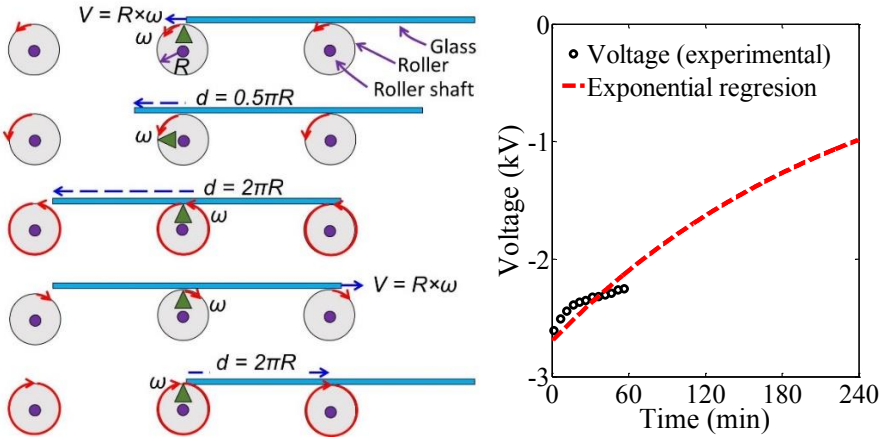

(a) (b)

Figure 10 - (a) time decay experiment procedure, (b) experimental results.

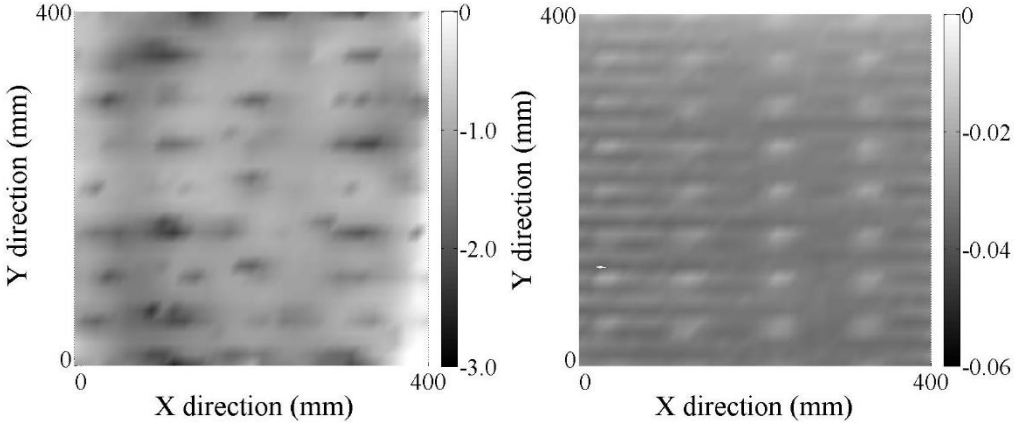

(a) (b)

Figure 11 - Surface potential results of the insulative rollers. (a) after 200 m glass displacement, (b) subsequently, utilizing ionizer.

3.2.4. Ionizer. As discussed in [1], since triboelectric charges are high in display panel manufacturing due to the high production speeds (to achieve profitability), utilizing ionizers is inevitable. For our experiments, the ionizer was only used as a precondition process. However, it was necessary to examine its performance on neutralizing the charge on the rollers. As such, the measured value by the instrument (i.e., the surface potential

when the probe is on the rollers) of the large insulative rollers before and after utilizing the ionizer are shown in Figure 11. In Figure 11 (a), it was observed that the insulative rollers after 100 m glass transfer had about -2.5 kV surface potential. However, after using the ionizer for 30 sec, the surface potential on the rollers was around 0 volts. This result indicated that our preconditions to use the ionizer for rollers before running the next experiment were done properly.

4. CONCLUSION

In this paper, a bidirectional roller conveyor system was fabricated to systematically study the triboelectric charging of the glass during the roller transfer process. Two different types of rollers with insulating and dissipative properties were made. Ultra-high-molecular-weight (UHMW) polyethylene material was used for the insulative rollers, and the dissipative rollers were made of UHMW polyethylene containing carbon particles. The measured resistances of the insulative and dissipative rollers were 6.9×10^{11} and $2.7\times10^{8}\ \Omega$, respectively. For each roller material two different sets of rollers were fabricated with the radius of RR = 30 and 90 mm with the thickness of TR = 10 mm, referred to as small dissipative (SD), small insulative (SI), large dissipative (LD), and large insulative (LI). To obtain the triboelectric characterization of the glass versus the transfer distance, a Faraday cup with an elevator system was mounted on the apparatus to measure the total charge on the glass. Two traveling distances (1 m and 0.5 m) with various transfer velocities (100 mm/s to 300 mm/s), and acceleration/deceleration (200 mm/s^2 and 300 mm/s^2) were studied. Moreover, RH variation (20% to 50%) on the triboelectric characterization of the glass was investigated. In addition, by utilizing a 2D automated

scanner, a comprehensive study including the 2D image of surface voltage distribution of the glass and rollers as well as a histogram of surface voltage distribution of the glass was presented. From the results, it can be concluded that:

- The amount of charge accumulated on the glass transferring by dissipative rollers was saturated faster at a smaller value than by insulative rollers.
- For shorter distances, the dissipative rollers exposed a greater charge on the glass in comparison with insulative rollers. However, after some distances the glass traveled by dissipative rollers was saturated and ultimately the triboelectric characterization of the glass due to insulative rollers would pass the triboelectric characterization of the glass due to dissipative rollers.
- Faster transfer velocity of the glass for each specific roller resulted in greater triboelectric characterization.
- Higher acceleration/deceleration of the glass led to greater triboelectric characterization.
- Decreasing the RH from 50%RH to 20%RH resulted in a 50% increase in the triboelectric charge.
- From the time decay experiment of the rollers, insulative rollers have a time decay of ~1.5×10^5. For dissipative rollers the time decay was too fast and not practical to measure it.
- For the same transfer velocity of the glass, larger rollers resulted in a lower triboelectric characterization on the glass. The reason might be due to surface to surface separation speed which is about three times slower for the large rollers.

Finally, from the comprehensive study of various parameters, a list of recommendations for industrial applications can be given as:

- Dissipative rollers are better for longer transfer distance,
- Larger rollers resulted in a lower triboelectric charging on the glass,
- There is a trade-off between speed of glass transfer (and also acceleration/deceleration) and triboelectric charge. Depending on the maximal charge levels acceptable the speed and acceleration need to be adjusted.

REFERENCES

[1] T. Murakami, H. Togari, and A. Steinman, “Electrostatic problems in TFT-LCD production and solutions using ionization,” In Electrical Overstress Electrostatic Discharge (EOS/ESD) Symposium Proceedings, pp. 365-370, 1996.

[2] D. Kim, C. Lim, S. Yoon, S. Jung, D. Oh, J. Kim, H. Kim, et al, “Electrostatic control and its analysis of roller transferring processes in FPD manufacturing,” In IEEE 35th Electrical Overstress/Electrostatic Discharge (EOS/ESD) Symposium, pp. 1-6, 2013.

[3] J. Yoo, D. Kim, W. Ho, J. Jeong, B. Park, and A. Steinman, “Comparing room ionization technologies in FPD manufacturing,” In IEEE 34th Electrical Overstress/Electrostatic Discharge (EOS/ESD) Symposium, pp. 1-6, 2012.

[4] D. S. Kim, “A study of electrostatic charging and discharging characteristics on glass in FPD manufacturing,” PhD dissertation, Korea University, June 2014.

[5] K. H. Kim, D. Pommerenke, Y. Gan, N. Goo, and S. Lee, “Multi-physics simulations for triboelectric charging of display panels during the roller transfer process." In IEEE 37th Electrical Overstress/Electrostatic Discharge (EOS/ESD) Symposium, pp. 1-8, 2015.

[6] K. H. Kim, A. Talebzadeh, D. Pommerenke, J. Birt, L. Guan, N. H. Goo, and Y. Kim, “A study on the triboelectric charging of display glass during the roller transfer process–modeling and characterization,” Journal of Electrostatics, vol. 86, pp. 24-33, 2017.

[7] A. Talebzadeh, M. Moradian, Y. Han, A. Patnaik, D. E. Swenson, and D. Pommerenke, "Dependence of ESD charge voltage on humidity in data centers: Part I-Test methods," ASHRAE Trans., vol. 121, pp. 58–70, 2015

[8] A. Talebzadeh, A. Patnaik, X. Gao, D. E. Swenson, and D. Pommerenke, "Dependence of ESD charge voltage on humidity in data centers: Part II-Data analysis," ASHRAE Trans., vol. 121, pp. 37–48, 2015

[9] X. Gao, A. Talebzadeh, M. Moradian, Y. Han, D. E. Swenson, and D. Pommerenke, "Dependence of ESD charge voltage on humidity in data centers: Part III-Estimation of ESD-related risk in data centers using voltage level extrapolation and Che bys HEV's inequality," ASHRAE Trans., vol. 121, pp. 49–57, 2015.

[10] A. Talebzadeh, M. Moradian, Y. Han, D. E. Swenson, and D. Pommerenke, "Electrostatic charging caused by standing up from a chair and by garment removal," Proc. 2015 IEEE Symp. Electromagn. Compact. Signal Integrity, pp. 57–62, 2015.

[11] A. Talebzadeh, M. Moradian, Y. Han, D. Swenson, and D. Pommerenke, "Effect of Human Activities and Environmental Conditions on Electrostatic Charging," IEEE Trans. on Electromagnetic Compatibility, vol. 58, no. 4, pp. 1266-1273, 2016.

[12] M. Moradian, A. Patnaik, Y. Han, F. Wan, X. Gao, D. Pommerenke, and D. E. Swenson, "Determination of the effect of humidity on the probability of ESD failure or upset in data centers," ASHRAE Trans., vol. 120, pp. 25-41, 2014.

[13] B. Moasa, E. Helerea, M. Ignat, and G. Telipan, "Experimental research on dissipative textile structures," 2014 IEEE International Conference on Optimization of Electrical and Electronic Equipment (OPTIM), pp. 155-160, 2014.

[14] G. Telipan, M. Ignat, L. Catanescu, and B. Moasa, "Electrostatic discharge testing of several ESD protective textiles used in electronic industry," 2014 IEEE International Conference and Exposition on Electrical and Power Engineering (EPE), pp. 602-605, 2014.

[15] F. Wan, V. Pilla, J. Li, D. Pommerenke, H. Shumiya, and K. Araki, "Time lag of secondary ESD in millimeter-size spark gaps," IEEE Trans. on Electromagnetic Compatibility vol. 56, no. 1, pp 28-34, 2014.

[16] M. Kohani, and M. Pecht, "New Minimum Relative Humidity Requirements Are Expected to Lead to More Medical Device Failures," Journal of medical systems vol. 40, no. 3, pp. 1-6, 2016.

[17] L. Liu, Electrostatic Generation and Control on Textiles, North Carolina State University, pp. 42-43, 2010.

[18] J. A. Wiles, et al., “Effects of Surface Modification and Moisture on the Rates of Charge Transfer between Metal and Organic Materials,” J. Phys. Chem. B, pp. 20296-20302, 2004.

[19] http://www.trekinc.com/products/347.asp

[20] W. D., Greason, I. M. Oltean, Z. Kucerovsky, and A. C. Ieta. "Triboelectric charging between polytetrafluoroethylene and metals." IEEE Trans. on Industry Applications, vol. 40, no. 2, pp. 442-450, 2004.

V. SHIELDING EFFECTIVENESS, COUPLING PATH, AND EMI MITIGATION FOR QSFP CAGES WITH HEATSINK

ABSTRACT

Quad form-factor pluggable (QSFP) interconnections shielding cages with heatsinks are often optimized for thermal, mechanical, and volume manufacturing. In this paper, shielding effectiveness (SE) of QSFP cages including two configurations of 1×1 and 1×6 with three cases of normal (i.e., rising) heatsink, without a heatsink, and with a modified heatsink is measured for the frequency range of 1-40 GHz using a dual reverberation chamber. For each measurement, three different vendors of optical modules are utilized and averaged SE is achieved for each case, indicating that the rising heatsink degrades the SE around 5 to 10 dB compare to the no heatsink or modified heatsink. Further, energy parcels and their trajectory concept are applied to visualize the coupling paths in a rising heatsink. The rising heatsink creates a new coupling path for EM waves to leak to the cage and emit from the chassis faceplate. From the energy parcel results, an EMI mitigation technique is proposed for the newly created coupling path by the rising heatsink and its performance is evaluated with SE measurements. Further, an active measurement with an evaluation board using a 40Gbps optical module is performed with and without the EMI mitigation technique.

Index Terms—QSFP interconnect; heatsink; shielding effectiveness; coupling path, EMI mitigation; TRP; reverberation chamber; energy parcel; EMI/EMC.

1. INTRODUCTION

QSFP interconnection is a compact transceiver used for telecommunication and data communication applications. Its features are four electrical lanes that operate at 10Gbps to provide 4×10 Gbps Ethernet systems [1]. The throughput of QSFP interconnection is further raised from 4×10 Gbps to 4×28 Gbps, known as QSFP28, to address 100 Gbps network applications [2]-[3]. Today, they have favorable application in high-end and low-end switches and routers, placed on the faceplate of the system chassis. For the electromagnetic interference (EMI) point of view, however, the big challenge is to maintain the radiation limit lower than a certain margin to meet electromagnetic compatibility (EMC) regulatory requirements. Approaching further higher data rates for network systems from 100Gbps to 200/400 Gbps is currently under development based on doubling the density of QSFP interconnections, so-called QSFP-DD, in which eight lanes operate at up to 25 Gbps via NRZ modulation or 50 Gbps via PAM4 modulation providing 200 Gbps and 400 Gbps speed, respectively [4]-[5].

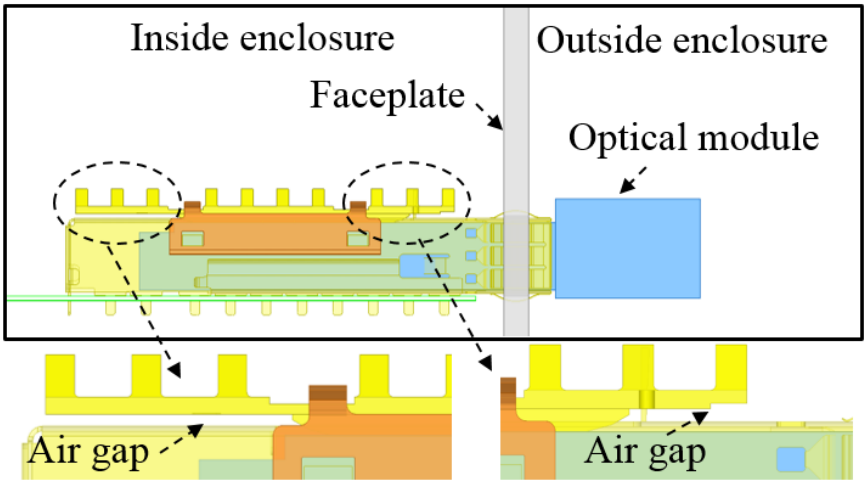

Figure 1 - Rising heatsink when optical module is inserted.

The introduction of double density technologies is expected to further increase radiation emission by a few dB because of the doubled transmitted power in the QSFP-DD interconnections. Thus, it is required to revisit the design of the key components which are placed on the front-end of the system chassis faceplate consisting of the QSFP interconnection, QSFP shieling cage, and the optical module to make them more effective against emission. One of the components that is particularly investigated in this paper, is the QSFP shielding cages possessing a heatsink. The heatsink is required to cool down the optical modules placed inside the QSFP shielding cage [6]. However, when the optical module is inserted, the heatsink rises as depicted in Figure 1. The air gap created by a rising heatsink can degrade the shielding effectiveness (SE) of the cage. Extensive efforts have been made over the years to study the EMI associated with high-speed high-density interconnections including edge-coupled PCB backplane connectors [7]-[11], and board-to-board interconnections (i.e., SFP and QSFP) [12]-[14]. The interconnections often contribute to radiation emission and potentially increase the system noise. Some EMI mitigation techniques have been evaluated to reduce emission from interconnections [15]-[16]. Furthermore, the EMI coupling paths and the resulting unintentional currents that lead to radiation in the optical link are described in [17]-[20]. The board-to-board interconnects and the flex cables in optical modules are the dominant sources of emission in active operation of the modules [17], [18], and [20]. However, the QSFP shielding cages have not been investigated yet. They are often optimized for thermal, mechanical, and volume manufacturing, but EMI performance is only intuitively considered. Imperfections allow system noise, typically from ASICs, ICs, PCB routing, and interconnections to leak in the QSFP shielding cages and emit from the chassis faceplate. Improving the EMI SE of the

QSFP shielding cages improves the overall EMI performance of networking systems to meet global and customer-driven EMC regulations. In this paper, understanding the effect of the rising heatsink on the SE performance of a QSFP cage is investigated as shown in Figure 1. Two different cage configurations of 1×1 and 1×6 cages are selected. The SE of QSFP is measured for the frequency range of 1-40 GHz using a dual reverberation chamber [21]-[23]. Measuring the SE of the cage is referred to as "passive measurement" because the optical module is not operating and there is no signal path to the QSFP interconnection. To visualize possible coupling paths, the concept of energy parcel is applied. It shows the energy flow through the newly created gaps at the rising heatsink. Then, an EMI mitigation technique is proposed and its performance is evaluated with the passive measurements. Finally, an active measurement with a module compliance board (MCB) using 40 Gbps optical module is performed with and without the EMI mitigation technique.

2. SHIELDING EFFECTIVENESS MEASUREMENT

A spare actual PCB line card with 0.3 cm thickness is used for the SE measurement, which focuses on the system noise leakage in QSFP cages and the emission out of the chassis/enclosure faceplate. As such, only the shielding cage was mounted on the PCB line card. The stirred dual reverberation chamber is used to obtain the SE of the QSFP cage. Figure 2 depicts the measurement setup. On the noisy side, Tx antenna provides the EM waves and on the quiet side, received power is measured by Rx antenna. For the design of experiment, three different vendors of optical modules are utilized for the measurement. To eliminate the design variation on the optical modules and focus only on their mechanical

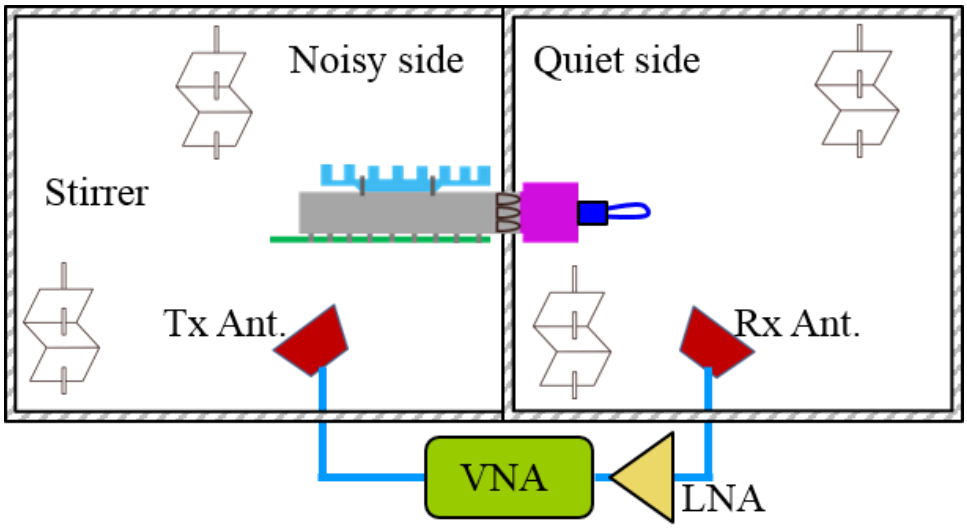

Figure 2 - Setup diagram for SE measurement.

feature, two types of aluminum cuboids are made with similar exterior dimension of optical modules. Cuboid #1 is similar to the optical modules and raises the heatsink. Cuboid #2, however, has a smaller height in the middle and doesn't raise the heatsink. The normal and modified heatsinks as well as the cuboids are shown in Figure 3.

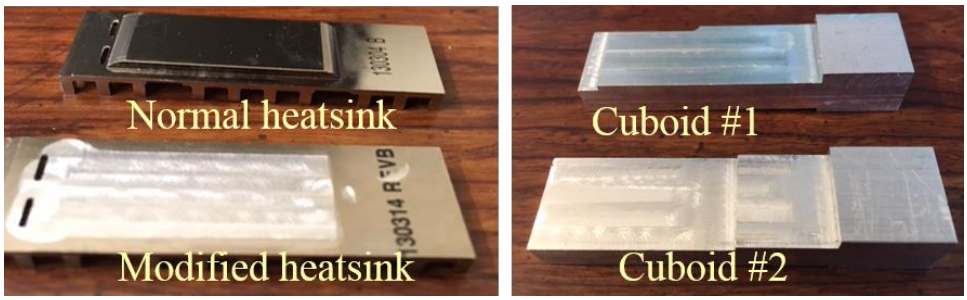

(a) (b)

Figure 3 - (a) heatsinks, (b) cuboids.

To explore the effect of a rising heatsink on the SE of the QSFP cage, different conditions are explored including a cage with a normal heatsink (Figure 4-left), a cage

without heatsink (Figure 4-middle), and a cage with a modified heatsink in which the pedestal part is removed (Figure 4-right).

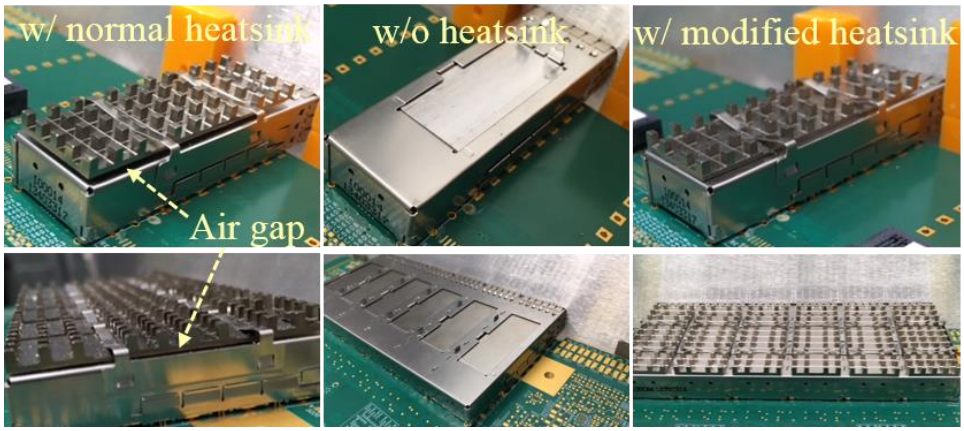

Figure 4 - Various cage configurations. 1×1 (top) and 1×6 (bottom).

2.1. CAGE CONFIGURATION OF 1×1

The SE of QSFP cage is obtained relative to the baseline measurement. In this study, the faceplate without the cage (i.e., an open aperture) is considered for the baseline measurement, as represented in Figure 5 (a) for the 1×1 cage and Figure 5 (b) for the 1×6 cage. Fig. 5 (c) depicts the cross section of the faceplate. The EM waves leak out from either the gap between the cage and the faceplate, or the gap between the cage and the optical module. The QSFP cages are designed with spring finger contacts (also known as a gasket) around their mouth. The spring finger is supposed to close any gap between either the cage and faceplate, or the cage and the module. However, the mechanical tolerance of the design results in an imperfection and lead the EM waves out of the faceplate. The IEEE standard for SE measurement is defined as [24]:

$$SE[dB] = 10\log_{10}\frac{P_1}{P_2} \tag{1}$$

where P_1 is the measured power in W at the receiver (or the quiet) side of the dual reverberation chamber when the faceplate with an open aperture is placed between two chambers. Similarly, P_2 is the measured power in W at the quiet chamber, when the faceplate with the cage is placed between two chambers. Because three different vendors of optical modules are utilized, the averaged SE over the modules is obtained as:

$$\overline{SE}[dB] = 10\log_{10}\frac{P_1}{\langle P_2 \rangle_{MO}} \tag{2}$$

where $<P_2>_{MO}$ is the average received power over the different modules. Figure 6 shows the averaged SE of the cage for two separate frequency bands of 1-18 GHz and 18-40 GHz.

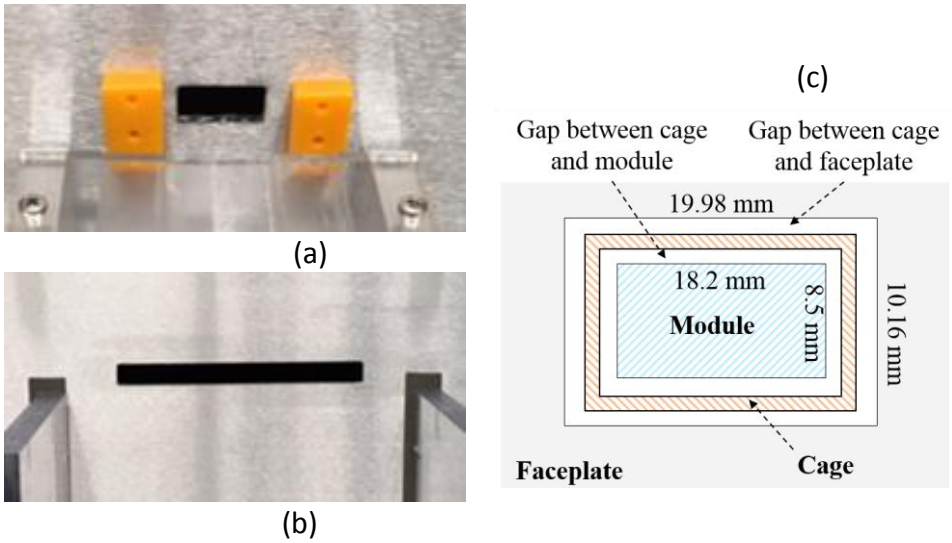

Figure 5 - (a) open aperture for 1×1 cage, (b) open aperture for 1×6 cage, (c) the cross-section of the faceplate when the module is inserted.

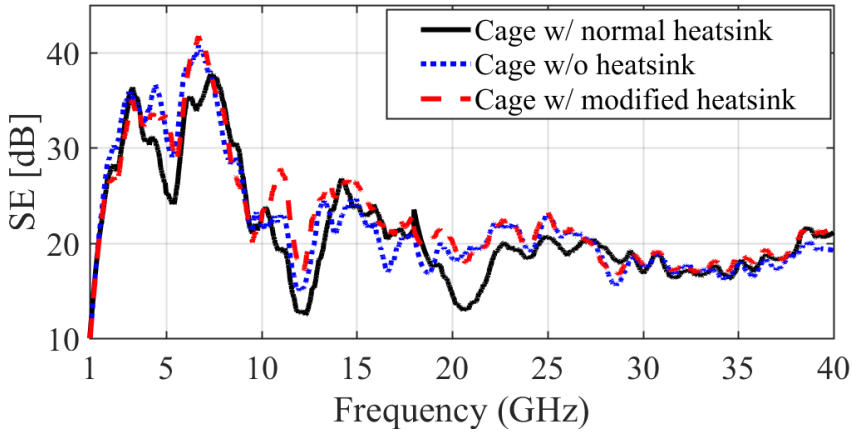

Figure 6 - Averaged SE of the 1×1 cage over three different modules.

The SE of the cage with the modified heatsink has the highest SE over the whole frequency range than the two other cases because the modified heatsink is not raised and, thus, no air gap is created. The cage with no heatsink exhibits a better SE than the cage with a normal (rising) heatsink. This observation indicates that the cage with a rising heatsink provides a leakage path for EM waves inside the cage, and further on via the opening to the quite chamber. Thus, the SE of the cage with the normal heatsink is a few dB lower than the cage with the modified heatsink. Especially at some frequencies like 5, 11, and 22 GHz, the difference is more than 5 dB. These frequencies are associated with the resonance frequencies of the slots (air gap) between the cage and faceplate, and between the cage and the modules as depicted in Figure 5c. The largest gap is between the faceplate and the cage at 60.28 mm, while the smallest gap is between the cage and the module at 53.4 mm. Assuming these lengths are one wavelength, the corresponding frequencies are 4.97 GHz and 5.61 GHz, respectively. The frequency of ~11 and ~22 GHz are associated to two and three wavelengths long. The faceplate with these two slots behaves as an efficient slot antenna at these resonance frequencies. The rising heatsink strengthens the

EM waves leaking out at these resonances, which is the reason the SE of the cage with a rising heatsink reduced about 5 dB at these frequencies. Further, the SE of the cage is reduced at the frequency below 2 GHz. In general, 0 dB SE means the received power from the faceplate possessing the cage and the module is equal to the received power from an open aperture. However, the faceplate with a rectangular open aperture (19.98 mm×10.16 mm) has a TE_{10} mode cut-off frequency of 7.5 GHz. So, even though the SE of the cage is low at a frequency below 2 GHz, the received power from the open aperture is very weak and not noticeable. For further exploration, the SE of the cage is compared with the two types of cuboids and the results are presented in Figure 7. The resonance frequency of 5 GHz is not as strong as before. Further, the resonance frequency of 22 GHz shifts to a lower frequency, which can be due to a better mechanical contact of aluminum cuboids to the cage. However, the cage with the rising heatsink has about 5 dB lower SE than the cage with no rising heatsink at two frequency bands of 10-14 and 16-19 GHz.

2.2. CAGE CONFIGURATION OF 1×6

The averaged SE over the modules for 1×6 cage is shown in Figure 8, which manifests that the cage with a rising heatsink has the lowest SE compared to the cage with either a modified heatsink or without the heatsink at a wider frequency range from 4 to 24 GHz in comparison to the 1×1 cage. Calculating the resonance frequencies of the slots for the 1×6 cage is beyond the interest of this paper. However, because of multiple slots with relatively close dimension in each cage and between cages, a broadband trend for the 1×6 cage is appropriated which indicates that the rising heatsink deteriorates the SE of the cage because of an additional new path for EM waves to couples inside the cage.

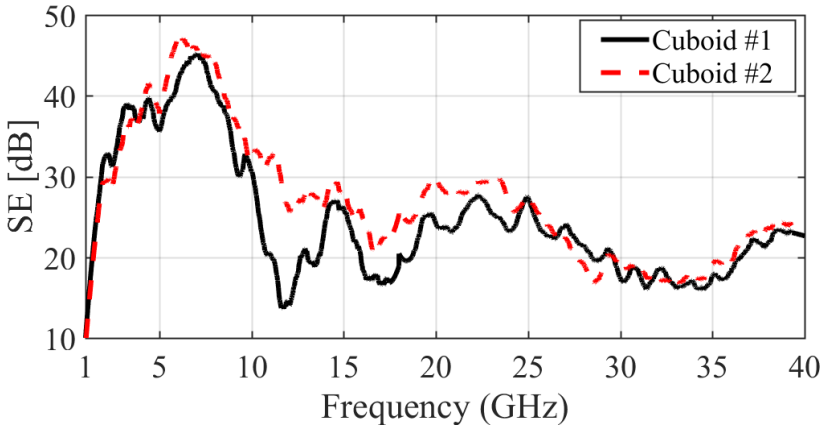

Figure 7 - The SE of the 1×1 cage with two types of cuboids.

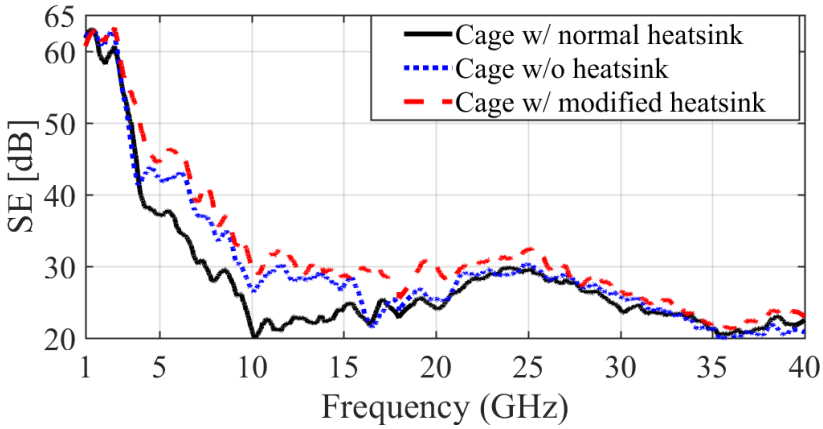

Figure 8 - Averaged SE of the 1×6 cage over three different OM vendors.

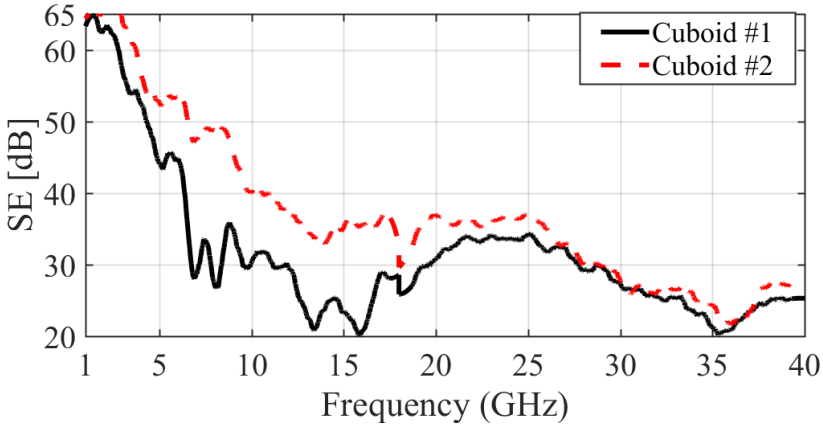

Figure 9 - The SE of the 1×6 cage with two types of cuboids.

Also, the SE of the 1×6 cage is obtained when the cuboids are placed in the cage. Six identical cuboids are fabricated for each type (cuboid #1 and #2). The SE of the cage with cuboids is shown in Figure 9. The difference in the SE of the cages with rising and non-rising heatsinks is relatively larger than the 1×1 cage (Figure 7), which demonstrates that the SE degradation due to the rising heatsink is worse for a larger number of cages.

Table 1 - Averaged SE of cage with optical modules at 10.31 GHz.

Condition	1×1 cage	1×6 cage
Cage w/ normal heatsink	23.37	20.48
Cage w/ modified heatsink	24.33	28.87

Table 2 - SE of the cage with cuboid at 10.31 GHz.

Condition	1×1 cage	1×6 cage
Cuboid #1	26.9	31.86
Cuboid #2	33.2	40.73

Because the 40 Gbps optical modules have the fundamental frequency of 10.31 GHz, the averaged SE of the cage over the modules at this frequency is given in Table 1. The reduction in averaged SE of rising heatsinks is about 8 dB in the 1×6 configuration relative to the modified heatsinks; this value is 1 dB for the 1×1 cage configuration. A comparison of the SE of the cage possessing a heatsink by inserting the cuboids is presented in Table 2 for the frequency of 10.31 GHz. The SE of the 1×1 cage with cuboid #2 is about 6 dB greater than the cage with cuboid #1 (i.e., rising heatsink). This value is 8.87 dB for

the 1×6 cage configuration. The results show that avoiding a rising heatsink will improve the SE of the cage. The improvement can be greater for bigger cage configurations. The potential coupling paths from inside to outside the enclosure with the rising heatsink is depicted in Figure 10. It is expected that the EM waves penetrate the cage from the path between the heatsink and the cage. This path is all around the cage and, thus, guides the EM waves through the cage. Also, EM waves can go through the cage from the bottom as there is a small gap between the cage and the line card PCB.

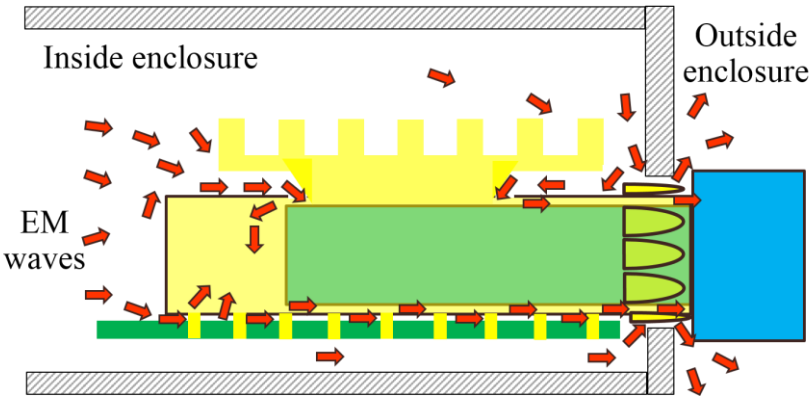

Figure 10 - Potential coupling path in rising heatsink.

3. ENERGY PARCELS THEORY

Understating of the EM coupling in electronic devices is a challenge for EMC engineers [25]-[32]. Several methods have been established to visualize the EM coupling including ray-tracing [25], diffuse scattering [26], reaction theorem [27], and so on. However, visualization of the EM coupling based on energy parcels and their trajectory [31]-[32] is a powerful and relatively easy to address the rising heatsink problem.

3.1. BRIEF INTRODUCTION

The rising heatsink problem. In this method, an analogy between the flow of EM energy and fluid flow is presented to visualize the EM energy path between an emitter and a receiver antenna. Hongyu Li, et. al, in [31]-[32] showed that the flow of EM energy can be imagined as a group of energy parcels propagating in space with certain velocities. Energy parcels are helpful to ease visualization of EM energy path. The visualization of the energy flow is defined by the Poynting vector, which demonstrates that the EM energy obeys the law of the conservation of energy. Assume in a region *V* characterized by ε, μ, σ and enclosed by surface *S*, with distribution of EM sources J_i and M_i, and the EM fields of *E* and *H*, the differential form of the instantaneous Poynting's theorem is [33]:

$$\nabla.(\vec{E}\times\vec{H}) = -[\vec{H}.\vec{M_i} + \vec{E}.\vec{J_i}] - \frac{\partial}{\partial}[\mu\frac{\vec{H}.\vec{H}}{2} + \varepsilon\frac{\vec{E}.\vec{E}}{2}] - \sigma\vec{E}.\vec{E} \tag{3}$$

In free space region without EM sources, (3) is simplified to:

$$\nabla.(\vec{E}\times\vec{H}) = -\frac{\partial}{\partial}[\mu\frac{\vec{H}.\vec{H}}{2} + \varepsilon\frac{\vec{E}.\vec{E}}{2}] \tag{4}$$
$$\vec{S} = \vec{E}\times\vec{H}$$

Vector *S* represents the energy flux or power density (i.e., the instantaneous Poynting vector). Hongyu Li showed that the flow of energy and fluid flow comprise the same partial differential equation, and, thus, the theories and methodologies of fluid dynamics can be

applied to electromagnetic energy flow to describe its motion. The instantaneous velocity of EM energy parcels is defined as:

$$\vec{v}(m/s) = \frac{\overrightarrow{S}\,(\mathrm{J/m^2 s})}{u(\mathrm{J/m^3})}$$
$$u = \mu\frac{\vec{H}.\vec{H}}{2} + \varepsilon\frac{\vec{E}.\vec{E}}{2} \qquad (5)$$

where *u* is the total magnetic and electric energy density. Time-averaged EM energy flow can be considered as a steady flow. The velocity of the energy parcels in timed-averaged is constant and is defined as:

$$\vec{v}_{av} = \frac{\vec{S}_{av}}{u} = \frac{\mathrm{Re}[\vec{S}]}{u} \qquad (6)$$

Equation (6) shows that the averaged velocity of the EM energy flow is a function of the real part of the complex Poynting vector. Therefore, the trajectory of energy parcels in timed-average flow can be obtained by calculating the streamline (tangential line) of the real part of the complex Poynting vector. The time-averaged flow of an energy parcel will be effective to identify and visualize propagation of EM waves in space or EM guided structure (e.g., transmission lines) because there is a time-averaged energy transmitted through space or in the EM guided structure. Streamline computation algorithms are available in many numerical electromagnetic solvers including ANSYS HFSS. To illustrate the idea, two examples are presented: Two dipole antennas (Tx and Rx) are placed

at a λ distance as shown in Figure 11. To obtain the energy path from the transmitter to the receiver antenna based on energy parcel and their trajectory method, the reverse calculation needs to be done. In other words, the negative sign of the real part of Poynting vector should be calculated at the receiver port to indicate how much energy is received at the receiver port from the Tx antenna. Figure 11 (a) displays the streamlines of the real part of the Poynting vector with a negative sign at the receiver antenna port. For the second example, a perfect electric conductor (PEC) is placed between the two antennas. A slot with 0.5λ length and the width of λ/20 at the frequency of interest (10.31 GHz) is designed in the middle of the PEC wall, which is perpendicular to the dipole antenna orientation. The EM waves can penetrate the slot at the response frequency and reach the Rx antenna. The tracked energy path from the receiver port is shown in Fig. 11b. The same amount of energy reaches the receiver port; however, the EM energy path is different and is through the slot.

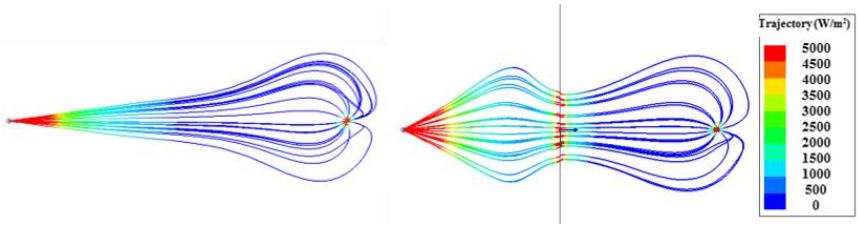

(a) (b)

Figure 11 - Reversed tracked energy parcels from the Rx (right antenna) to the Tx antenna. (a) in free space, (b) in free space at the presence of PEC wall with slot.

3.2. APPLICATION FOR QSFP SHIELDING CAGE

The rising heatsink reduces the SE performance of the QSFP cages, as shown and discussed in previous sections. The possibility of a new coupling path for EM waves

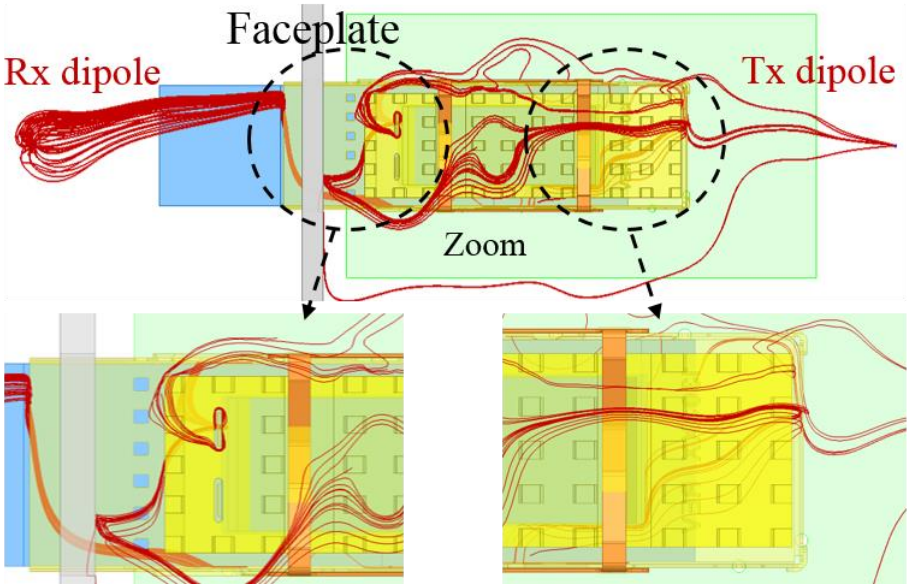

(a)

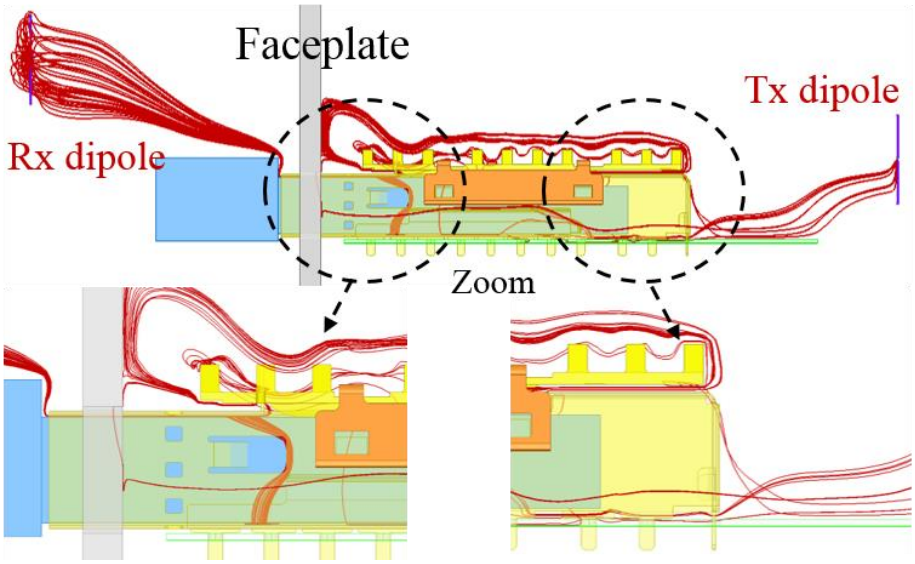

(b)

Figure 12 - Reversed tracked energy parcels from the receiver antenna (Rx) to the transmitter antenna (Tx) (a) top view, (b) side view.

created by a rising heatsink can be investigated by the energy parcels method. As such, a simulation model is built in ANSYS HFSS. Cuboid #1 is used to lift the heatsink. A PEC faceplate with 2 mm thickness is placed at the mouth of the cage. Two dipole antennas are

placed before and after the faceplate. The dipole antennas are designed for the frequency of 10.31 GHz, which is the fundamental frequency of 40 Gbps optical modules. The distance of the transmitter dipole antenna from the edge of the cage is 35 mm, which is greater than a wavelength (30 mm). The cage is almost placed in the far-field zone of the transmitter antenna so plane waves from the transmitter reach the cage. The receiver antenna is also in the far-field zone at 35 mm from the edge of the cuboid. The location of the two antennas is chosen arbitrarily with only a horizontal distance far enough from the edges to be assumed the cage is in far-field of the antennas. The streamlines of the real part of the Poynting vector with a negative sign is plotted at the receiver port to show how the EM energy from the Tx antenna reaches the Rx antenna. The EM waves penetrate the cage and leak out from the faceplate. Energy parcel concept illustrates possible coupling paths. Fig. 12 (a) exhibits the top view of the EM energy path which is reversely tracked back to the Tx antenna at the receiver port. The zoomed in subfigures show how the area between the heatsink and the top of the cage contribute as a path for the EM energy to penetrate inside the cage from the back and front of the heatsink. The side view of the same result is presented in Fig. 12 (b). The subfigures display the zoomed in area in the front and the back of the cage. The rising heatsink functions as a guided structure for the EM waves.

3.3. IDENTIFYING THE DOMINANT LEAKAGE PATH

Two possible leakage paths from the inside of the chassis/enclosure to the faceplate consist of the air gaps between the cage and the module (path #1), and between the faceplate and the cage (path #2), as shown in Figure 5c. The dominant leakage path can be identified by using the energy parcel method. For this purpose, the Tx antenna is located

at the one side of the cage and has an angle of θ with *z*-axes, as illustrated in Figure 13 (a). On the other side, four Rx antennas placed at four sides of the cuboid, in Figure 13 (b).

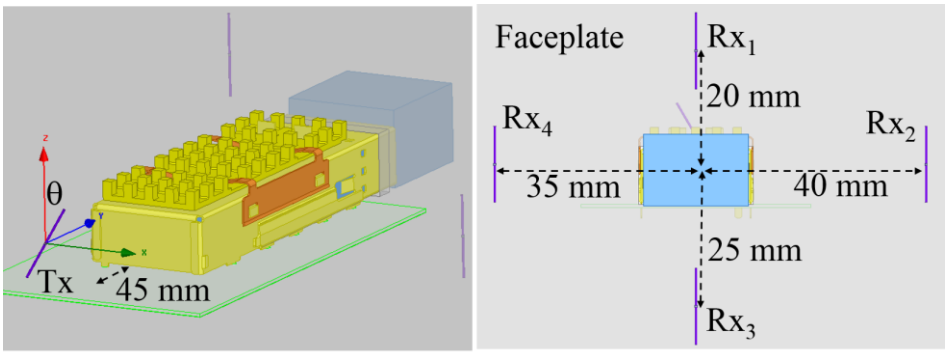

(a) (b)

Figure 13 - Location of (a) Tx antenna, (b) four Rx antennas.

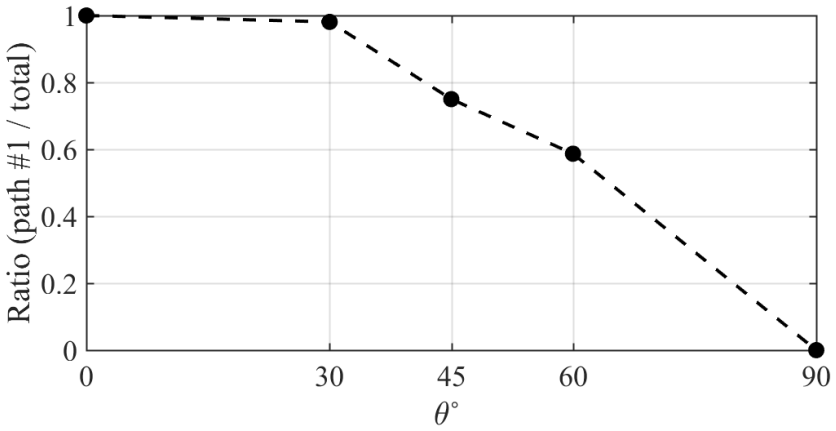

Figure 14 - Ratio of streamlines going through the path #1 to the total.

Rotating the Tx antenna around the *z*-axes provides plane waves with different polarization angle, in which θ of 0˚ and 90˚ are associated to the vertical and horizontal polarization, respectively. The streamlines (in the range of ~25 counts for each Tx-Rx combination) is tracked back from the Rx antenna ports to the Tx antenna. By counting the

number of streamlines going through each path, the dominant leakage path is determined between path #1 and path #2. The ratio of the streamlines in path #1 and the total number of streamlines are calculated and are shown in Figure 14. For the wide variation of θ from 0 to 60, the ratio is greater than 0.5 which indicates that path #1 is the dominant path for the coupling from inside the enclosure/chassis to the faceplate. The greatest ratio happens for $\theta = 0^{\circ}$ which is a pure vertical polarization for the EM waves propagating from the Tx antenna.

Figure 15 (a) shows the streamlines from Rx_4 to Tx with $\theta = 0^{\circ}$. The dominant leakage path with vertical polarization is from path #1. In fact, the EM waves couple into the cage and then reach Rx_4. The rising heatsink creates a parallel plate structure at the air gap between the heatsink and the top of the cage which behaves as a guided structure for the EM waves to couple inside the cage. However, the parallel plates only guide the plane waves with a vertical polarization. Fig. 15 (b) represents an example of the streamlines from Rx_4 to Tx with $\theta = 60^{\circ}$ which combines both vertical and horizontal polarizations. The EM waves reach the Rx antenna from the both paths, but with the majority of path #1.

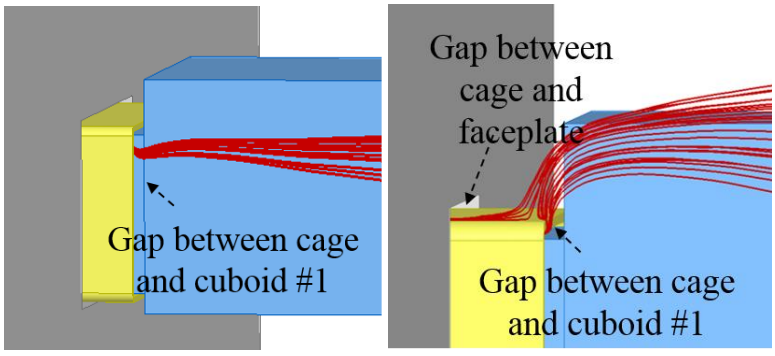

Figure 15 - (a) streamlines of Rx4 for θ=0˚, (b) streamlines of Rx4 for θ=60˚.

4. APPLYING EMI MITIGATION TECHNIQUE

To mitigate the EMI resulted in a rising heatsink, a window frame gasket is placed between the cage and the heatsink. Using an elastomeric gasket is preferred as it can be expanded when the module is inserted. From a thermal point of view, the heatsink must touch the optical module for the highest thermal connectivity so, the mechanical forces created by the newly inserted gasket should be considered to avoid any degradation in the heatsink performance. However, in this paper, the goal is to only show the gasket performance in improving the SE of the cage. A 2 mm width fabric-over-foam (FoF) gasket strip is cut as a window frame shape around the top of the 1×1 cage. Fig. 16a shows the placement of the gasket around the cage on a spare PCB line card for SE measurement. Similarly, three different vendors of modules are inserted into the cage and the average SE is obtained over the modules as shown in Fig. 17 for with and without the gasket. The SE of the cage is improved by a couple of dB in the whole frequency range. Better than 7 dB improvement is seen in the three response frequencies of about 5.5, 11, and 22 GHz.

The SE of the cage at the frequency of 10.31 GHz is compared in Table 3. About 8 dB improvement is achieved in SE of the cage possessing the gasket. Implementing the gasket for a larger cage configuration can result in even better performance. Improving the EMI SE of the QSFP shielding cages can improve the overall EMI performance of networking systems to meet global and customer-driven EMC regulations.

To evaluate the gasket in active operation of the modules, an MCB is utilized for 40 Gbps modules, as shown in Figure 16 (b). The electrical input signals are 10.31 Gbps NRZ with a $2^{31}-1$ pseudo-random bit sequence (PRBS). The measurement setup is depicted in Fig. 18. The optical module is powered ON with a DC power supply.

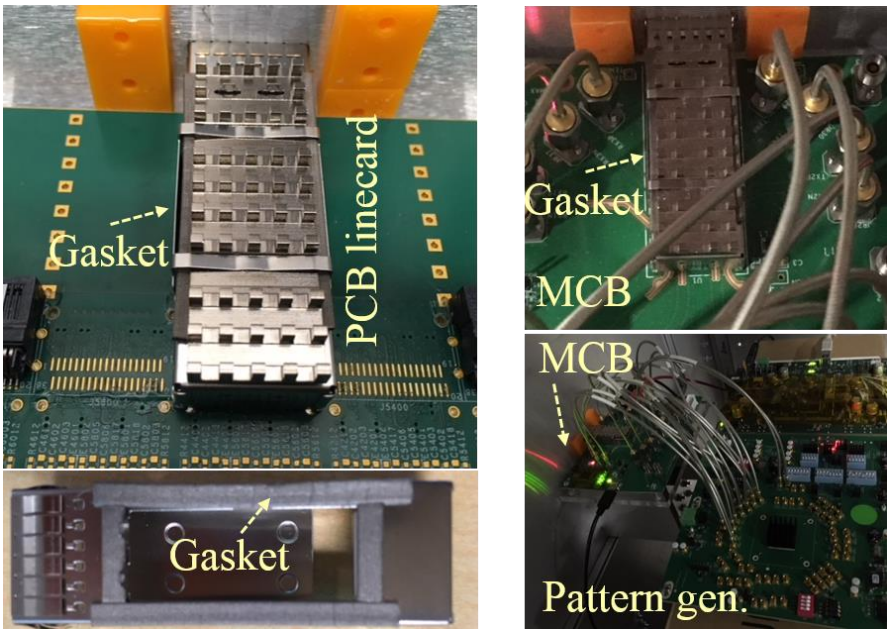

(a) (b)

Figure 16 - Gasket placement in (a) spare PCB line card for the SE measurement, (b) MCB for active measurement.

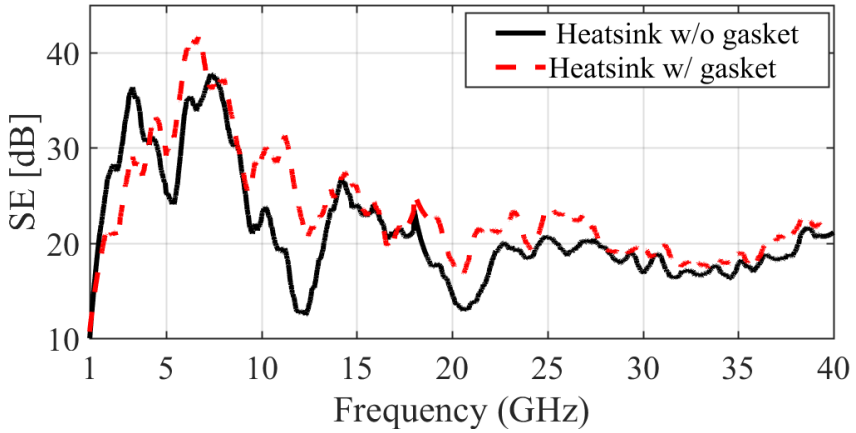

Figure 17 - Comparison between the averaged SE of the cage w/ and w/o gasket.

Table 3 - SE of the cage with normal heatsink at 10.31 GHz.

Condition	SE [dB]
Cage w/ gasket	29.96
Cage w/o gasket	23.37

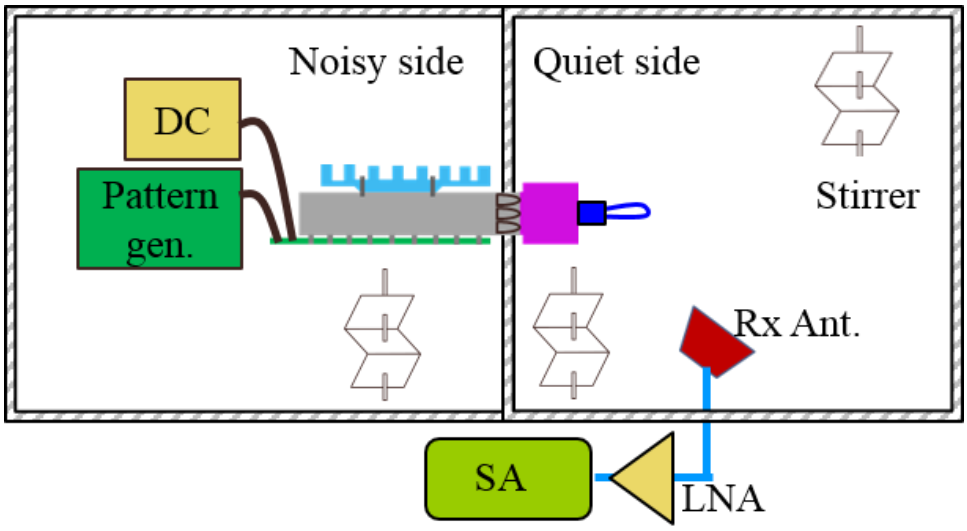

Figure 18 - Diagram of the active measurement set up.

The pattern generator transferred four traffics lanes of data to the QSFP connector. The electrical to optical transition occurs in the optical module; the optical cable provides the loopback and the optical signal transferees back to an electrical signal in the module meaning full data traffic is provided to the module. The QSFP shielding cage with a rising heatsink is mounted on the evaluation board. The total received power is obtained on the quiet side of the chamber. The second examination is the cage with the gasket. For each measurement, three different vendors of optical modules are used and the total received power is plotted in Fig. 19. With the gasket, the emission is reduced by 2 to 3 dB which indicates that implementing the gasket has a beneficial effect in shielding of the system. In addition, the optical module is considered as the dominant source of emission from the faceplate chassis. Thus, adding the gasket between the heatsink and the QSFP cages is likely to have a positive impact on the entire system in comparison to adding a gasket somewhere buried in the system (i.e., may be beneficial locally but not yield any measurable benefits at the system level).

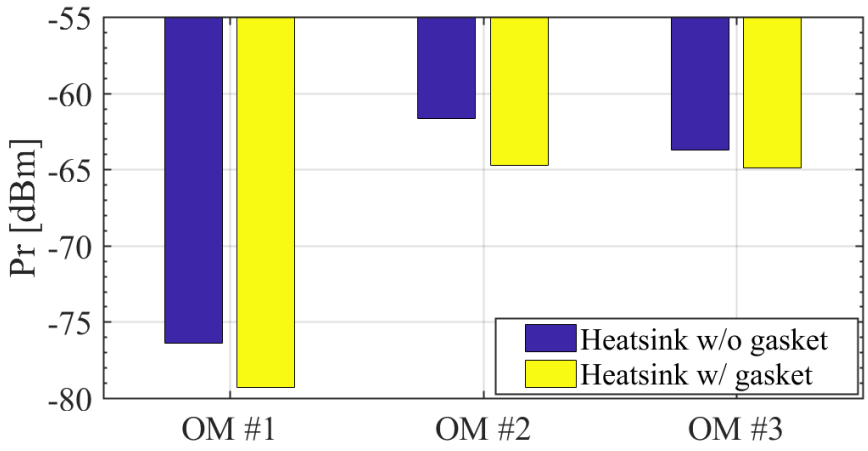

Figure 19 - Comparison of the total received power at the Rx side when different optical modules are used in active measurement.

5. CONCLUSION

The shielding cages of QSFP interconnections are often designed for thermal, mechanical, and volume manufacturing and their EMI performance is intuitively considered. Furthermore, introducing double density technology for QSFP interconnections makes it imperative to use a heatsink on the top of the cage to cool the 200 Gbps optical modules. The heatsinks shape (i.e., the pedestal under the heatsink) is for a thermal contact to the optical modules. Therefore, when optical modules are inserted into the cage, the heatsinks are raised which creates an air gap between the cage and the heatsink that can degrade the EMI performance of the shielding cage. In this paper, the effect of a rising heatsink on SE performance of the QSFP cage is explored. Two configurations of 1×1 and 1×6 QSFP cages are studied and the SE of the cages are measured for the frequency range of 1 to 40 GHz using a dual reverberation chamber. Three conditions are investigated for the cage including the cage with the normal heatsink, the cage without the heatsink, and the cage with the modified heatsink. Further, three different vendors of

optical modules are utilized for the examination. The averaged SE over the modules is obtained. The SE of the cage with a rising heatsink is 5 to 10 dB lower at the resonance frequencies (about 5.5, 11, and 22 GHz) of the gap path between the faceplate and the cage, and the cage and the optical module. Additionally, two types of aluminum cuboids are fabricated in which one rises the heatsink and the other one does not. For the first time, energy parcels and their trajectory method is applied to visualize the coupling path in a rising heatsink. The rising heatsink provides a new coupling path for EM waves to leak to the cage and emit from the chassis faceplate. The dominant leakage path is also identified by using the energy parcel method. The gap between the cage and the cuboid is the dominant path and the rising heatsink acts as a guided structure (parallel plates) to leak the waves to the inside the cage. Implementing a window frame gasket around the cage is introduced as an EMI mitigation technique. Its performance is evaluated with SE measurements and about 8 dB improvement is achieved at a frequency of 10.31 GHz. Further, an active measurement with the evaluation board using a 40 Gbps optical module is performed with and without the gasket; the emission is reduced by 2 to 3 dB at the frequency of 10.31 GHz when the gasket is implemented. Adding the gasket between the heatsink and the QSFP cages is likely to have a positive impact on the entire system compares to adding a gasket somewhere buried in the system which may provide localized mitigation but not yield any measurable benefits at the system level.

REFERENCES

[1] Small Form-Factor Pluggable (SFP) Transceiver Multi Source Agreement (MSA), Sept 14, 2000, http://schelto.com/SFP/SFP%20MSA.pdf.

[2] J. Anderson, and M. Traverso, "Optical transceivers for 100 gigabit Ethernet and its transport [100 gigabit ethernet transport]." IEEE Communications Magazine 48, no. 3 (2010).

[3] C. Cole, "Beyond 100G client optics." IEEE Com. mag., vol. 50, no. 2, 2012.

[4] J. Lee, et al. "Demonstration of 112-Gbit/s optical transmission using 56GBaud PAM-4 driver and clock-and-data recovery ICs." In ECOC, pp. 1-3., 2015.

[5] QSFP-DD MSA, http://www.qsfp-dd.com

[6] M. Hsu, and H. Lin. "Heat dissipation improvement design for QSFP connector." In 10th IMPACT, pp. 374-377, 2015.

[7] B. Archambeault, S. Connor, M. Halligan, J. Drewniak, and A. Ruehli. "Electromagnetic radiation resulting from PCB/high-density connector interfaces." IEEE Trans. on EMC, vol. 55, no. 4, pp. 614-623, 2013.

[8] H. Chen, S. Connor, T. Wu, and B. Archambeault. "The effect of various skew compensation strategies on mode conversion and radiation from high-speed connectors." In IEEE Int. Symp. on EMC, pp. 328-332, 2013.

[9] X. Tian, M. Halligan, L. Gui, X. Li, K. Kim, S. Connor, B. Archambeault et al. "Quantifying radiation and physics from edge-coupled signal connectors." IEEE Trans. on EMC vol. 57, no. 4, pp. 780-787, 2015.

[10] H. Chen, S. Connor, M. Halligan, X. Tian, X. Li, B. Archambeault, J. Drewniak, and T. Wu. "Investigation of the Radiated Emissions From High-Speed/High-Density Connectors." IEEE Trans. on EMC vol. 58, no. 1, pp. 220-230, 2016.

[11] M. Halligan, X. Tian, X. Li, S. Connor, D. Beetner, and J. Drewniak. "Quantifying High-Density Connector Radiation in a Lossy Multisignal Environment." IEEE Trans. on EMC vol. 58, no. 1, pp. 270-277, 2016.

[12] J. Li, and J. Fan. "Radiation Physics and Design Guidelines of High-Speed Connectors." IEEE Trans. on EMC, vol. 58, no. 4, pp. 1331-1338, 2016.

[13] J. Zhou, H. Runjing. "High-Speed SFP+ Signal Integrity Simulation and Measurement." Jour. of Com. and Comp., vol. 11, pp. 371-377, 2014.

[14] A. Talebzadeh, et al. "SI and EMI performance comparison of standard QSFP and flyover QSFP connectors for 56+ Gbps applications." In IEEE Int. Symp. on EMCSI, pp. 776-781, 2017.

[15] J. Li, X. Li, S. Toor, H. Fan, A. Bhobe, J. Fan, and J. Drewniak. "EMI coupling paths and mitigation in a board-to-board connector." IEEE Trans. on EMC vol. 57, no. 4, pp. 771-779, 2015.

[16] C. Hsiao, T. Wu, C. Chiu, S. Wang, C. Wang, W. Wang, and Y. Lin. "Radio-frequency interference mitigation strategies for high-speed connectors." In IEEE EDAPS, pp. 56-59., 2013.

[17] J. Li, Jing, S. Toor, A. Bhobe, J. Drewniak, and J. Fan. "Radiation physics and EMI coupling path determination for optical links." In IEEE Int. Symp. on EMC, pp. 576-581, 2014.

[18] L. Zhang, X. Li, X. Jiao, J. Li, S. Toor, A. Bhobe, D. Pommerenke, and J. Drewniak. "EMI Coupling Paths and Mitigation in Optical Transceiver Modules." Vol. 59, no. 6, pp. 1848-1855, IEEE Trans. on EMC, 2017.

[19] D. Kawase, H. Oomori, M. Shiozaki, and H. Kurashima. "EMI suppression of 10Gbit/s optical transceiver by using EBG structure." In Int. Symp. on EMC, pp. 33-38, 2011.

[20] H. Oomori, M. Shiozaki, and H. Kurashima. "Development of a practical electro-magnetic interference (EMI) simulation in high speed optical transceivers." In 59th IEEE ECTC, pp. 1908-1913, 2009.

[21] H. Krauthauser. "On the measurement of total radiated power in uncalibrated reverberation chambers." IEEE Trans. on EMC vol. 49, no. 2, pp. 270-279, 2007.

[22] X. Zhou, J. Li, H. Fan, A. Bhobe, P. Sochoux, and J. Yu. "High-frequency EMC design verification through full-wave simulations and measurements in reverberation chamber." In IEEE Int. Symp. on EMC, pp. 299-305, 2013.

[23] IEC 61000-4-21 (2003): Electromagnetic Compatibility. Part 4-21: Testing and Measurement Techniques – Reverberation Chamber Testing Methods.

[24] IEEE Standard Method for Measuring the Effectiveness of Electromagnetic Shielding Enclosures, IEEE Standard 299, 2006.

[25] T. Kurner, D. Cichon, and W. Wiesbeck. "Concepts and results for 3D digital terrain-based wave propagation models: An overview." IEEE Jour. on selected areas in Com., vol. 11, no. 7, pp. 1002-1012, 1993.

[26] V. Degli-Esposti, D. Guiducci, A. de'Marsi, P. Azzi, and F. Fuschini, "An advanced field prediction model including diffuse scattering," IEEE Trans. Ant. Propag., vol. 52, no. 7, pp. 1717–1728, 2004.

[27] J. Malmstrom, H. Henrik, and B. Jonsson. "On Mutual Coupling and Coupling Paths Between Antennas Using the Reaction Theorem." IEEE Trans. on EMC, 2017, early access.

[28] S. Shinde, X. Gao, K. Masuda, V.V. Khilkevich, D. Pommerenke, "Modeling EMI Due to Display Signals in a TV", IEEE Trans. on EMC, no. 99, pp. 1-10.

[29] Y. Cao, Y. Wang, L. Jiang, A. Ruehli, J. Fan, and J. Drewniak. "Quantifying EMI: A Methodology for Determining and Quantifying Radiation for Practical Design Guidelines." vol. 59, no. 5, pp. 1424-1432, IEEE Trans. on EMC, 2017.

[30] S. Shinde, et al., "Radiated EMI Estimation from DC-DC Converters with Attached Cables based on Terminal Equivalent Circuit Modeling", IEEE Trans. on EMC, Dec 22, 2017.

[31] H. Li, V. Khilkevich, and D. Pommerenke. "Identification and Visualization of Coupling Paths-–Part II: Practical Application." IEEE Trans. on EMC vol. 56, no. 3, pp. 630-637, 2014.

[32] H. Li, V. Khilkevich, and D. Pommerenke. "Identification and Visualization of Coupling Paths—Part I: Energy Parcel and Its Trajectory." IEEE Trans. on EMC vol. 56, no. 3, pp. 622-629, 2014.

[33] C. A. Balanis, Advanced Engineering Electromagnetics. Hoboken, NJ, USA: Wiley, 1989.

SECTION

2. CONCLUSIONS

This dissertation is composed of five papers that focuses on triboelectric charge voltage generation during daily activities in data centers, triboelectric charge voltage generation during glass transfer system in display manufacturing, and shielding effectiveness of quad small form-factor pluggable (QSFP) interconnections cage with a heatsink and visualizing the coupling path by applying the energy parcels concept to electromagnetic (EM) waves.

In the first three papers, the generation of electrostatic charge is considered for the cases of walking (well defined pattern and random), standing up from a chair, and for taking off a sweater at various different tempratures and releative humidity and dew points variation from -13.13 to 13.89 °C. Further, the effect of utilizing ESD-mitigation shoes and flooring system on building the static charge and the discharge process are presented. Data anlalyses were perfomed by definition of walking, standing, event volatges, decay time constant, ESD effectivness factor, and relative humidity variation (RHV) paramter.

In the fourth paper, triboelectric charge generation on the glass is explored during the glass transportation by a roller conveyor system in display manufacturing. The paper presents an intensive study to understand the underlaying parameters including the effect of roller material (insulative vs. dissipative), roller radius (small vs. large), transfer velocity (slow vs. fast), transfer acceleration (medium vs. high), traveling distance (200 m vs. 400 m). In addition, a comprehensive study of the surface potential distribution on the glass and rollers by utilizing a 2D automated scanner is given.

In the fifth paper, the shielding effectiveness of QSFP interconnections cages with heatsinks, which are often optimized for thermal, mechanical, and volume manufacturing, is investigated. Energy parcels and their trajectory concept are applied to EM waves to visualize the coupling paths in a QSFP cage with a rising heatsink. The rising heatsink creates a new coupling path for EM waves to leak to the cage and emit from the routers/switches chassis faceplate. An EMI mitigation technique is introduced and evaluated by SE measurement for the frequency of 1-40 GHz, and by an active operational of 40 Gbps optical module in dual reverberation chamber.

VITA

Atieh Talebzadehghahroudi was born in Tehran, Iran, in 1988. She received her B.Sc. degree in Electrical Engineering from Shahed University, Tehran, Iran, in 2010 and M.Sc. degree in Electrical Engineering from Amirkabir University of Technology, Tehran, Iran, in 2013. She joined the EMC Laboratory at the Missouri University of Science and Technology in Summer 2014 as a Ph.D. student. In May 2018, she received her Ph.D. in electrical engineering from Missouri University of Science and Technology. Her research interests included EMC/EMI and SI analyzes of high speed interconnects, triboelectric charging analyzes, sparkles electrostatic discharge, and power integrity of high-speed circuits. Atieh was a member of IEEE EMC society and a member of Eta Kappa Nu (HKN) IEEE honor society. She had been awarded multiple awards from different professional societies including the Dean's Ph.D. Scholar Award in 2017, Technical Paper Award of ASHRAE annual conference PR Material in June 2016, the first place of IEEE EMC/SI Student Hardware Design Competition in August 2016, and the Best Student Paper Award finalist in the IEEE International Symposium on EMC 2015.